SENSITIVITY AND SEA SURFACE TEMPERATURE ANALYSES OF WRF MODEL FOR PREDICTING HEAVY RAINFALL EVENTS OBSERVED IN EASTERN BLACK SEA AND MEDITERRANEAN REGIONS OF TURKEY

A THESIS SUBMITTED TO
THE GRADUATE SCHOOL OF NATURAL AND APPLIED SCIENCES
OF
MIDDLE EAST TECHNICAL UNIVERSITY

BY

HEVES PİLATİN

IN PARTIAL FULFILLMENT OF THE REQUIREMENTS
FOR
THE DEGREE OF MASTER OF SCIENCE
IN
EARTH SYSTEM SCIENCE

AUGUST 2020

Approval of the thesis:

SENSITIVITY AND SEA SURFACE TEMPERATURE ANALYSES OF WRF MODEL FOR PREDICTING HEAVY RAINFALL EVENTS OBSERVED IN EASTERN BLACK SEA AND MEDITERRANEAN REGIONS OF TURKEY

submitted by **HEVES PİLATİN** in partial fulfillment of the requirements for the degree of **Master of Science** in **Earth System Science, Middle East Technical University** by,

Prof. Dr. Halil Kalıpçılar
Dean, Graduate School of **Natural and Applied Sciences**, METU _____

Prof. Dr. Bülent G. Akınoğlu
Head of the Department, **Earth System Science**, METU _____

Prof. Dr. İsmail Yücel
Supervisor, **Department of Civil Engineering**, METU _____

Prof. Dr. Elçin Kentel Erdoğan
Co-Supervisor, **Department of Civil Engineering**, METU _____

Examining Committee Members:

Assoc. Prof. Dr. M. Tuğrul Yılmaz
Department of Civil Engineering, METU _____

Prof. Dr. İsmail Yücel
Department of Civil Engineering, METU _____

Assoc. Prof. Dr. Koray K. Yılmaz
Department of Geological Engineering, METU _____

Asst. Prof. Dr. Cüneyt Baykal
Department of Civil Engineering, METU _____

Asst. Prof. Dr. Bahtiyar Efe
Department of Meteorological Engineering, SAMU _____

Date: 27.08.2020

I hereby declare that all information in this document has been obtained and presented in accordance with academic rules and ethical conduct. I also declare that, as required by these rules and conduct, I have fully cited and referenced all material and results that are not original to this work.

Name, Last name : Heves Pilatin

Signature :

ABSTRACT

SENSITIVITY AND SEA SURFACE TEMPERATURE ANALYSES OF WRF MODEL FOR PREDICTING HEAVY RAINFALL EVENTS OBSERVED IN EASTERN BLACK SEA AND MEDITERRANEAN REGIONS OF TURKEY

Pilatin, Heves
Master of Science, Earth System Science
Supervisor : Prof. Dr. İsmail Yücel
Co-Supervisor: Prof. Dr. Elçin Kentel Erdoğan

August 2020, 204 pages

With this thesis it is aimed to enhance the prediction accuracy of the Weather Research and Forecasting (WRF) model on the extreme precipitation events of Mediterranean and Eastern Black Sea regions of Turkey. While the first part of sensitivity analysis was conducted for the physical parameters (microphysics, cumulus and PBL) and the initial boundary conditions, the second part has only focused on the impact of sea surface temperature (SST). After choosing 4 microphysics, 3 cumulus, 2 PBL and 2 input meteorological sources options, in total 96 scenarios have been tested through the first part of sensitivity analysis for each region. Among all of the schemes, generally for microphysics Eta / Ferrier (ES) scheme, for cumulus Grell Freitas (GFES) sheme and finally for PBL Mellor Yamada Janjic (MYJ) scheme performed better than the other options in Mediterranean event cases. However, for Eastern Black Sea region, Aeresol Aware Thomspon (AATS) and WRF Single Moment 6 (WSM6) as microphysics, Betts Miller Janjic (BMJ) and GFES as cumulus and MYJ as PBL scheme become prominent. Again, WRF model usually performs better by using the Global

Forecasting System (GFS) meteorological input dataset in Mediterranean region whereas it produces more realistic forecasts for Eastern Black Sea, if it uses ERA5 Reanalysis (ERA5, ECMWF) meteorologic data. For SST analysis, three SST data sources were selected to use. Through detailed examination, the Medspiration and NCEP sources were found successful for the prediction of the Mediterranean event cases. In Eastern Black Sea region, the two satellite based sourced datasets (Medspiration and GHRSST) performed better than the other two.

Keywords: Sensitivity Analysis, WRF, Sea Surface Temperature, Extreme Precipitation Events

ÖZ

TÜRKİYENİN DOĞU KARADENİZ VE AKDENİZ BÖLGELERİNDEKİ SAĞANAK YAĞIŞLI HAVA OLAYLARINI TAHMİN ETMEK İÇİN OLUŞTURULAN WRF MODELİ DUYARLILIK VE DENİZ YÜZEY SICAKLIĞI ANALİZLERİ

Pilatin, Heves
Yüksek Lisans, Yer Sistem Bilimleri
Tez Yöneticisi: Prof. Dr. İsmail Yücel
Ortak Tez Yöneticisi: Prof. Dr. Elçin Kentel Erdoğan

Ağustos 2020, 204 sayfa

Bu tezdeki çalışmalarla amaçlanan, Türkiye'nin Akdeniz ve Doğu Karadeniz bölgelerindeki ekstrem yağış olayları ile Hava Araştırma ve Tahmin modeli olarak da bilinen WRF'u kullanarak; bu bölgeler için model tahmin doğruluğunu arttırmaktır. Bu bağlamda, biri fizik parametrelerinin (mikrofizik, kümülüs ve yüzey tabaka sınır) ve girdi verilerinin, diğeri ise deniz yüzey sıcaklığının (DYS) ekstrem yağışlara etkisini incelemek adına iki farklı duyarlılık analizi yapılmıştır. İlk çalışmada denenmek üzere, 4 mikrofizik, 3 kümülüs, 2 PBL ve 2 veri kaynak seçenekleri olmak üzere toplam 96 senaryo belirlenmiş ve modele konulmuştur. Bütün seçenek ve analizlerin sonucunda Akdeniz'de; mikrofizik için Eta / Ferrier (ES), kümülüs için Grell Freitas (GFES), PBL ve veri kaynağı için ise sırasıyla Mellor Yamada Janjic (MYJ) ve GFS daha iyi performans göstermiştir. Doğu Karadeniz'de çalışılan olaylar bazında, Aeresol Aware Thomspon (AATS) and WRF Single Moment 6 (WSM6) mikrofizik, Betts Miller Janjic (BMJ) and GFES kümülüs, MYJ yine PBL ve bu sefer ERA5 Re-analiz (ERA5, ECMWF) girdi veri

seçenekleri öne çıkmıştır. DYS analizine gelindiğinde ise 3 farklı deniz yüzey sıcaklığı veri kaynağı belirlenmiş ve bu kaynakların olay tahminlerindeki başarıları kıyaslanmıştır. Buna göre Akdeniz üzerinde çalışan model, Medspiration ve NCEP datasetleri kullandığında daha gerçekçi sonuç verirken; bu model Doğu Karadeniz bölgesi için uydu bazlı kaynaklar olan GHRSST ve Medspiration ile çalıştığında daha iyi sonuçlar üretmiştir.

Anahtar Kelimeler: Duyarlılık Analizi, WRF, Deniz Yüzey Sıcaklığı, Ekstrem Yağış Olayları

to my beloved family

ACKNOWLEDGMENTS

First of all, I would like to give my biggest thanks to my supervisor and my mentor ***Prof. Dr. İsmail Yücel*** for his guidance, advice, encouragement, trust and patience with gratitude. I would also thank to ***Prof. Dr. Elçin Kentel Erdoğan*** as my Co-Advisor and ***Assoc. Prof. Dr. M. Tuğrul Yılmaz*** for their support and assistance throughout the studies conducted under this thesis.

Without their love, friendship, encouragement and continuous support, I could not achieve to complete this study as it is done now. Therefore, I would like to give my sincerest thanks to my dearest friends: ***Berina Mina Kılıçarslan*** and ***Research Assistant Eren Düzenli*** for always being there for me, no matter what.

Last but not least, I would like to thank and say my deepest gratitude to my family by using this platform. I would be always grateful for their endless love, patience and trust that they show to me. After this thesis, I am once again realizing that they are my biggest luck in this life. So, I personally thank to my mother ***Ayla Pilatin*** and my father ***Kenan Pilatin*** who always wait for me with open arms and I also want to thank to my partner in life, ***Olcay Bacakoğlu*** for his understanding, love, honesty and encouragement that he gives me for many years.

This study is supported and funded by The Scientific and Technological Research Council of Turkey (TUBITAK) with the grant number 110Y193.

TABLE OF CONTENTS

LIST OF TABLES

TABLES

LIST OF FIGURES

FIGURES

LIST OF SYMBOLS

SYMBOLS

AATS : Aerosol Aware Thompson Scheme

ACM2 : Asymmetric Convective Model Version 2.0 Scheme

BMJ : Betts Miller Janjic Scheme

CAPE : Convective Available Potential Energy

CCN : Cloud Condensation Nuclei

CERSAT : The Centre European Remote Sensing d'Archivage et de Traitement

CIN : Convective Inhibition

COSMO : The Consortium for Small-scale Modeling

CSI : Critical Success Index

ECMWF : The European Centre for Medium-Range Weather Forecasts

ERA5 : ECMWF Reanalysis 5th Generation

ES : Eta / Ferrier Scheme

FAR : False Alarm Ratio

FBI : Frequency Bias Index

GFES : Grell-Freitas Scheme

GFS : The Global Forecast System

GHRSST : The Group for High Resolution Sea Surface Temperature Level 4 Ultra High Resolution

IFREMER : Institut Français de Recherche pour L'Exploitation de la Mer

K : The Eddy-diffusivity for Heat and Eddy-viscosity for Momentum

KFS : Kain-Fritsch Scheme

KS : Kessler Scheme

LCL : Lifting Condensation Level

MBE : Mean Bias Error

MEDS : The Medspiration L4 Ultra High Resolution SST Data

GDM : General Directorate of Meteorology

MM5 : The Fifth Generation NCAR/Penn State Mesoscale *Model*

MMAB : Marine Modeling and Analysis Branch

MYJ : Mellor- Yamada-Janjic Scheme

NCAR : National Center for Atmospheric Research

NCEP : National Centers for Environmental Prediction

NOAA : National Oceanic and Atmospheric Administration

NWP : Numerical Weather Prediction

PBL : Planetary Boundary Layer

PC : Percent Correct

POD : Probability of Detection

R : Correlation Coefficient

RMSE : Root Mean Square Error

RRTM : Rapid Radiative Transfer Model

RTG_SST_HR : The real-time, global, sea surface temperature

SD : Standard Deviation Error

SST : Sea Surface Temperature

TOPSIS : Technique for Order of Preference by Similarity to Ideal Solution

YSU : Yonsei University Scheme

WRF : Weather Research Forecasting

WRF ARW : Advanced Research WRF

WRF NMM: Non-hydrostatic Mesoscale Model

WSM6 : WRF Single Moment 6 Class Scheme

CHAPTER 1

INTRODUCTION

1.1 Introduction

Due to global warming and climate change over the years, the number of catastrophic events around the world and their impacts on life are becoming more important. As they cause the major changes in the precipitation types, amount and the water cycle that create some meterological disasters. For instance, some regions may suffer from the floods because of the sudden extreme precipitation occurences whereas the lack of rain at other regions may cause the widespread droughts (Yucel & Onen, 2014). At this point, the forecasting of these events is crucial to take precautions before it happens because their frequencies get often while their magnitudes are also growing so fast that makes them basically threat to the life and the property on the earth.

Additionally, some of the main needs that are essential to sustain the life such as the agricultural production, food security and economy, are also directly affected by the sudden extreme precipitation events (Conforti, 2018). Since the irregulary in precipitation patterns cause to diminish agricultural activities and threat the food security as well as the water reservoirs for the future. This leads great risk to health, hunger and economy crises all around the World.

The researches and the weather forecasts for future are mainly done by the numerical weather prediction (NWP) models where both mesoscale and synoptic/regional simulations of atmosphere can be achieved with temporal and spatial variations for the long and short periods. Currently, the Weather Research and Forecasting (WRF) model is the most commonly used regional forecasting model among all NWPs such as COSMO, MM5, GFS and ECMWF. The study conducted by Abualkishik,

(Abualkishik, 2018) supports this claim via referring the WRF is a community supported model by the users of all around the world. Hence, it is opened to public and flexible and also it has strong software utilities' architecture which mostly enables it to provide more accurate results than the other NWP models (Abualkishik, 2018).

However, of course, like in the other NWP models, the sensitivity analysis of WRF is essential to identify the parameters that have most influence on the model predictions. Knowing the parameters having great impacts, enables the users to determine the best options for the configuration. The'best options' refer the configuration options that lead the model providing the most accurate forecasts, closest to the reality.

Here, the key point is following the path of how the model builds its dynamic atmospheric system. Since the WRF is a 'fully compressible nonhydrostatic model', it uses the governing equations in order to calculate atmospheric physics (UCAR, 2019). Therefore, the equations used in the WRF model forecasts, can alter through the different approachs / schemes that are prefered to use for establishing the physics of its cloud system. This indicates that the schemes of model physics, are quite important in the model predictions as well as the physical parameters of atmospheric system itself such as radiation, cumulus, microphysics and etc. Since each of them can affect the results after all.

Just as the physical parameters, the initial boundary conditions of WRF model also has huge impact on the predictions because the model takes the starting weather conditions of the run period from there. Then, it builds up its future predictions based on this dataset.

So overall, both the initial boundary conditions and the selected approachs to be used in physical parameters can be considered as the most sensitive parts of WRF model that can change the forecasts entirely.

From this perspective, the sensitivity analysis of WRF model in the first part of this thesis is planned to conduct through these parts. Since the best configuration options have been tried to find for heavy precipitation events, only some of the physical parameters that are known for having the direct effect on rainfall production, have been chosen to focus under this study. These parameters are listed as follows: cumulus, microphysics and planetary boundary layer. The initial boundary conditions to include into the WRF model sensitivity analysis, on the other hand, are selected among commonly used meteorological datasets like Global Forecasting System (GFS) and The European Centre for Medium-Range Weather Forecasts (ECMWF - ERA5).

In the second part of this thesis, Sea Surface Temperature (SST) impact on heavy precipitation production has been investigated by using the best physical and initial boundary configuration options for each region, which were found from the previous sensitivity analysis results.

In some cases, the SST changes can trigger the intense precipitation event occurences over the regions. Since certain catastrophic rainfalls that regularly influence the World climate cycle such as summer monsoons in India or the tropical cyclones, are considered as the SST sourced events, its impacts on precipitation can be taken as synoptic. Yet, some researches claim that especially on the mountainous regions near to the sea, the heavy rainfall production may be triggered by the rapid changes in SST. From this perspective, it may be possible to say, the scale of SST triggered occurences can also be mesoscale.

So, does SST really trigger or contribute the intense precipitation event occurence around a region? The answer of this question has been tried to find out in the second portion of this thesis. Actually, this can be also thought as an another perspective of sensitivity analysis for WRF because SST is one of the variables in meteorogical dataset that is also used to define the initial boundary conditions in the model. For this purpose, one heavy precipitation event for each of Mediterranean and Eastern Black Sea regions has been studied. Additionally, the model configurations

determined to be used in this study, are directly taken from the results of the sensitivity analysis conducted in the first part of the thesis.

1.2 Literature Review

The literature review is the key term of any research before it has conducted. Since it offers the specific questions to be answered by the study as well as the right conditions and the detailed strategy to get those answers. Hence, for having comprehensive aims to obtain, this thesis uses many reference studies as the backbone of its two analyses.

For instance, in sensitivity analysis, the goal is always finding the parameters that affect the model forecasts most. To be able to make a proper analysis, every possible option which are considered as having huge impact on precipitation occurence are included into this part of thesis. Some of these option are the orographical and climatic effect on WRF. As it is already known from many sensitivity studies conducted so far (e.g. Rontu, 2013; Elvidge, et.al., 2019; Iriza, et.al., 2015; Arthur et al., 2018), the orographic features and the climatic regimes of a region have incontrovertible impact on the weather prediction simulations.

As mentioned in Yucel et.al's (2014) and Jee et.al's (2016) articles, the sensitivity analyses of weather prediction models generally focus on initial boundary conditions and some physical components of atmosphere such as cumulus, microphysics, planetary boundary layer components, especially for precipitation studies as they can entirely change the model predictions. The specific parameterization studies of these components (Arakawa, 1974; Bister, 1998; Bright et.al, 2002; Mayor et.al, 2015; Hong, 2010) also proof this theory.

The initial boundary conditions and the physical schemes to use in the sensitivity analysis of thesis are determined based on their working mechanisms and some reference studies (Zeyaeyan et.al, 2017; Rebora et.al, 2013; Argüeso et.al, 2011;

Flesch et.al, 2012; Gelpi et.al, 2016; Hong et.al, 2009a; Miao et.al, 2014) which share similar climatic features with Mediterranean and Eastern Black Sea regions. According to recent studies of Senatore and his colleagues (Senatore et.al, 2014; 2020), SST has also undeniable impact on WRF prediction accuracy since the continuous circulation of vertical fluxes are transfered by the interface between the sea surface and the atmosphere (Bigg et.al, 2003). As these and many other studies (Jee et.al, 2017; Cisneros et.al, 2016; Robinson et.al, 2012; Senatore et.al, 2014; Senatore et.al, 2020) suggest that some mesoscale extreme precipitation events are triggered by the changes in SSTs, particularly for the regions with complex topography. Because this effect is wished to be investigated, the second part of the thesis focuses on the WRF model precipitation performances via using different SST sources.

1.3 The Scope of Thesis

While the weather forecast is a must to plan the daily life, it is also a good tool to establish the overall picture of the future. By looking at the model's predictions, any catastrophic event like heavy precipitation, storm, tornado can be detected earlier so that the possible risks may born from these events can be eleminated before they happen. Additionally, the continuous forecasts for the long and short time periods on any region and the globe itself, can give a helpful representation about the changes occuring in the water cycle, the annual mean precipitation – temperature data and the shifting in climate regimes. Since the starting point of this cycle is atmosphere, it is vital to obtain an accurate weather prediction outcome from the NWP models. However, the accuracy of the model varies via the study area and its topographical properties, the meterological data used, the physical parameters selected and many other factors for every run because the NWP models use these factors together to mimic the complete atmospheric simulation in the real life. Therefore, the models are sensitive to extrinsic parameters that can change the whole forecast results.

For the weather predictions conducted in Turkey, it is already known that the General Directory of Meteorology (GDM) uses only one model configuration with WRF model on all regions of the country. The GDM's configuration options are given in **Table 1.3.1**.

Table 1.3.1 The WRF model configuration options of GDM

Grid Space / Horizontal Resolution	Initial Boundary Condition Data	Cumulus	Microphysics	PBL	Shortwave Radiation	Longwave Radiation	Land Surface
4 km	Integrated Forecast Systems (IFS)	-	WRF Single Moment Class 3 and 5	Yonsei University	Dudhia Shortwave Scheme	RRTM Longwave Scheme	5 Layer Thermal Diffusion

Yet, as it was mentioned above, the prediction accuracy of model has been enhanced by the working mechanisms and content of many atmospheric components. Therefore, it is not much possible to believe that one configuration suits every region and climate in Turkey well and produces the 'most realistic' forecast for the heavy precipitation events. The biggest motivation underlies the sensitivity analysis is to determine the special model configuration options which usually offer the most successful rain predictions in Mediterranean and Eastern Black Sea regions and improving the model forecast performance and accuracy to the reality.

Since this kind of detailed sensitivity analysis has not been done before in Turkey, the study carries great importance for atmospheric research and also contributes the best chance to observe the impact of climate change on precipitation regimes which is also the other motivation under the thesis.

Similar comments can be said for SST analysis. The WRF model provides different outcomes when an external updated SST source has been used in its configuration. Othervise, the SST data is taken constant for each day of the run period which does not suit with the real case. Thus, observing the impact of this parameter on forecast and again finding the 'best option' (among SST sources) for future operational studies, are the aims of this study. As the power of climate change is rising, the frequency and the impact size of convective heavy precipitation events triggered by the changes in SSTs, are also increasing.

1.4 Description of Thesis

This thesis study consists of 5 chapters with two seperate studies:

- Initially, the aim of the studies and the general principles to follow while conducting those, are explained by **Chapter 1**.

- In **Chapter 2**, the methodology is represented. Accordingly, the study areas, the event dates, the numerical weather prediction model, its main working steps, are placed into this chapter.

- **Chapter 3** shows the model configuration arragements in both sensitivity and SST analyses. The first three subsections of this chapter explain the selection criteria of the input and physical parameters be used in Sensitivity Analysis and how the model configurations has been arranged through the

mentioned study whereas Chapter 3.4 & Chapter 3.5 cover the event dates, the selection and the arrangement processes of SST sources for SST Analysis.

- The results of sensitivity and SST analyses for each event date and region that are evaluated by various perspectives, are offered via **Chapter 4**.

- As the last chapter of this thesis **Chapter 5,** discusses the general outcomes obtained from both studies, highlights the important factors and finally offers some suggestions for future climate studies.

CHAPTER 2

METHODOLOGY

2.1 General Information

The flowchart of methodology that has been followed through this thesis, is given in **Figure 2.2.1** By looking at this figure, it can be easily seen that for both parts or studies, the WRF model is common. Then, the sensitivity study showed under 'PART I' has conducted by determining the extreme precipitation event dates and station locations and choosing the initial and boundary conditions and the physical parameters of WRF.

The results of this study are evaluated by many different aspects. Depending on the general outcomes from all of these aspects, the best configuration options which give the most accurate prediction, have been chosen for each study area. After this step, the second part of the thesis (PART II) has been carried out. Once again, the heavy rainfall event dates and the SST data sources are estimated but the important point here has been illustrated by orange line comes from the PART I. As this line indicates that the best options determined from sensitivity analysis, are directly used during the model configuration of SST analysis. By this way, both of the studies are connected to each other. Afterwards, the obtained results from the four different SST sources' model performances are investigated with some different analyses and tried to find the best performer source among all for the extreme precipitation forecasts.

2.2 The Study Areas

The studies that are aimed to conduct under this thesis, are chosen from the events occured on two regions of Turkey: Mediterranean and Eastern Black Sea. The main reason behind this decision is actually finding the similarities as well as the diversities that the WRF model applies onto its forecasts based on the region. Since the climates of these regions are quite different from each other whereas the orographic features are close.

As the name itself implies, Mediterranean climate dominates the Mediterranean region. The summers usually pass dry and high temperatures while the winters are moderate. On the other hand, Eastern Black Sea region has oceanic climate with warm and humid summers, wet and cold winters. Both of the regions have mountains at the coastal area and these mountains are located as parallel to the sea. Therefore, the altitude, the complex topography and the climatic impacts from the seaside towards the inlands are quite similar among these two regions. Hence, as a first step of sensitivity analysis conducted on Turkey, initially these two regions are selected to study and it is aimed to see how the model sensitivity on forecast accuracy has changed due to their climate regions but still have common orographical features.

Normally, all of the studies examined in the scope of this thesis are applied on the specific basins in Mediterranean and Eastern Black Sea regions. According to that, Antalya and Eastern Black Sea basins are determined for Mediterranean, Eastern Black Sea heavy precipitation events, respectively.

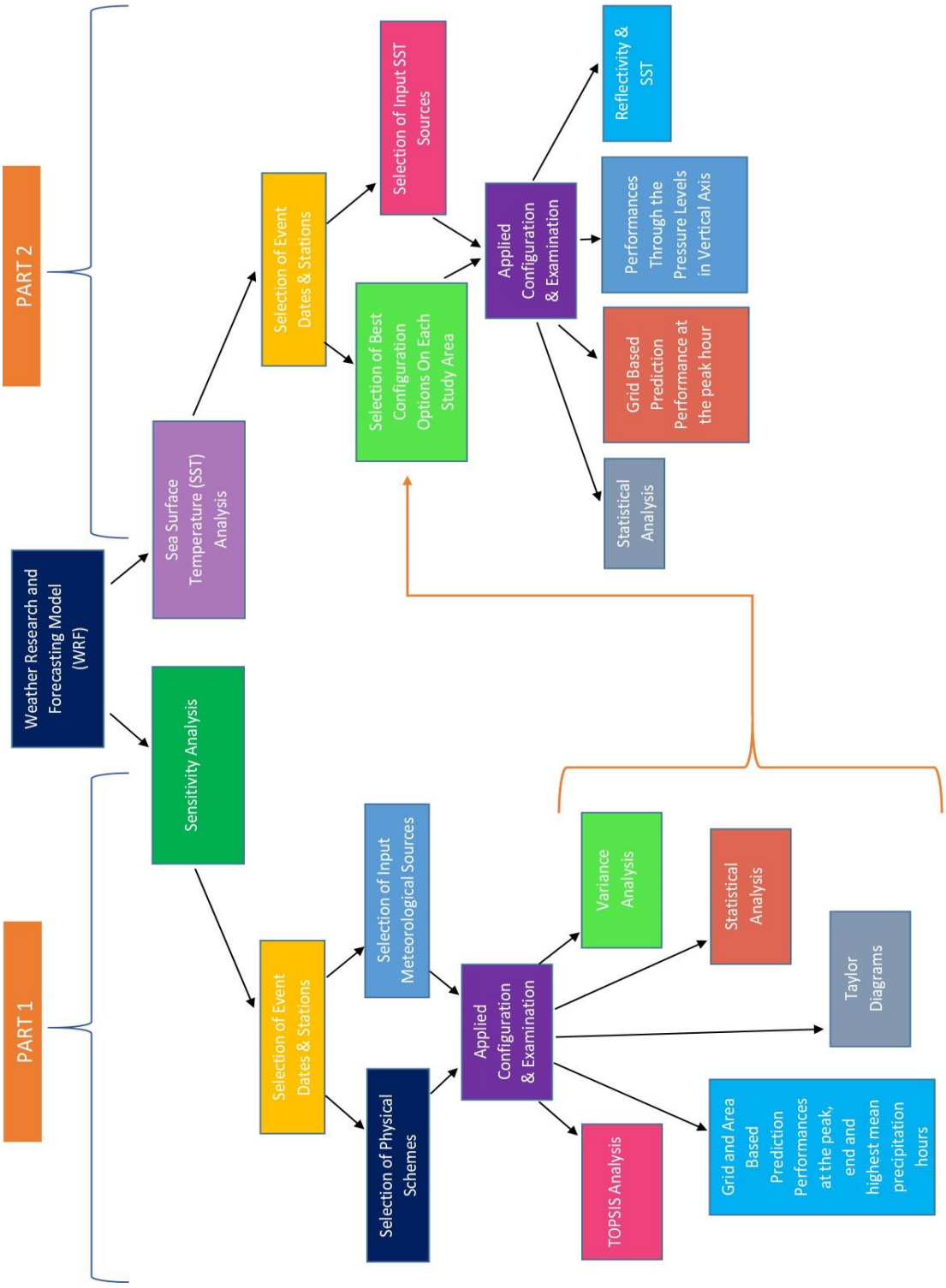

Figure 2.2.1 Methodology Overview

2.3 Selection of Extreme Precipitation Events and Observation Stations for Each Region

The hourly precipitation data recorded via the observation stations for the last 10 years, between 2008.01.01 – 2017.12.31, is acquired from GDM. Throughout this dataset and the information about the events, the numbers of heavy precipitation frequencies took place in each season has shown on **Table 2.3.1** and **Table 2.3.2**.

Based on these tables, the maximum number of extreme precipitation events in Antalya basin (Mediterranean region) occured during autumn season. Comparing to other seasons, with 23 events, the autumn forms almost one third of the sum of total event numbers at this region. For Eastern Black Sea basin (Eastern Black Sea region) the result is the same. Here, more than half of the other seasons' total event number were recorded in autumn season. Nearly the half of 100 events in Eastern Black Sea on the other hand, were observed in summer season. This examination indicates that the autumn is a rainy season that influence the most of the extreme events taking place in both areas; even though the event frequencies also vary from one year to another as well as the seasons.

Therefore, the years and the seasons of selected events carry great importance while trying to find the best configuration conditions for each region. One autumn and one summer events are selected for each of region so that beside orographical and climatic features, the seasonal effects on the study areas can also be included into the WRF sensitivity analysis.

Table 2.3.1 Numbers of extreme precipitation events recorded in Antalya Basin through the seasons between 2008 - 2017

	2008	2009	2010	2011	2012	2013	2014	2015	2016	2017	TOTAL
SPRING	0	0	0	3	2	0	1	1	0	7	14
SUMMER	1	1	0	0	0	1	1	2	1	5	12
AUTUMN	0	5	4	1	1	1	5	2	0	4	23
WINTER	0	3	4	0	3	1	1	1	0	0	13
SUM OF ALL											62

Table 2.3.2 Numbers of extreme precipitation events recorded in Eastern Black Sea Basin through the seasons between 2008 - 2017

	2008	2009	2010	2011	2012	2013	2014	2015	2016	2017	TOTAL
SPRING	1	2	2	0	0	2	0	4	0	2	13
SUMMER	6	13	4	3	4	3	3	4	4	1	45
AUTUMN	0	7	2	4	6	1	4	6	3	5	38
WINTER	0	1	1	0	0	1	0	0	0	1	4
SUM OF ALL											100

The hourly precipitation data of the last decade (2008.01.01 – 2017.12.31) are delivered from GDM for all available observation stations located in the study areas However, since this study only focuses on Antalya and Eastern Black Sea basins, the stations which are not located within the boundaries of these basins, are eliminated from the others.

After this step, 50 observation stations for Antalya, 109 observation stations for Eastern Black Sea have remained. Yet, still not all of these stations have the continuous dataset for each time step or the precipitation data percentage to be used in the validation process. Because of this reason, the quality control analysis has been applied on the stations. In quality control analysis, the stations which their means during the event period are equal to '0' and and also the stations which provide less than 95 % of valid data during the model run time (73 hours for this study) of that event were disqualified from the set. Thus, the analysis was not conducted by considering the stations' data for the whole 10 years period but investigating them based on their data quality during 3 days event period.

The selection process of observation station that are planned to use in Sensitivity Analysis is shown by **Figure 2.3.1**.

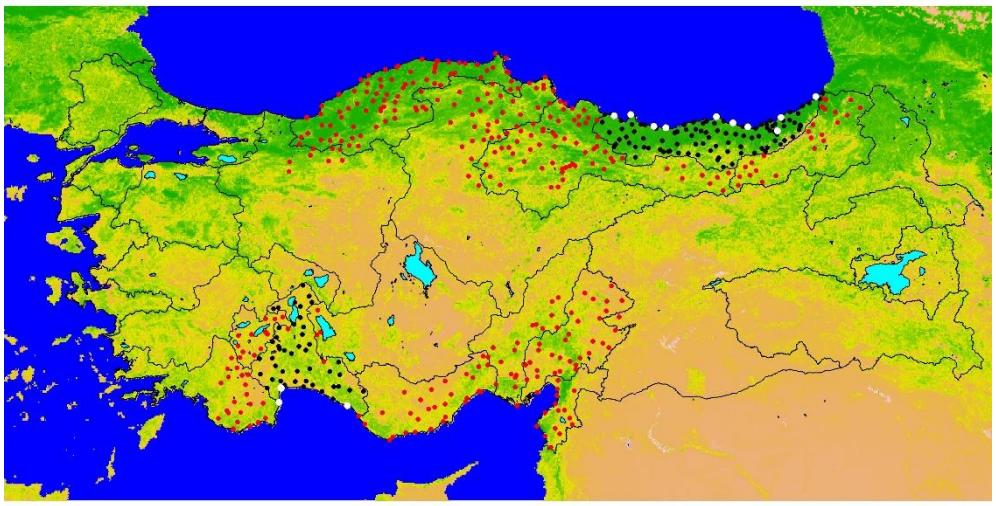

Figure 2.3.1 The location of 511 observation stations in Mediterranean and Black Sea regions represented on the map. Red points indicate the stations do not locate within the boundaries of study areas whereas white points refer the stations that could not pass the quality control analysis. Black points show the actual stations which can satisfy both conditions

In **Table 2.3.3** and **Table 2.3.4**, the possible event dates and the total number of stations survived from data quality control analysis for each event, additionally the ID number, coordinates and the peak precipitation amount of main station in which maximum hourly rain recorded during that event period, are represented for Mediterranean and Black Sea regions, respectively. The cumulative precipitation and the peak hour when maximum precipitation dropped over the region, are calculated based on 73 hours dataset period of each event date. Apart from it, the percentage of total precipitation stated under 'Precipitation Data (%)' column has prepared by using all avaliable rain data of the valid stations according to their event periods.

Table 2.3.3 The characteristic features of heavy precipitation events occured in Antalya Basin between 2008 - 2017

Event Date	Main Station's Number	Latitude (°)	Longitude (°)	Maximum Precipitation (mm)	Cumulative Precipitation (mm)	Maximum Precipitation Hour	Percentage of Precipitation (%)	Total Number of Stations to be used in Validation Study
20.09.2008	17927	37.0968	31.5952	37	91.6	69	12	14
6.01.2009	17310	36.5507	31.9803	33	60.6	47	24	13
13.02.2009	17302	36.8851	30.6828	48	144.4	37	32	14
20.09.2009	17310	36.5507	31.9803	23	30.2	40	3	14
13.10.2009	17310	36.5507	31.9803	43.8	120	56	18	14
14.10.2009	17310	36.5507	31.9803	43.8	120	32	20	14
3.12.2009	17895	36.9393	30.898	19	83.6	30	29	12
15.12.2009	17895	36.9393	30.898	43.6	118.8	50	29	13

Table 2.3.3 (cont'd) The characteristic features of heavy precipitation events occured in Antalya Basin between 2008 - 2017

18.12.2009	17310	36.5507	31.9803	6.8	41.6	38	20	13
28.12.2009	17302	36.8851	30.6828	42.8	151.6	46	16	14
23.01.2010	17954	36.7895	31.441	23.6	83.4	19	23	14
28.01.2010	17895	36.9393	30.898	13.8	186.6	51	27	14
7.02.2010	17302	36.8851	30.6828	12.6	128.8	49	36	13
24.02.2010	17954	36.7895	31.441	22	48	50	14	14
25.11.2010	17895	36.9393	30.898	22	59	7	26	13
10.12.2010	17927	37.0968	31.5952	12.2	109.4	43	45	3
14.12.2010	17927	37.0968	31.5952	11.6	184.8	39	45	3
16.12.2010	17927	37.0968	31.5952	15.2	272.8	48	53	4
2.04.2011	17310	36.5507	31.9803	37	141.4	54	30	12
3.04.2011	17310	36.5507	31.9803	37	152	30	39	13
12.06.2011	17302	36.8851	30.6828	15.6	24.2	63	9	13
9.10.2011	17927	37.0968	31.5952	56.8	162	47	35	7
1.01.2012	17954	36.7895	31.441	14.4	111.2	22	39	6
6.01.2012	17954	36.7895	31.441	13.8	109	69	44	14
10.01.2012	17302	36.8851	30.6828	18.2	57.2	53	49	13
18.04.2012	17826	38.1047	30.5577	7.4	18.6	38	9	13
19.05.2012	17954	36.7895	31.441	25.4	36.6	28	25	14
18.12.2012	17927	37.0968	31.5952	11.6	201.4	50	54	14
14.02.2013	17954	36.7895	31.441	43.2	65.6	64	20	26
17.07.2013	17240	37.7848	30.5679	23	44.8	35	4	26
25.11.2013	17895	36.9393	30.898	26.8	118.2	48	29	26

Table 2.3.3 (cont'd) The characteristic features of heavy precipitation events occured in Antalya Basin between 2008 - 2017

7.06.2014	18013	36.866	31.775	23.6	34.7	60	11	30
18.08.2014	18015	36.9703	30.4339	6.9	7.3	34	2	30
23.10.2014	17915	36.8604	31.0627	61	258.2	69	30	26
24.10.2014	17917	36.8886	31.2494	53.4	267	45	40	25
25.10.2014	17917	36.8886	31.2494	53.4	297.8	21	35	25
14.11.2014	18307	37.0987	30.6425	28	109.1	34	21	29
12.12.2014	18016	36.9501	30.6025	38.7	123.3	35	19	30
26.12.2014	18306	36.9517	31.1189	13.1	49.6	47	21	14
12.01.2015	18016	36.9501	30.6025	78.2	310.8	48	40	31
27.03.2015	18111	37.3792	30.8228	20.8	107.9	60	42	32
21.06.2015	18047	37.0468	31.7971	11.1	13.9	14	3	32
1.08.2015	17927	37.0968	31.5952	22.6	39	20	4	34
22.10.2015	17954	36.7895	31.441	78.2	236.2	47	29	35
23.10.2015	17954	36.7895	31.441	78.2	255.4	23	34	36
20.09.2016	18014	37.1046	30.9345	51	86.9	70	10	36
3.05.2017	17240	37.7848	30.5679	24.5	40.2	42	3	43
22.05.2017	18111	37.3792	30.8228	21.4	49	35	9	41
30.05.2017	17917	36.8886	31.2494	53.4	54	44	9	43
4.06.2017	17926	37.0565	30.191	24.4	27	59	5	44
5.06.2017	17926	37.0565	30.191	24.4	25.6	35	5	44
17.06.2017	18610	37.2478	31.7747	28	33.1	38	4	44
19.06.2017	17917	36.8886	31.2494	29.9	64.7	31	8	44
4.08.2017	18846	38.4558	31.0531	27	27.7	39	8	34

Table 2.3.3 (cont'd) The characteristic features of heavy precipitation events occured in Antalya Basin between 2008 - 2017

5.08.2017	18846	38.4558	31.0531	27	31.3	15	7	32
6.08.2017	18611	36.7886	32.2792	18.3	19.5	13	5	34
21.08.2017	18609	37.3017	30.1767	14	27.3	38	3	32
30.08.2017	18844	37.5242	31.1881	59.2	66.2	38	4	34
24.10.2017	17954	36.7895	31.441	31.3	131.7	47	20	41
25.10.2017	17954	36.7895	31.441	31.3	144.3	23	25	44
29.10.2017	17310	36.5507	31.9803	22.8	82.8	35	15	42
27.11.2017	17954	36.7895	31.441	29.6	163.2	68	28	43

Table 2.3.4 The characteristic features of heavy precipitation events occured in Eastern Black Sea Basin between 2008 - 2017

Event Date	**Main Station's Number**	**Latitude (°)**	**Longitude (°)**	**Maximum Precipitation (mm)**	**Cumulative Precipitation (mm)**	**Maximum Precipitation Hour**	**Percentage of Precipitation (%)**	**Total Number of Stations to be used in Validation Study**
29.05.2008	-	-	-	-	-	-	-	-
22.06.2008	-	-	-	-	-	-	-	-
30.06.2008	-	-	-	-	-	-	-	-
3.07.2008	-	-	-	-	-	-	-	-
8.07.2008	-	-	-	-	-	-	-	-
14.09.2008	-	-	-	-	-	-	-	-

Table 2.3.4 (cont'd) The characteristic features of heavy precipitation events occured in Eastern Black Sea Basin between 2008 - 2017

18.09.2008	-	-	-	-	-	-	-	-
6.06.2009	-	-	-	-	-	-	-	-
18.06.2009	-	-	-	-	-	-	-	-
30.06.2009	-	-	-	-	-	-	-	-
15.07.2009	-	-	-	-	-	-	-	-
17.07.2009	-	-	-	-	-	-	-	-
21.07.2009	-	-	-	-	-	-	-	-
22.07.2009	-	-	-	-	-	-	-	-
25.07.2009	-	-	-	-	-	-	-	-
27.07.2009	-	-	-	-	-	-	-	-
28.07.2009	-	-	-	-	-	-	-	-
8.08.2009	-	-	-	-	-	-	-	-
10.09.2009	-	-	-	-	-	-	-	-
16.09.2009	-	-	-	-	-	-	-	-
17.09.2009	-	-	-	-	-	-	-	-
20.09.2009	-	-	-	-	-	-	-	-
23.09.2009	17042	41.4065	41.433	23	154.8	35	43	9
28.09.2009	17624	41.143	37.293	14.4	50.8	29	43	9
6.10.2009	17040	41.04	40.5013	11.6	46.2	30	13	12
28.10.2009	17040	41.04	40.5013	14.4	24.8	54	19	11
30.10.2009	17628	41.1777	40.8993	19	141	26	64	11
20.11.2009	-	-	-	-	-	-	-	-
21.11.2009	-	-	-	-	-	-	-	-

Table 2.3.4 (cont'd) The characteristic features of heavy precipitation events occured in Eastern Black Sea Basin between 2008 - 2017

21.12.2009	17628	41.1777	40.8993	8.4	57.6	13	26	4
4.01.2010	17040	41.04	40.5013	7.2	41.2	57	22	11
16.06.2010	17042	41.4065	41.433	26	80.8	31	21	13
17.06.2010	17042	41.4065	41.433	26	88.8	7	26	14
14.07.2010	17040	41.04	40.5013	41.8	118	42	16	14
24.07.2010	17628	41.1777	40.8993	24.2	87.2	62	22	14
26.08.2010	17040	41.04	40.5013	39.8	200.8	43	14	14
14.09.2010	17042	41.4065	41.433	27.6	103.2	43	15	13
23.09.2010	17628	41.1777	40.8993	27.4	129.4	21	21	14
30.09.2010	17628	41.1777	40.8993	28.4	103	67	17	13
22.07.2011	-	-	-	-	-	-	-	-
12.08.2011	17033	40.9838	37.8858	23.2	62.2	68	23	14
18.08.2011	17033	40.9838	37.8858	31.8	168.4	52	14	14
24.09.2011	17040	41.04	40.5013	33.2	211	33	27	13
25.09.2011	17628	41.1777	40.8993	33.6	128	65	32	13
12.10.2011	17569	40.6193	40.4435	4.2	22	71	21	2
18.10.2011	-	-	-	-	-	-	-	-
25.06.2012	17088	40.4598	39.4653	2.6	8.6	43	6	3
29.07.2012	17040	41.04	40.5013	40.4	64.8	51	4	13
31.07.2012	17040	41.04	40.5013	40.4	88.6	3	7	13
6.08.2012	17624	41.143	37.293	34.4	180.8	31	20	14
22.09.2012	17042	41.4065	41.433	49.2	310.6	52	21	14
23.09.2012	17042	41.4065	41.433	49.2	306.8	28	18	14

Table 2.3.4 (cont'd) The characteristic features of heavy precipitation events occured in Eastern Black Sea Basin between 2008 - 2017

4.10.2012	17686	40.5592	38.4397	9.6	20.6	38	10	14
9.10.2012	17040	41.04	40.5013	22.6	67	36	21	14
11.10.2012	17040	41.04	40.5013	16.2	31.6	48	17	14
12.10.2012	17040	41.04	40.5013	16.2	30.4	24	15	14
16.03.2013	17626	41.0325	39.5615	7.2	28.6	46	28	23
18.06.2013	17769	41.0503	40.8992	41.8	79.2	65	22	23
19.06.2013	17769	41.0503	40.8992	41.8	80.2	41	17	24
10.07.2013	17624	41.143	37.293	62.6	117.2	46	6	35
31.08.2013	17628	41.1777	40.8993	26.8	67.8	47	24	35
21.09.2013	17772	41.1528	41.0703	35.2	123.6	43	44	33
3.10.2013	17624	41.143	37.293	23.6	212.8	62	49	34
22.06.2014	18558	40.9146	38.1942	61	139.7	44	19	64
4.08.2014	18566	40.98972	40.42889	75.5	118.6	43	9	66
5.08.2014	17040	41.04	40.5013	46	119.4	19	13	45
24.09.2014	18554	41.3166	41.2928	55.3	174.5	28	21	62
18.10.2014	17040	41.04	40.5013	22.4	93.4	54	47	63
31.10.2014	18567	41.2703	41.1556	45.4	180.4	43	40	63
21.11.2014	17689	41.0405	37.4878	32.2	109	52	29	65
21.03.2015	18562	40.8522	38.5714	15.6	48.8	54	41	65
16.05.2015	18222	40.5894	38.2789	12.1	15	43	4	49
23.05.2015	18227	40.5686	39.2989	8.7	15.5	38	2	62
19.06.2015	18531	40.8561	37.2486	61.2	64.9	38	11	65
25.06.2015	18531	40.8561	37.2486	20.2	40.2	18	30	62

Table 2.3.4 (cont'd) The characteristic features of heavy precipitation events occured in Eastern Black Sea Basin between 2008 - 2017

23.08.2015	18554	41.3166	41.2928	36.9	225.7	2	13	78
24.08.2015	18568	40.8711	40.5825	32.6	102.3	26	14	78
29.08.2015	17624	41.143	37.293	44.6	77.6	8	5	79
7.10.2015	18560	41.0175	38.9519	38.6	235	39	34	77
13.10.2015	17800	40.9898	40.6083	39.8	151.4	61	38	24
14.10.2015	17800	40.9898	40.6083	39.8	169.8	37	37	24
15.10.2015	17800	40.9898	40.6083	39.8	166.6	13	26	80
11.11.2015	17569	40.6193	40.4435	32.2	78.8	56	45	75
12.11.2015	17569	40.6193	40.4435	32.2	77	32	46	74
31.08.2016	18567	41.2703	41.1556	64.9	279.4	57	18	76
1.09.2016	18567	41.2703	41.1556	64.9	279.4	33	18	76
4.09.2016	17628	41.1777	40.8993	53.4	201.2	34	18	78
21.09.2016	18231	41.0328	39.2144	81.1	299.7	34	23	75
28.09.2016	18560	41.0175	38.9519	30.8	71	44	26	78
25.10.2016	17781	41.0603	40.7417	19.9	168.7	30	35	77
14.11.2016	19059	40.9758	41.1125	40.1	398	31	27	87
14.04.2017	17775	40.98353	40.33194	8.8	24.4	32	17	87
20.06.2017	19060	40.8039	39.9689	23	42.9	59	28	91
15.08.2017	18905	41.0408	40.7669	36.4	68.5	64	8	81
23.09.2017	18554	41.3166	41.2928	51.5	248.2	63	24	60
27.09.2017	18905	41.0408	40.7669	33	135.8	72	21	65
1.10.2017	17040	41.04	40.5013	20.9	74.8	55	30	76
14.10.2017	18554	41.3166	41.2928	11.3	46.9	49	10	91

Table 2.3.4 (cont'd) The characteristic features of heavy precipitation events occured in Eastern Black Sea Basin between 2008 - 2017

16.10.2017	18554	41.3166	41.2928	25.9	104.2	33	30	90
23.12.2017	18527	40.9756	37.9672	7.6	70.1	7	59	58

As mentioned before, the one of the aims is to observe how the best configuration options of the model forecasts have changed through the seasonal difference over the same region. According to this aim, one summer and one autumn time events have been decided to use for each study area in the sensitivity analysis under this thesis. Therefore, two events are selected from **Table 2.3.3** to be conducted on Mediterranean region and two others are also determined from **Table 2.3.4** for Eastern Black Sea region.

The selected event dates can be seen in **Table 2.3.5**. It should also be kept in mind that the value of peak precipitation amount as well as having the high percentage of precipitation data and the valid stations number during the event periods (established as 73 hours in this analysis) are important factors to look during the event dates selection process.

Table 2.3.5 Selected event dates of regions to be used in Sensitivity Analysis

Selected Events Dates	**Mediterranean**	**Eastern Black Sea**
Autumn Event Date	27.11.2017	14.11.2016
Summer Event Date	30.08.2017	21.09.2016

2.4 Weather Research and Forecasting Model – WRF

With a basic definition, WRF is a tool to observe the state of art atmospheric simulation system (Abualkishik, 2018). It is a mesoscale NWP model and like other NWPs, it is designed for use in atmospheric research and operational forecasting applications.

Since the model is mesoscale, it can work on a wide range scales, starting tens of meters to thousands of kilometers from the Earth surface. However, WRF is generally preferred to use on synoptic/regional studies and it is one of the most common models comparing to other NWP. Since WRF has strong software utilities' architecture and it is an open source model that has been supported and improved by its users all the time. Therefore, it is much flexible (Abualkishik, 2018).

WRF includes two dynamic cores: the Non-hydrostatic Mesoscale Model (NMM) (Janjic, 2003) core and the Advanced Research WRF (ARW) (Skamarock et al. 2005) core. Each of these cores has developed by different institutions and contains diverse dynamic solvers which is the key component of the model system for processing on map projections, grid staggering (Arawaka E grid for NMM, C grid for ARW), vertical coordinate systems (Hybrid sigma-pressure for NMM, Mass-based terrain-following for ARW) and data assimilation capabilities (Bernardet et al., 2006; Balseiro, 2008).

NMM is a product of the National Centers for Environmental Prediction (NCEP) and had been converted from Eta model physics whereas ARW is created by the National Center for Atmospheric Research (NCAR) and had been converted from MM5 model physics (Bernardet et al., 2006).

NMM and ARW are nonhydrostatic models and they both can be used for similar applications:

- Idealized simulations (e.g. LES, convection, baroclinic waves)
- Parameterization research

- Data assimilation research
- Forecast research
- Real-time NWP
- Regional climate research
- Coupled-model applications
- Teaching

(UCAR, 2019)

Yet, they have quite implication variety in their simulations. ARW has more complex dynamic and more physical settings than NMM. Additionally, some studies (Bernardet et al., 2006; Szunyogh, 2015; Szoke et.al., 2007) which have been conducted by both cores to compare their forecast performances, claim that the model works with the ARW core gives better predictions on multiple downscaling nestings because it offers more dynamic and physical options to shape the model atmospheric system. Therefore, it can be considered that the WRF ARW core usually gives better predictions for multiple nested domains.

By looking at these judgements, WRF ARW core (Version 4.0) has determined to be used in both sensitivity and SST analyses of this thesis.

2.5 Operating Mechanism of WRF Model

There are two main process systems for WRF model to follow. The first one is a pre-processing system which is called WPS and it includes three parts: geogrid, ungrib and metgrid (UCAR, 2019). Static and dynamic features of every event are introduced to the model within these parts. After these steps have completed, the WRF model system is ready to be used in further steps to produce forecasts. This portion of the model includes real.exe and wrf.exe programs to be run, respectively (UCAR, 2019)

.

WRF model runs via the setting options specified in the namelists by the user. The model has two seperate namelists: namelist.wps and namelist.input. The first one, namelist.wps, is required to adjust for pre-processing system of the model (UCAR, 2019). It includes sections for each of three programs of WPS. In each section, the model has been formed about how to combine input data with study area and in which format that the output files will be created. By the second namelist, namelist.input, all of the model parameters are defined into the model, including the previous sections of WPS namelist and many more such as the physics, dynamics, body and control (UCAR, 2019). This namelist is very crucial as the WRF model itself provides forecasts by directly using the directives in the namelist.input.

The purposes and the working mechanisms of the process programs under the model are explained below.

2.5.1 Geogrid.exe

Geogrid is the first step of WPS system to be run. In this step, the projection, the geographic coordinates and the grid size (or the resolution) of study areas (domain) that are wished to be work by the model, are defined (UCAR, 2019).

Since the WRF model can be run for multiple small areas (nests) under a big common region (parent domain), it is very important to define the numbers of these nests correctly into the model namelists. According to this, the example **Figure 2.4.1** shows how the model domains are numbered in order to be specified in the namelists.

Let's assume, the locations of all domains are shown in **Figure 2.4.1**. As it can be observed from the illustration here, the biggest common domain among these options is "d01" and it can be considered as the 'parent domain' of the model but not for all nests because the parent domain of each nests indicates the one size bigger domain option (Carlos F. Balseiro, 2008; Davies, 2014).

In **Figure 2.4.1**, the colorful arrows pointing out from each nest refer that nest's parent domain. Based on this, while the parent domain of d02 and d04 is d01, the one size bigger domain of d03 is d02. It should be also kept in mind that the nests must be completely smaller than their parent domains and fit in it perfectly. None of the nests or the parent domains can intersect with each other.

.

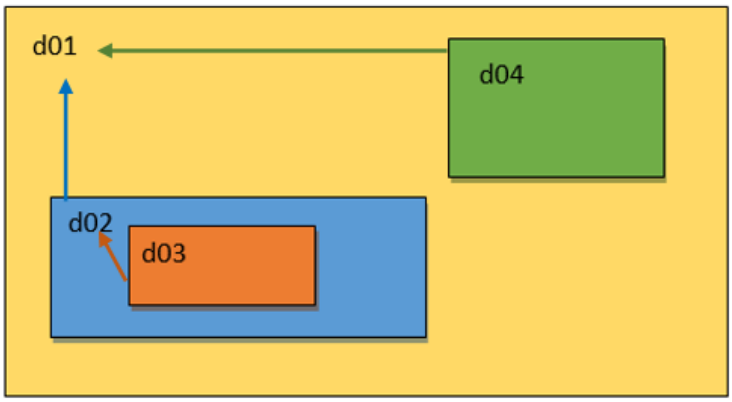

Figure 2.4.1 The illustration of the relation among the nests and their parent domains. "d" letter before the numbers indicate the "domain" word

Therefore, the parent_id section in both namelists (namelist.wps and namelist.input) are filled with each parent domain number based on this perspective (**Figure 2.4.2**).

The first column refers to the main parent domain so its ID is 1 but rest of columns represent the nests and their parent domains' IDs with respect to **Figure 2.4.1**.

	d01	**d02**	**d03**	**d04**
parent_id =	1,	1,	2,	1,

Figure 2.4.2 An example to how to fill the parent_id section in the namelists of WRF model. "d" letter before the numbers indicate the "domain" word

After geogrid process, as the static data (do not change depending on time), the orographic features of the study areas are builded up in the model configuration.

2.5.2 Ungrib.exe

As the second step of WPS system, ungrib program is highly important because the initial boundary conditions of the model are determined here (UCAR, 2019). WRF model has the starting and ending dates to make run in between that period and it also needs meteorological condition file of these days to feed its forecasts with the data provided from this source by specific interval hours so that the accuracy of the predictions have been improved. That meteorological dataset which contains the atmospheric data of each day of the run period is given to the model by ungrib program. Hence, ungrib.exe open the input meterological dataset and make it possible for the model to read it.

2.5.3 Metgrid.exe

The last program that is run under WPS, is metgrid.exe. So far, the static (orographical features from geogrid) and dynamic (meteorological input dataset from ungrib) data have given into the WRF model. Yet, these are not combined over the domain area. Therefore, these two components are needed to be match to be able to mimic real atmospheric conditions. At this point, metgrid does that job by horizontally interpolating (UCAR, 2019) the input data over the domain area. It should be kept in mind that the metgrid program produces an output per by every interval hour for each domain.

2.5.4 Real.exe

After all WPS steps are completed, WRF process system is ready to read and differenciate the parameters as initial and boundary condition files. Initial condition file includes constant atmospheric and orographic variables provided by the first two steps of WPS whereas the boundary condition file is filled with the variable that will change through the time (Carlos F. Balseiro, 2008).

This step is applied for wrf.exe program so that it can easily read the inputs and make the WRF run (UCAR, 2019).

2.5.5 Wrf.exe

Finally the WRF model is ready to run. Since everything (horizontally and vertically) has already arranged before, the model now can produce the forecasts for the specified run period by wrf.exe program (UCAR, 2019).

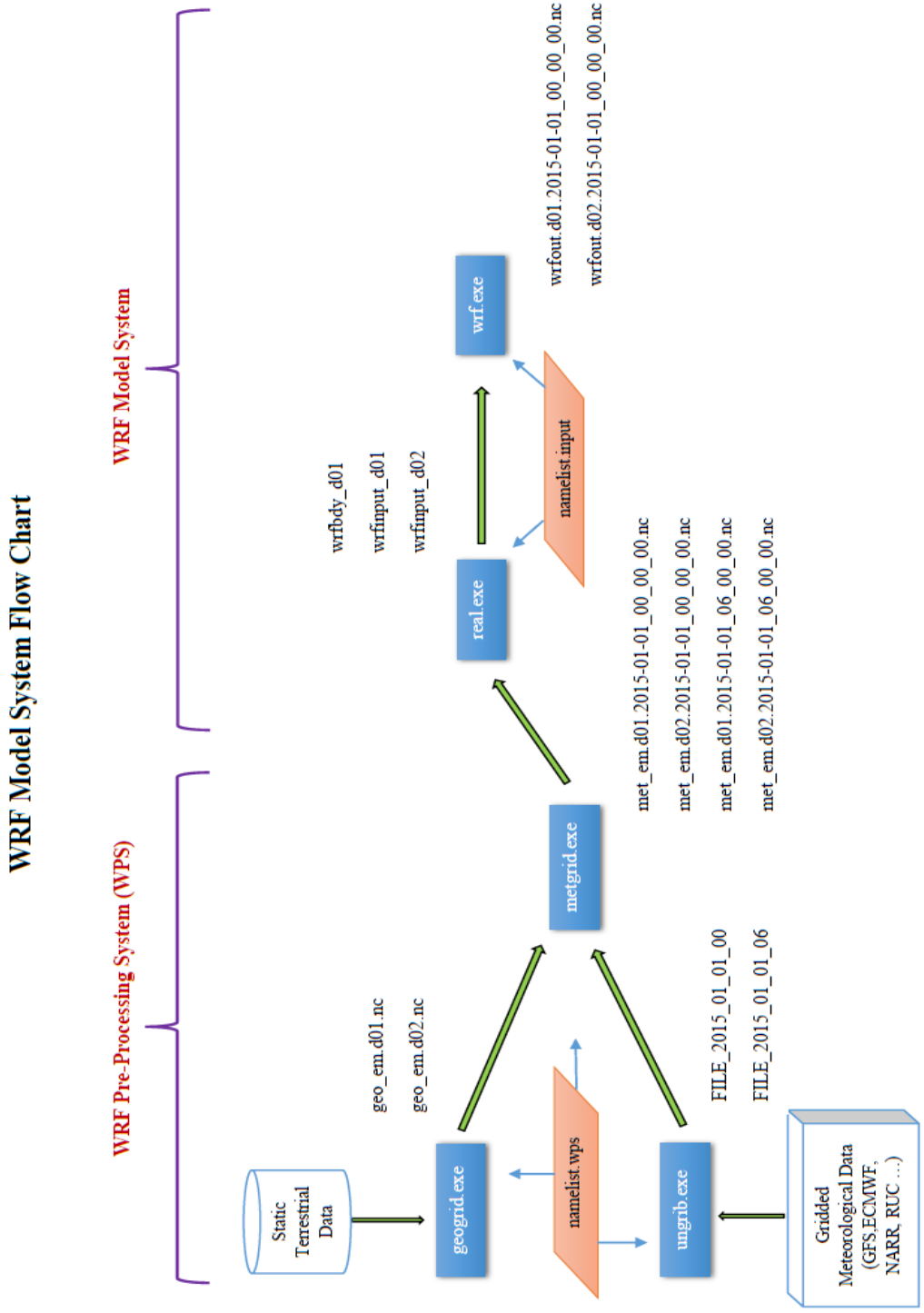

Figure 2.4.1 Flowchart of WRF Model System

(UCAR, 2019)

CHAPTER 3

MODEL CONFIGURATION ARRANGEMENTS

PART I - Sensitivity Analysis

Through the reference studies (Argüeso et al., 2011; Gelpi et al., 2016; Zeyaeyan et al., 2017; Yao et al., 2017; Sikder et al., 2016; Jee & Kim, 2017) that are conducted on similar climatic regions, it has found that the microphysics, cumulus and planetary boundary layer (PBL) are the most powerful physical components of the atmospheric system for precipitation forecasts in NWP models. Therefore, only these three parameters of physics are included into the sensitivity analysis.

The input meteorological dataset, as mentioned before, is also another essential parameter for WRF model predictions because the model takes the initial boundary conditions by using this dataset. Normally, WRF generates prediction for each hour from its calculated simulations but first the model needs to know the initial states of atmosphere as the starting point. The input meteorological dataset supplies this information to the model. However after the initial hour, the model keeps to update its atmospheric boundary conditions by using this dataset for every time interval. The time interval is determined via the user and it is usually preferred as 3 or 6 hours (UCAR, 2019).

With respect to the conducted studies under this thesis, the interval time to update boundaires has been determined as 6 hours (21600 seconds). This period is valid for all forecasts that will run by both the sensitivity and SST analyses.

As the model redefines the boundary conditions from this dataset during the run period, that actually helps to its prediction profile to be kept through the real aspect of the event so the accuracy has enhanced.

The selections of physical parameter schemes and the meteorological datasets which have been decided to use through the sensitivity analysis of heavy precipitation events occured on Mediterranean and Eastern Black Sea regions, are explained in the following pages.

3.1 Selection of Input Datasets

The Global Forecast System (GFS) (Peng, 2014a,b) and the ERA5 Reanalysis (ERA5) (ECMWF, 2020) datasets are selected for the meteorological data sources to be used in the WRF model sensitivity analysis of this thesis.

The GFS is provided under the same named model (The Global Forecast System model) product via the National Centers for Environmental Prediction (NCEP). Since it is a coupled model, it combines four seperate models: an atmosphere model, an ocean model, a land/soil model, and a sea ice model (Iracema et al., 2014). The coupled models are important to describe an accurate picture of weather conditions because they mimic the real Earth system.

Additionally, because they compose the four seperate models, the GFS dataset includes all the seperate models' variables together. However, the specific feature of this dataset to be selected to use in the current study, is containing only the forecasts results. This indicates that the outcome of the previous day forecast has been entered as the input meteorological data for the next forecast. The GFS does not include observational data (Iracema et al., 2014). In this sense, it may be said that the GFS dataset actually shows the model forecast's performance by using its resulted prediction as the new input dataset of the coming model run. The GFS dataset can be found out up to 16 days in the future. The horizontal resolution or the grid space in this source's data is around 28 kilometers.

The ERA5 Reanalysis, on the other hand, is a product of European Centre for Medium – Range Weather Forecast (ECMWF). It is also a coupled model that contains the multiple variables on the atmospheric, oceanic, land/soil models

(Hersbach et al., 2020). Since this is a reanalysis product, it contains both the forecast and the observation data in its sets.

Through the ERA5 process (Hersbach et al., 2020), the forecast has been run for 12 hours. Here, 12 hours refer the assimilation window (**Figure 3.1.1**). This time period has been decided, is because according to the researchers the optimal forecast range that gives the most accurate prediction is 12 hours. At the end of this time period, the first forecast has been produced. Then, the observation stations' data on the same interval are collected and added to the system. By adjusting the previous forecast with the real observational data, the corrected forecast can be established.

After this step, the forecast re-run one more time. That's why, this meteorological input data type is called 'reanalysis'. By looking at the difference between previous and corrected forecasts on the y axis of this graph, once again the importance of the input dataset on the initial boundary conditions can be observed clearly. The ERA5 Reanalysis dataset has been provided for 137 levels from the surface up to a height of 80 km and like GFS, the horizontal resolution or the grid space in this source's data is around 28 – 30 kilometers.

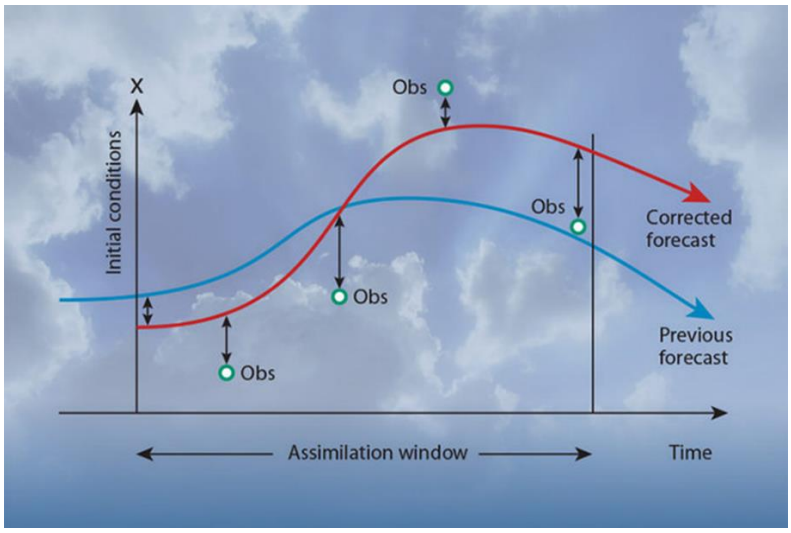

Figure 3.1.1 The mechanism of how ERA5 Reanalysis dataset has obtained by ECMWF (Hersbach et al., 2020)

As the ERA5 Reanalysis data combines the reality with the forecast and make the corrected predictions, it is expected to give more accurate results for the past time event forecasts and this is the main reason why it has been included into the planned sensitivity analysis. Correspondingly, there is no chance for a reanalysis data provided for the future predictions because it needs the observation records to continue in time. Therefore, the ERA5 Reanalysis data can be valid or updated to the users within 5 days of real time, not any further.

To sum up, the GFS and the ERA5 Reanalysis meteorological data sources are selected due to the presence of the observational data and the methods of creating these datasets.

3.2 Selection of Parameterization Schemes

For this study, the parameters that are known to be more effective on rainfall occurence are selected to be used in the sensitivity analysis so that their levels of impact can be analysed. Based on this perspective, the analysis has been aimed to conduct for only cumulus, microphysics and planetary boundary layer (PBL) parameterizations. Therefore, while various approachs (schemes) to be used in the calculations of these physics are selected for the sensitivity analysis, only one approach (scheme) has determined for the other physical components in the model configurations.

3.2.1 Cumulus Parameterization

In atmospheric system, all physical components work together. For instance, according to Arawaka's report (Arakawa, 2004), the cloud formation is directly related with the momentum and heat fluxes that are carried up and down through the planetary boundary layer (PBL). Since these fluxes are formed by the emission,

absorption and the reflection of radiation in atmosphere – oceans coupling, the solar energy can also be considered as one of the main components of whole the cloud system (Arakawa, 2004; Stensrud, 2012).

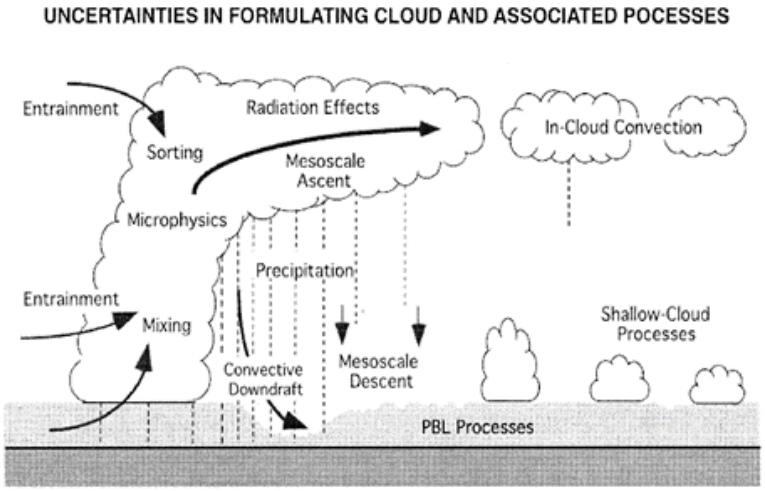

Figure 3.2.1 General Representation of the clouds and their related processes (Arakawa, 2004)

Based on the impact size and power of these components, some synoptic and mesoscale circulations such as cyclones, tornadoes, thunderstorms (Stensrud, 2012) can be generated. By this way, the cloud system influences on not only the dynamic atmospheric system but also the hydrological cycle of the World (Arakawa, 2004).

There are two types of precipitation: convective and non-convective. The convective precipitation is produced by the cumulus clouds whereas non-convective precipitation has provided from microphysics processes. That's why, it is critical to include these two parameters into sensitivity analysis of WRF model, especially if this study has conducted to observe the forecast performance efficiency for the intense precipitation events.

Due to various physical - chemical interactions within the cumulus and the surrounding atmosphere, the size and height of cumulus clouds can change a lot. This also shapes the type of cumulus clouds (deep or shallow) and their effects on the atmosphere and the land. However, that does not mean that the same type of clouds also behaves exactly the same. Since the cumulus behaviours are formed by the orographic and atmospheric features (temperature, wind, humidity etc.) of the region they accumulated over. Therefore, as represented on **Figure 3.2.2** The need for cumulus parameterization, even in a single location, the cumulus clouds depths and impacts may vary (Jakop & Miller, 2003).

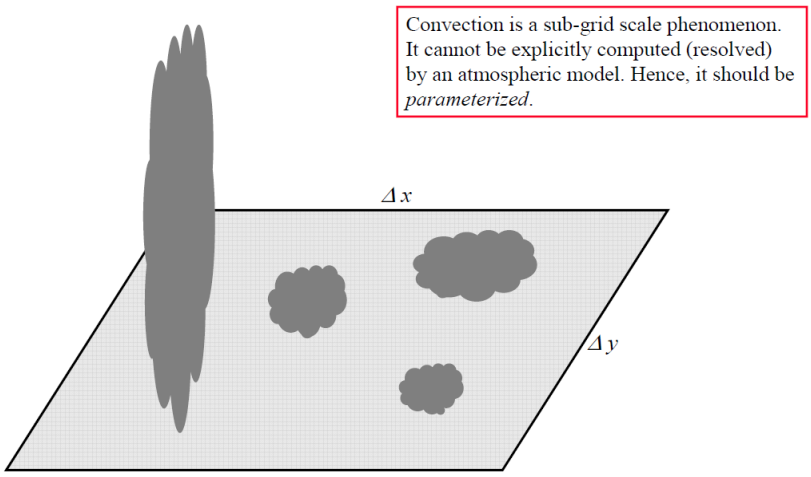

Figure 3.2.2 The need for cumulus parameterization

(Mironov, 2015)

The convection is a sub-grid process so to be able to observe the collective effects of these cluster clouds, the cumulus parameterization can be used in the numerical weather prediction models. As the objective of cumulus parameterization is to obtain a 'closed system' for predicting weather and climate (Stensrud, 2012). Taking cumulus clouds as a cluster, is important to built that closed system and to produce more accurate convective precipitation especially for the investigation of large grid size models by using sub-grid scales (Parker, 2002).

The reason why cumulus parameterization is much needed in larger grids comparing to small grid sizes, is because the surface fluxes that are mostly effective on sub-grid cumulus cloud formation, may miscalculated and become unstable for the larger scale models but with the cumulus parameterization these grids can be downsized to the sub-grid scale so the accuracy of the model simulation has enhanced.

Here, the closure assumption carries great importance for the cumulus parameterization as it offers a relation or describes the statistical interactions between the sub-grid-scale convection and the large scale model predicted variables such as the Convective Available Potential Energy (CAPE), moisture content, boundary layer characteristic of the ensemble cumulus clouds (Stensrud, 2012; Suhas & Zhang, 1955). The problem with the closure assumption is choosing the right type of parameterization and closure variable that can actually match with the current convection. Thus, the relation between the closure variable and the convection is essential in cumulus parameterization.

There are many different approachs (schemes) to calculate the cumulus physics of atmospheric system in the WRF model. These schemes have various triggering functions to active and sustain the convection in their system. Since by using triggering functions, the temperature, momentum and the moisture profiles of atmospheric layers has redistributed throughout the vertical grid columns of model. This process continues until the convection inside the column has deactivated (Pennelly, et.al, 2014). Some of the common triggering functions are stated as follows:

- **Convective Available Potential Energy (CAPE):** "the maximum energy available to an ascending air parcel" (represents the deep layer existance). The energy which is available to lead the way for convection.

- **Cloud Depth:** help to determine the possible convection type; shallow or deep

- **Convective Inhibition (CIN):** "the energy necessary to lift a parcel pseudoadiabatically to its level of free convection" (low level sub-cloud convergence)

- **Moist Convection:** occurs when the warm air rises and the excess water vapor in the air parcel condenses to form a cloud

- **Sub-grid-scale convection:** comprising one or more clouds within a grid box

(Stensrud, 2012)

Most of the time, the model builds up its cloud system and decides the time period and the power of cumulus activity based on these variables by using the cumulus parameterization schemes. Especially, the CAPE, the CIN and the cloud depth are quite important decision makers for shaping this system (Zheng, et.al, 2016).

According to the article of D.J. Parker (2002), both the CAPE and CIN are two primary thermodynamic parameters of the deep convection systems. While the CAPE indicates how the upward winds will be strong if the convective storms develops, the CIN refers the minimum lifting energy to be overcomed (to reach its level of free convection, LFC) so the deep convection has activated (Suhas & Zhang, 1955). Therefore, the CIN usually acts like a starting point of a convective system to overcome its inhibition level and pass the control to the CAPE in order to grow the atmospheric system from the surface based storms to larger deep scale storms (Parker, 2002).

For instance, some cumulus schemes -the mass fluxes type schemes- use the CAPE as a triggering parameter of the convection (Gerard et al., 2013) as it helps to rearrange the mass flux gradients such as the concentration, moisture, heat or momentum between the surface and the cumulus clouds, breaks the stability of atmosphere and brings convective precipitation into the model predictions. Thus, it

feeds the convection activity (deep storms) until there is not much of it left in the system

Generally two types of cumulus parameterization are used in the numerical weather models: adjustment and mass flux. Mass flux parameterization calculates the cumulus mass flux profiles and termodynamic variables whereas the adjustment type of parameterization, as name indicates, adjusts the modeled resolved heat and moisture fluxes based on pre-specified profiles (Gerard et al., 2013).

Even though, the WRF model offers many cumulus parameterization options to the users, only 3 of them are decided to use in the sensitivity analysis of model physics in the scope of this thesis. These are Kain-Fritsch (KFS) (Kain, 2004) and Betts-Miller-Janjic (BMJ) (Betts et.al, 1986a,b) and Grell-Freitas (GFES) (Grell et.al, 2014). These schemes have continuously improved and commonly used for cumulus parameterization. However, among many, these three schemes are selected based on their calculation assumptions and their performances on some reference studies which are also conducted for similar climate patterns with Mediterrean and Eastern Black Sea regions.

The Kain – Fritsch (KFS) scheme uses the mass fluxes assumption for its deep cumulus calculations. The KFS determines the cumulus depth (shallow or deep) based on the Lifting Condensation Level *(*LCL*)*. If the LCL as the updraft source layer, determined from mixing vertically-adjacent layers over the 60 hPa nearest the ground is colder than the environmental LCL temperature then it descents, if it is warmer then it ascents (Stensrud, 2012).

Here, the essential point for KFS scheme to decide the minimum cloud depth where the vertical velocity remains positive whether the cloud is a shallow or deep cumulus. Based on this approach, if the vertical velocity remains positive over a cloud depth with 2-4 km or less, shallow cumulus (the LCL is colder than the environmental LCL temperature) but if this depth bigger than 4 km (the LCL is warmer than the environmental LCL temperature), deep cumulus has activated in KFS parameterization (Stensrud, 2012). Yet, to be able to trigger the shallow cumulus, still the ascending parcel must have an LCL temperature warmer than its environment.

Since the KFS is a mass fluxes scheme, for both shallow and deep cumulus cases, the scheme modifies the temperature, moisture and the mixing ratios along the vertical layers. Especially in deep cumulus, all grid-scale mass fluxes as well as the entrainment and detrainment components of the cloud system are considered and their mass distributions are vertically readjusted. This process continues until 90% of the CAPE is removed from the system. Unless the deep convection has not activated, only than the shallow convection has activated (Stensrud, 2012).

The Betts Miller Janjic (BMJ) on the other hand, is a adjustment scheme which means it uses a reference profile to modify the temperature and moisture fluxes (separate for T and q) through the vertical layers (Stensrud, 2012; Jeworrek et al., 2019). In regards to this approach, the model identifies the most unstable and has non-zero CAPE parcel in at least 200 hPa pressure levels. Based on this selected parcel's pressure and CAPE energy, the scheme determines the levels that this parcel's ascent in the air, including the cloud base and top. Then, the most appropiate path to follow for ascending the air parcel has been decided among many other possibilities. This path is called the 'reference profile' to be used in BMJ scheme and it generally produced from the field campaign observations in tropical convections (Stensrud, 2012). After the profile has been determined, the vertical traces of temperature and moisture in the model are arranged depending on the reference

point. While the traces are adjusted, their vertical entalpy do not change through the different pressure levels.

Like the KFS scheme, the BMJ has also some conditions to trigger the scheme activation. In the KFS, the scheme decides the type of cumulus (shallow or deep) by looking at the cloud depth distance (3-4 km from the surface). Here in the BMJ, the cloud depth determined in terms of pressure. If the cloud depth over the selected point on the reference profile, is less than 200 hPa (Stensrud, 2012), the shallow cumulus becomes activated in the scheme. However, if it is more than 200 hPa then the deep cumulus convection is triggered in the system. The enthalpy of the temperature and the moisture, conserve for both shallow and deep convections in the BMJ's approach.

The Grell-Freitas (GFES) is very similar to the Kain – Fristch (KFS) approach as it also uses the mass flux assumption in its scheme calculations (Jeworrek et al., 2019). Yet, the GFES scheme can make a smooth transition from the sub-grid cumulus scale for convective precipitation to cloud-resolving microphysic scales for non-convective precipitation (UCAR, 2019). Therefore, the GFES has more scale aware assumption comparing to the KFS scheme.

Regarding to some of the similar researches, the KFS and the GFES schemes and their performances are considered as better to obtain convective heavy precipitation events in which the rain has suddenly formed and vanished, comparing to the BMJ. This outcome has been reached by the idea of the cloud base usually becomes dry and stable within the KFS and the GFES schemes after the precipitation falls out. Yet, in BMJ approach, not all moisture levels can be removed at the cloud base with convective precipitation as to be able to continue the deep convection (Jeworrek et al., 2019), there should be some moisture remained at the cloud base level. That's why, the BMJ can be considered as the better cumulus scheme performer for the synoptic / frontal precipitation events (Jeworrek et al., 2019).

However, since there is not a certain answer to give about their performances, three of them are wished to include into this sensitivity analysis for both Mediterrean and Eastern Black Sea regions.

3.2.2 Microphysics Parameterization

In weather forecasting models, as mentioned before, all physical parameters are connected to each other. Among these parameters, the microphysics is quite important component of the cloud system (Sonkaew, et.al 2016).

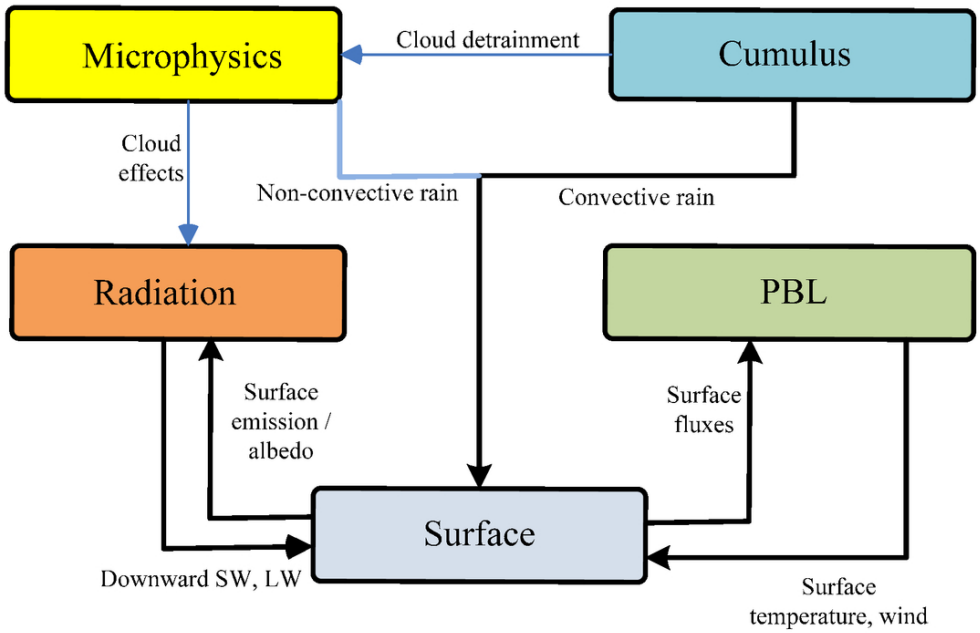

Figure 3.2.3 Main physical components of the atmospheric system and their relations with each other

(Jarno, et.al 2014)

The microphysics processes have control on the cloud formation as they are dealed with one of the essential liquid presence for the world's mechanism to maintain: 'moisture' (Zheng, et.al, 2016).

Moisture or moist processes can change the phase of water species. Hence, the water vapor, cloud droplets, rain droplets, snow, ice crystals, graupel and hail are some of the types of microphysical species that are worked with the numerical weather prediction models (Eltahan, et.al, 2017). The microphysics investigates the physical phase processes to identify the shape, size and mixing ratio of the water species by looking at the latent heat exchanges in the system (Stensrud et.al,2010).

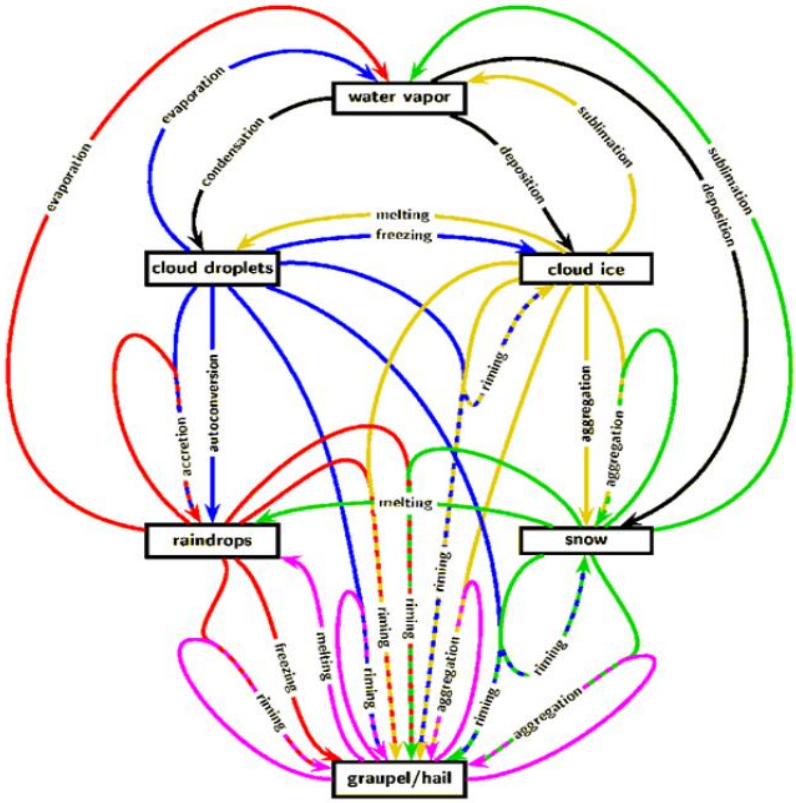

Figure 3.2.4 Water species and the cycles among them. The black lines indicate loss of water vapor; red lines indicate loss of rain drops; blue lines indicate loss of cloud droplets; yellow lines indicate loss of cloud ice; green lines indicate loss of snow; and purple lines indicate loss of graupel/hail

(Stensrud et.al,2010)

That's why, the microphysics basically represents the phase, amount and mixing ratios of these species in the cloud. Additionally, it is useful to observe the interaction between the other components of the cloud system. For instance, as it can be observed from **Figure 3.2.3**, the detrainment (some air drawn out from the cloud to surrondings) of the cumulus cloud changes all microphysics calculations. As the various water species's mixing ratios and their amounts are directly affected via any change in the cumulus so they are needed to be determined again. Based on these calculations, the cloud depth and its stability can be identified.

While the depth of the cloud (the deepness) are growing, the penetration of the radiation that comes from the sun through the cloud becomes harder (Eltahan & Magooda, 2017). It mainly reflects and since this situation affects the total radiation budget reached the Earth surface, the surface fluxes also change. Depending on them, the vertical turbulent mixing so the flux exchanges in the planetary boundary layer (PBL) have activated. As a result of all, this will influence the cloud formation first and then the other physical parameters all over again.

Based on these facts, it can be easily said that microphysics plays the key role in the weather and the climate system as well as the hydrological cycle (Eltahan & Magooda, 2017). Additionally, it should be kept in mind that the non-convective precipitation in forecasting models are produced from the microphysical dynamics. Therefore, the microphysic parameterization is essential in the sensitivity analysis of atmospheric physics.

The microphysics schemes that will be included to be tested in the sensitivity analysis, have been decided by their working principles and some similar reference studies. Through this perspective, the Kessler (KS) (Kessler, 1995), Eta / Ferrier (ES) (Ferrier et.al, 2002), Lin et al. / WRF Single Moment 6 (WSM6) (Hong et.al, 2006) and Aerosol Aware Thompson (AATS) (Thompson, 2014) schemes are selected for the sensivity analysis of heavy rainfall events occured in Mediterranean and Eastern Black Sea regions of Turkey.

However, these schemes are not needed to be used all microphysical species in their parameterizations calculations. While some of them focus on the liquid and gas form of the water like rain droplets, cloud droplets, water vapor and use only their processes (e.g. Kessler scheme), others may combine the liquid, gas and frozen microphysical species together such as Eta and WSM6 (Stensrud et.al,2010). This variability can be seen in **Figure 3.2.5**. The particle distributions of the water species are taken as the picture of the air circulation of that region.

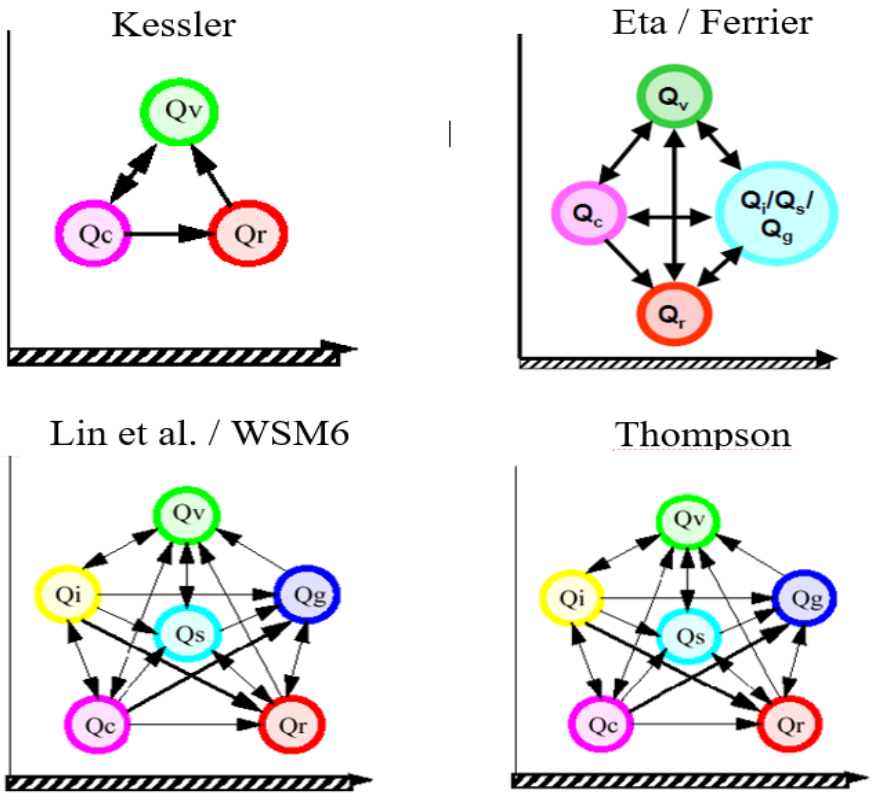

Figure 3.2.5 Microphysics Parameterization Schemes. Mixing ratios Qv (water vapor), Qc (cloud water), Qi (cloud ice), Qr (rain), Qs (snow) and Qg (graupel) are modeled

(Sonkaew, et.al 2016)

The Thompson scheme's representation on **Figure 3.2.5**, refers the Aerosol Aware Thompson (AATS). Since their working principles are quite similar, the Thompson scheme mixing ratios of water species and their relations have been shown on this figure. The AATS is a double moment scheme which means it can predict both the mixing ratios and the total number of concentration of at least one specie whereas the single moment schemes such as the Kessler or the WSM6, can not make any prediction about the total concentration of a specie but calculate only the mixing ratios. This condition makes the double moment schemes more flexible and capable for giving the accurate microphysical process simulation in model predictions.

Since the double moment parameterization scheme can predict the maximum total number of concentration (N_0) of at least one specie, it can give the particle size

distribution for that specie (Stensrud et.al,2010). The more microphysical specie concentrations are predicted, the more realistic particle size's range can be supplied. Therefore, it is a benefit for the cloud droplets distribution determination.

Another advantage for the double moment schemes is the sedimentation or the size – sorting. Because the particle sizes can be determined from the maximum the total number of concentration for a diameter of zero (N_0), the relation between those particle sizes and their fall speeds can be useful for the model to represent the sedimentation state of the atmosphere (Stensrud et.al,2010; Hong et al, 2004). This implies that the larger particles fall faster than the small size particles. Therefore, working on a climate where the snow, hail, graupel and rimed iced are commonly observed, the double moment schemes are considered better in terms of giving the closest forecast results to the reality because they are more sensitive about the microphysical particle sizes and distribution.

Yet both of the types are not perfect. The single moment schemes are relatively much more efficient and easy to compute as the double moment schemes are very sensitivite to the particle sizes which creates uncertanity on deciding the concentration. Apart from this, the double moment schemes can adopt different environments but still the validation is harder than the single moment (Stensrud, 2010; Kaufeld, 2010).

Moreover to the approach differences between these schemes were mentioned above and also shown in **Figure 3.2.5**, each sheme uses various water species and their relations in its calculations. That's why, using the microphysic parameterization scheme that is coherent with the climate of working region, may create a significant diversity among the schemes' performances in the model forecasts.

For instance, if the climate on the study region (the domain) has cold and wet winters, the Kessler microphysics scheme may not be considered as suitable to run for the weather forecast of that region during the winter season. Since the Kessler approach, includes only the liquid (Qc, Qr) and vapor phase (Qv) of the water in its calculations whereas the rest three selected schemes (Eta, WSM6, AATS) take snow, graupel,

hail or ice forms of the water into consideration for the parameterization (Stensrud et.al,2010). Therefore, it may expect to obtain more accurate non-convective precipitation results from the models working with those three schemes.

In the scope of this study, the Aerosol Aware Thompson (AATS) is defined as the fourth option to try in the sensitivity analysis of WRF model. The main reason of this choice actually lies under the name itself. This scheme makes the calculations by considering the potential aerosols in the air (UCAR, 2019). Being aware of the aerosols is important because the aerosol particles act as the cloud condensation nuclei (CCN) which means they create a base for the water vapor to condensate to the liquid phase (Lim, 2010). As the water vapor condensates the liquid and stucks onto these particles, the cloud droplets' sizes that should be naturally formed in the cloud is getting smaller. This leads them to collide and coalescence less and eventually can not provide enough rain droplets which is also known as precipitation (Song & Zhang, 2011). Hence, if more aerosol particles exist in the cloud, the cloud becomes more dry and warm, the precipitation amount decreases and because of the high number of particles, the radiation has scattered more through the clouds. The AATS scheme includes the water and ice-friendly aerosols while shaping the atmospheric state (UCAR, 2019). The initial and the boundary conditions of the model has builted by considering the aerosol variables.

Consequently, having both single and double moment schemes as well as using multiple working mechanisms in calculations, offer great opportunity to observe which microphysical scheme/s contribute to the model for giving the most accurate predictions on each region.

3.2.3 Planetary Boundary Layer Parameterization

For weather forecasting models, not just the cumulus clouds or their chemistry but also the interaction between the atmosphere and the Earth surface is crucial to consider. From this perspective, planetary boundary layer (PBL) becomes a must

parameter which represents the turbulent vertical mixing of thermodynamic and kinematic profiles such as the heat, momentum or atmospheric constituents like moisture (Hu et.al, 2010). To be able to parameterize these fluxes through the atmosphere, various PBL schemes are used and their boundaries are generally assumed up to three kilometers from Earth surface (Cohen et.al, 2015).

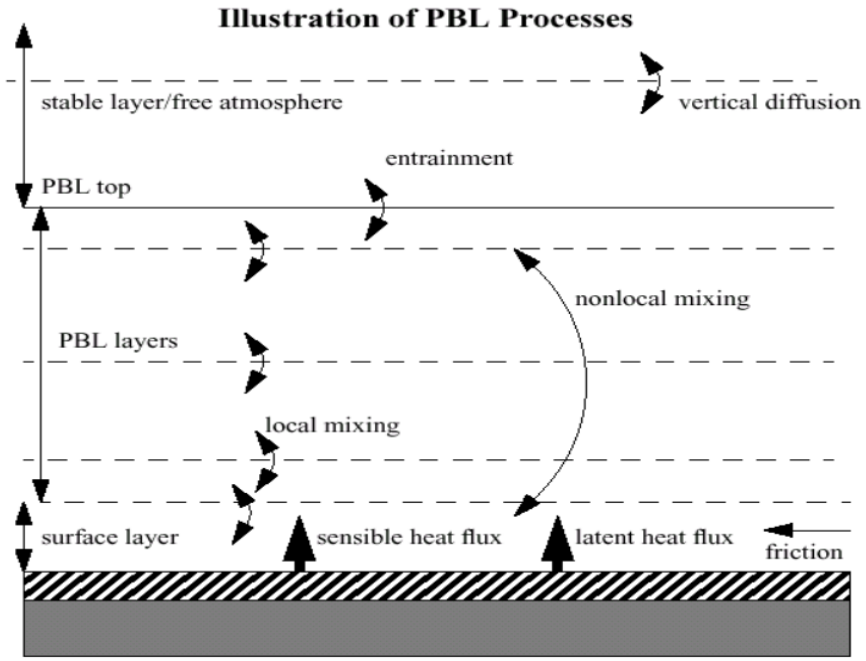

Figure 3.2.6 General Representation of the PBL Interactions and Related Processes (Dudhia, n.d.)

Although the goal here is providing the vertical turbulent mixing fluids (heat or moisture) by eddy fluxes at the turbulent boundary layers because each scheme adopts a difference assumption, their performances on every model domain will be different (Cohen et.al, 2015).

Planet boundary layer has two types of schemes: local and non-local. The difference between these approaches is, as seen in **Figure 3.2.6**, the interaction between the layers. While the local schemes take the adjacent vertical levels solely, the non-local

schemes can reach to much more deeper layers in PBL where the vertical turbulent mixing is also estimated among the distant levels (Cohen, et.al, 2015).

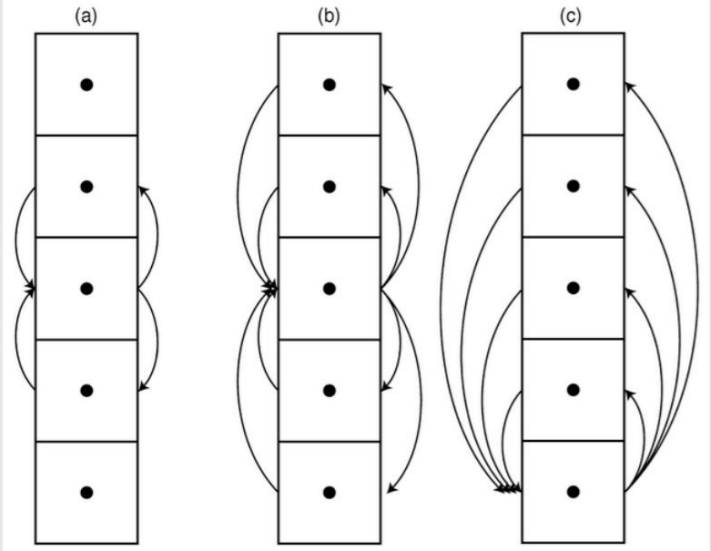

Figure 3.2.7 Representation of the mechanics of the local and non-local closures a) interactions in local closures b) and c) interactions in non-local closures

(Collins, 2016)

The common PBL models are Mellor- Yamada-Janjic (MYJ) (Mellor et.al, 1982) by using the local approach, whereas Yonsei University (YSU) (Hong et al, 2006b) and the asymmetric convective model, Version 2 (ACM2) (Pleim, 2007a) are the non-local model types. Actually, ACM2 is a hybrid model that combines a transilient term with local mixing (Hu et.al, 2010).

In planetary boundary layer, since the turbulent motions of the momentum, heat or moisture are provided with eddies (Tagesson, 2012), there is direct dependence between the diffusivity coefficients of eddies and the local instability (or stability) at that level of air (Jansirani, et.al, 2016). Therefore, the model equations use K (the eddy-diffusivity for heat and eddy-viscosity for momentum) in their formulas to represent the turbulent movements (the K theory) where the liquid can be traced and

observed through the distribution of this turbulence along the mixing length (Jansirani et.al, 2016; Tagesson, 2012). At the end, they illustrate the state of air whether it is stable or unstable.

Among these two models (MYJ, YSU), depend on the spatial and temporal differences, the closest one to the reality may change from a research to another. Yet, based on the various studies so far conducted at various locations, there are still some general aspects for each model.

For instance, as a local scheme MYJ, is usually the less sensitive PBL model to build the model's height. According to Mellor and Yamada's study (1982), the MYJ is generally more useful scheme for the stable or neutral air conditions rather than unstable since it takes the local gradients (pressure, concentration, temperature at that point), it is easy to focus on the small eddies' turbulent transfer. Although this is important, the real turbulence in atmosphere is provided by the large eddies as they can transport the fluid (heat, moisture) to the longer distances (Cohen, et.al, 2015). Therefore, the MYJ is a local scheme which is too moisty near the surface with a very thin layer and that makes it incapable of producing the strong vertical turbulent mixing (Hu, et.al, 2010).

The non-local PBL approaches, on the contrary, usually give more accurate predictions about the turbulent kinetic mixing in models, more appropiate for the convective air systems rather than the MYJ. The reason lies behind this statement, because of the non-local schemes, as mentioned before, parameterize many adjacent and distant layers so their level of model heights (the mixing length) are thicker, which may start from the boundary layer to the top layer of PBL (Cohen et.al, 2015). So they are much more influenced by the surface layer fluxes interactions such as the wind speed and direction, potential surface temperature, latent and sensible heat (represented non-local mixing in the **Figure 3.2.6**) and their effects on turbulence are carried through the deep layers.

When considering a full day, it can be said, most of the turbulent mixing occurs in day time rather than night time. That's why, investigating how the model

performances change during a day is also important. In some cases, the rised temperature (warm and dry) during the day, may cause strong turbulence (convective) which creates unstable air conditions at the boundary layer (Cohen et.al, 2015). For this perspective, the YSU might be the model that can offer more accurate forecast for this time period of the day.

However, as the day turns to night, the air usually becomes more stable (eddy diffusivity / viscosity declines near the surface) (Hu et.al, 2010). The MYJ may be a better option now but it still does not have a systematic sensitivity for the height, not interact with the surface fluxes.

Overall, the YSU seems the most sensitive PBL model for the determination of model mixing lenght where the vertical turbulent movements of fluids are caused by the eddy fluxes. Even though, this gives an advantage to the WRF model for building a convective system in its predictions, it does not indicate that YSU is always the 'right scheme' to be used in all type of event simulations. As like the other physical components of atmosphere, the PBL activity has also shaped by the orographic, climatic, seasonal and even the hour of event features. That's why, both the MYJ and YSU are selected to use in the model simulations of the events which are determined to be conducted under this sensitivity analysis.

3.3 WRF ARW Model Set Up for Sensitivity Analysis

From Chapter 2.3, the event dates determined to be used in the sensitivity analysis have shown on **Table 3.3.1**.

Table 3.3.1 Selected event dates and determined model run periods for Sensitivity Analysis

Region	Event Season	Event Date	Main Station	Peak Precipitation Amount (mm)	Model Run Period

Table 3.3.1 (cont'd) Selected event dates and determined model run periods for Sensitivity Analysis

Mediterranean	Autumn	28.11.2017	Manavgat / Antalya	29.6	26.11.2017 – 29.11.2017
Mediterranean	Summer	30.08.2017	Sutculer / Isparta	59.2	29.08.2017 – 01.09.2017
Eastern Black Sea	Autumn	14.11.2016	Camlihemsin / Rize	40.1	13.11.2016 – 17.11.2016
Eastern Black Sea	Summer	21.09.2016	Besikduzu / Trabzon	81.1	20.09.2016 – 24.09.2016

It has been planned to work on the model with one parent and one child (nest) domain for each region. To be able to obtain the effects of the interaction between the parent and the nests on the predictions, two-way nesting option has been applied. The parent domain is common for both Mediterranean and Eastern Black Sea regions and the sea impacts on the model predictions are wanted to investigate in this analysis for both regions. Therefore, the parent domain has drawn from little outside of the Turkey borders and placed between 43.5 – 38.7N, 23.5 – 29.9E with a horizontal (spatial) resolution 9 km (**Figure 3.3.1**).

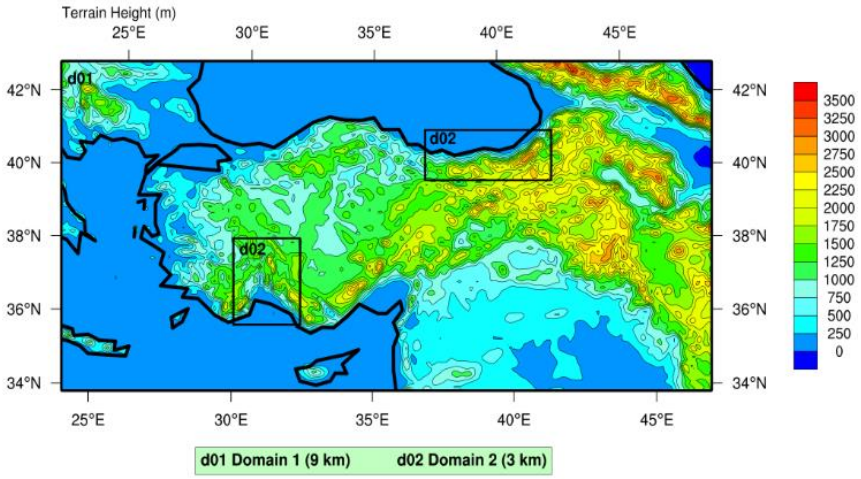

Figure 3.3.1 The representation of determined domains to be used in WRF model configuration for each region. d01 at the top left corner, represents Domain 1 with 9 km grid size (common for both Mediterranean and Eastern Black Sea regions), d02 indicates Domain 2 with 3 km grid size for each region, respectively

The area is covered by 232 grids in West-east and 111 grids in South-north direction. The nested domains, on the other hand, are seperately determined. Here, the key is to cover the main basin area. The nest domain on Mediterranean region is placed in 47.5 – 32.4N, 34.5 – 36.4E coordinates. The horizontal resolution is 3 km and the grid points are decided as 73 and 88 for West-east and South-north directions, respectively. The nest of Eastern Black Sea region has also been specified with 3 km resolution in horizontal aspect but its grids aligned through West-east direction are estimated as 136 and 52 for South-north direction. The area overlays 47.5 – 41.6N, 23.5 – 36.9E.

Table 3.3.2 General outline of WRF model configurations determined for two regions

Regions	**Mediterranean**		**Eastern Black Sea**	
	Domain 1	Domain 2	Domain 1	Domain 2
Coordinates	43.5 – 38.7N, 23.5 – 29.9E	47.5 – 32.4N, 34.5 – 36.4E	43.5 – 38.7N, 23.5 – 29.9E	47.5 – 41.6N, 23.5 – 36.9E
Grid Numbers	232 grids in West-east and 111 grids in South-north	73 grids in West-east and 88 grids in South-north	232 grids in West-east and 111 grids in South-north	136 grids in West-east and 52 grids in South-north
Grid Sizes or Horizontal Resolution	9 km	3 km	9 km	3 km

Table 3.3.2 (cont'd) General outline of WRF model configurations determined for two regions

Vertical Metgrid Levels	32	32	32	32
Soil Levels	4	4	4	4
Pressure Top (p_top, hPa)	50	50	50	50
Interval Seconds (Δt)	21600 s (6 h)	21600 s (6 h)	21600 s (6 h)	21600 s (6 h)
GFS Horizontal Resolution	0.25º (around 28 km)	0.25º (around 28 km)	0.25º (around 28 km)	0.25º (around 28 km)
ERA5 Horizontal Resolution	0.25º (around 28 km)	0.25º (around 28 km)	0.25º (around 28 km)	0.25º (around 28 km)

Apart from cumulus, microphysics and PBL, the WRF model also uses radiation and land surface parameters to build up the atmospheric system. Yet, because these parameters are not included into sensitivity analysis, only one scheme has been determined for each of them.

As it has already known that the radiation is one of the major component of climate change as it regulates the Earth's energy bugdet. The Earth energy balance is basically the relation among the incoming solar radiation and the outgoing infrared radiation. Moreover, solar radiation determines the surface temperature which is critical parameter for both land and the atmospheric models so as precipitation

analyses. As mentioned in Chapter 3.2.1, by absorbing or reflecting the radiation, the clouds affect the current weather or the climate differently. For instance, some clouds allows the solar radiation (the sunlight) to react the surface of the Earth whereas some of them, mostly the deeper cumulus clouds, react the sunlight as reflection to the space and not allow reaching the surface.

Even though the radiation schemes' options are various in the WRF model, through the perspective of this sensitivity analysis, only one radiation is used in all physical combinations. Therefore, the sensitivity effect of radiation on the precipitation has not been looked up in this study. Yet, that does not change the importance of selecting appropriate radiation scheme to use in the analysis itself.

Among many alternatives, the 'Rapid Radiative Transfer Model (RRTM)' radiation scheme is selected to be used in all configurations in the sensitivity analysis of WRF model. This scheme is one of the most common radiation options prefered by the users because it can specify the size of hydrometeors (water vapor, CO_2, ozone and trace gases) regardless of cloud type or amount for radiation calculations (UCAR, 2019).

Dudhia shortwave scheme, on the other hand, has selected because it one of the common options that represents a simple downward integration of solar flux (UCAR, 2019). This scheme is simple, fast and inexpensive to compute. During its calculations, it accounts clear – sky absorption (where it is assumed that no cloud exist) and scattering by water vapor, trace gases and aerosols but not ozone (Dudhia, n.d.).

Land surface is also important physical parameter in numerical weather forecasting models (NWPs). Since it is basically the layer we walked on and it is kind of the coverage between the underlying soil and the atmosphere. Therefore, it can be considered that the land surface processes occur at this interface. The impacts of these processes are pretty visible to realize such as the evaporation of surface water, melting snow, the runoff or condensation water on vegetation turn into leaf drips as well as transpiration (Orth, et.al, 2016).

Thus, land surface processes shape the lower boundary conditions of the atmospheric models. Since the vertical turbulent mixing (kinetic movements) of heat, water and the blowing wind within this boundary layer are redistributed as well as the pollutants or the other constituents of atmosphere over the surface by its processes (Zhao, et.al, 2015; Hahmann, 2005). However, most of the time atmospheric prediction models, e.g the WRF, are not much sensitive to this parameter. Even though, the land surface is kind of a bridge among the atmosphere, the hydrological cycle and the biosphere, it is more crucial for the hydrological models, e.g.WRF-Hydro (Hahmann, 2005).

For the sensitivity analysis, Unified Noah Land Surface Model has been chosen as the land surface parameterization scheme of WRF model. Although there are not huge differences among the schemes of land surface, still the selected one has four layers (10, 30, 60, 100 cm thick) to calculate the soil temperature and moisture (Ek, 2013; UCAR, 2019). Additionally, it offers fractional snow cover and frozen soil physics into the model which contributes the accuracy of land processes.

Lastly, as one of the common used methods, Eta Similarity scheme has determined for the surface layer physics option in WRF namelists. This scheme works with Monin-Obukhov theory principles (UCAR, 2019) where the mean of surface fluxes such as the momentum, water vapor, sensible and latent heat fluxes are determined by scaling lengths (thermal roughness length and surface roughness, zero plane displacement) and scaling velocity (friction velocity) (Bianco, 2008) and this enables the scheme offers horizontally homogenous surface layer.

Table 3.3.3 Radiation and Land Surface Schemes to be used in Sensitivity Analysis

Shortwave Radiation (ra_sw)	**Longwave Radiation (ra_lw)**	**Surface Layer (sf_sfclay)**	**Land Surface (sf_surface)**
Dudhia Shortwave Scheme (1) (Dudhia, 1989)	RRTM Longwave Scheme (1) (Conley, 2011)	Eta Similarity Scheme (2) (Bianco, 2008)	Unified Noah Land Surface Model (2) (Chen et al, 2001)

After the selection processes for both input meteorological and physical schemes to be tested by WRF model in sensitivity analysis, the whole list of configuration ensembles are given on **Table 3.3.4**. As it can be seen from the columns' names, this table demonstrates the number of scenarios and their run options in terms of the domain size, physical parameters and input datasets. Selected approachs of every physical parameter are matched with each other and produce new configuration. Because of this, in total 96 scenarios are determined to examine the prediction performance through the scope of sensitivity analysis.

Here, it is clear that each simulation number contains two scenarios where one of them indicates the parent domain (9 km, domain 1) while the second one is prepared for the nested domain (3 km, domain 2) configuration in WRF model. Based on this order between two domains, the even numbered scenarios refer the nested domain whereas the odd numbered scenarios represent the parent domain ensembles.

Additionally, for the nest domain's (3 km horizontal resolutions) scenarios, no cumulus parameterization has been applied (**Table 3.3.4**), this is the reason why their cumulus columns are filled with '0', which means 'turned off'. Since the objective of cumulus parameterization is to obtain a closed system for predicting weather events. It is usually used for convective precipitation calculations in the model

because this type of rain events generally occur local and placed as distributed on the large scale of grids (Jeworrek et al., 2019). Therefore, it is very hard to observe their total impacts on the model's atmospheric system without using a parameterization scheme. From this perspective, for the model domains determined with a lower horizontal resolution (> 4 km), the cumulus parameterization is considered as 'benefical' on the prediction of convective systems (Jeworrek et al., 2019). However, when the resolution is better which means smaller than that range (≤ 4 km) like the resolution of domain 2 in this study (3 km), the cumulus clouds can be easily resolved by the microphysics (Jeworrek et al., 2019; Done et al, 2004; Gilliland et al, 2007) of each grid without requiring a parameterization scheme. Thus, the cumulus parameterization in the studies of this thesis, has not been activated on the nested domain's (domain 2, 3 km) model simulations.

Thus, overall there are 96 different configurations are estimated to test in WRF model forecasting performance for the sensitivity analysis of this thesis. The 48 of them belong to the domain 1 (9 km) whereas the other half contains domain 2 (3 km)scenarios. Yet, because the model runs over both domains together, each of two domain scenarios are taken under one simulation number (from Simulation Number column of **Table 3.3.4**). Since there are also only two options available in input meteorological dataset type, the half of 96 scenarios are determined to be worked with GFS dataset whereas the rest uses ERA5 dataset in their model simulations. Apart from these, all of the physical parameters' schemes are aligned through the list of scenario configurations.

Table 3.3.4 The model configurations used in the Sensitivity Analysis

Scenario	Grid Sizes or Resolution (km)	Microphysics	Cumulus	PBL	Input Dataset Type	Simulation No
Scenario 1	9	KS (1)	KFS (1)	YSU (1)	GFS	1
Scenario 2	3	KS (1)	0	YSU (1)	GFS	
Scenario 3	9	ES (5)	KFS (1)	YSU (1)	GFS	2
Scenario 4	3	ES (5)	0	YSU (1)	GFS	

Table 3.3.4 (cont'd) The model configurations used in the Sensitivity Analysis

Scenario 5	9	WSM6 (6)	KFS (1)	YSU (1)	GFS	3
Scenario 6	3	WSM6 (6)	0	YSU (1)	GFS	
Scenario 7	9	AATS (28)	KFS (1)	YSU (1)	GFS	4
Scenario 8	3	AATS (28)	0	YSU (1)	GFS	
Scenario 9	9	KS (1)	BMJ (2)	YSU (1)	GFS	5
Scenario 10	3	KS (1)	0	YSU (1)	GFS	
Scenario 11	9	ES (5)	BMJ (2)	YSU (1)	GFS	6
Scenario 12	3	ES (5)	0	YSU (1)	GFS	
Scenario 13	9	WSM6 (6)	BMJ (2)	YSU (1)	GFS	7
Scenario 14	3	WSM6 (6)	0	YSU (1)	GFS	
Scenario 15	9	AATS (28)	BMJ (2)	YSU (1)	GFS	8
Scenario 16	3	AATS (28)	0	YSU (1)	GFS	
Scenario 17	9	KS (1)	GFES (3)	YSU (1)	GFS	9
Scenario 18	3	KS (1)	0	YSU (1)	GFS	
Scenario 19	9	ES (5)	GFES (3)	YSU (1)	GFS	10
Scenario 20	3	ES (5)	0	YSU (1)	GFS	
Scenario 21	9	WSM6 (6)	GFES (3)	YSU (1)	GFS	11
Scenario 22	3	WSM6 (6)	0	YSU (1)	GFS	
Scenario 23	9	AATS (28)	GFES (3)	YSU (1)	GFS	12
Scenario 24	3	AATS (28)	0	YSU (1)	GFS	
Scenario 25	9	KS (1)	KFS (1)	MYJ (2)	GFS	13
Scenario 26	3	KS (1)	0	MYJ (2)	GFS	
Scenario 27	9	ES (5)	KFS (1)	MYJ (2)	GFS	14
Scenario 28	3	ES (5)	0	MYJ (2)	GFS	
Scenario 29	9	WSM6 (6)	KFS (1)	MYJ (2)	GFS	15
Scenario 30	3	WSM6 (6)	0	MYJ (2)	GFS	
Scenario 31	9	AATS (28)	KFS (1)	MYJ (2)	GFS	16
Scenario 32	3	AATS (28)	0	MYJ (2)	GFS	
Scenario 33	9	KS (1)	BMJ (2)	MYJ (2)	GFS	17
Scenario 34	3	KS (1)	0	MYJ (2)	GFS	
Scenario 35	9	ES (5)	BMJ (2)	MYJ (2)	GFS	18
Scenario 36	3	ES (5)	0	MYJ (2)	GFS	
Scenario 37	9	WSM6 (6)	BMJ (2)	MYJ (2)	GFS	19
Scenario 38	3	WSM6 (6)	0	MYJ (2)	GFS	
Scenario 39	9	AATS (28)	BMJ (2)	MYJ (2)	GFS	20
Scenario 40	3	AATS (28)	0	MYJ (2)	GFS	
Scenario 41	9	KS (1)	GFES (3)	MYJ (2)	GFS	21
Scenario 42	3	KS (1)	0	MYJ (2)	GFS	

Table 3.3.4 (cont'd) The model configurations used in the Sensitivity Analysis

Scenario 43	9	ES (5)	GFES (3)	MYJ (2)	GFS	22
Scenario 44	3	ES (5)	0	MYJ (2)	GFS	
Scenario 45	9	WSM6 (6)	GFES (3)	MYJ (2)	GFS	23
Scenario 46	3	WSM6 (6)	0	MYJ (2)	GFS	
Scenario 47	9	AATS (28)	GFES (3)	MYJ (2)	GFS	24
Scenario 48	3	AATS (28)	0	MYJ (2)	GFS	
Scenario 49	9	KS (1)	KFS (1)	YSU (1)	ERA5	25
Scenario 50	3	KS (1)	0	YSU (1)	ERA5	
Scenario 51	9	ES (5)	KFS (1)	YSU (1)	ERA5	26
Scenario 52	3	ES (5)	0	YSU (1)	ERA5	
Scenario 53	9	WSM6 (6)	KFS (1)	YSU (1)	ERA5	27
Scenario 54	3	WSM6 (6)	0	YSU (1)	ERA5	
Scenario 55	9	AATS (28)	KFS (1)	YSU (1)	ERA5	28
Scenario 56	3	AATS (28)	0	YSU (1)	ERA5	
Scenario 57	9	KS (1)	BMJ (2)	YSU (1)	ERA5	29
Scenario 58	3	KS (1)	0	YSU (1)	ERA5	
Scenario 59	9	ES (5)	BMJ (2)	YSU (1)	ERA5	30
Scenario 60	3	ES (5)	0	YSU (1)	ERA5	
Scenario 61	9	WSM6 (6)	BMJ (2)	YSU (1)	ERA5	31
Scenario 62	3	WSM6 (6)	0	YSU (1)	ERA5	
Scenario 63	9	AATS (28)	BMJ (2)	YSU (1)	ERA5	32
Scenario 64	3	AATS (28)	0	YSU (1)	ERA5	
Scenario 65	9	KS (1)	GFES (3)	YSU (1)	ERA5	33
Scenario 66	3	KS (1)	0	YSU (1)	ERA5	
Scenario 67	9	ES (5)	GFES (3)	YSU (1)	ERA5	34
Scenario 68	3	ES (5)	0	YSU (1)	ERA5	
Scenario 69	9	WSM6 (6)	GFES (3)	YSU (1)	ERA5	35
Scenario 70	3	WSM6 (6)	0	YSU (1)	ERA5	
Scenario 71	9	AATS (28)	GFES (3)	YSU (1)	ERA5	36
Scenario 72	3	AATS (28)	0	YSU (1)	ERA5	
Scenario 73	9	KS (1)	KFS (1)	MYJ (2)	ERA5	37
Scenario 74	3	KS (1)	0	MYJ (2)	ERA5	
Scenario 75	9	ES (5)	KFS (1)	MYJ (2)	ERA5	38
Scenario 76	3	ES (5)	0	MYJ (2)	ERA5	
Scenario 77	9	WSM6 (6)	KFS (1)	MYJ (2)	ERA5	39
Scenario 78	3	WSM6 (6)	0	MYJ (2)	ERA5	
Scenario 79	9	AATS (28)	KFS (1)	MYJ (2)	ERA5	40
Scenario 80	3	AATS (28)	0	MYJ (2)	ERA5	

Table 3.3.4 (cont'd) The model configurations used in the Sensitivity Analysis

Scenario 81	9	KS (1)	BMJ (2)	MYJ (2)	ERA5	41
Scenario 82	3	KS (1)	0	MYJ (2)	ERA5	
Scenario 83	9	ES (5)	BMJ (2)	MYJ (2)	ERA5	42
Scenario 84	3	ES (5)	0	MYJ (2)	ERA5	
Scenario 85	9	WSM6 (6)	BMJ (2)	MYJ (2)	ERA5	43
Scenario 86	3	WSM6 (6)	0	MYJ (2)	ERA5	
Scenario 87	9	AATS (28)	BMJ (2)	MYJ (2)	ERA5	44
Scenario 88	3	AATS (28)	0	MYJ (2)	ERA5	
Scenario 89	9	KS (1)	GFES (3)	MYJ (2)	ERA5	45
Scenario 90	3	KS (1)	0	MYJ (2)	ERA5	
Scenario 91	9	ES (5)	GFES (3)	MYJ (2)	ERA5	46
Scenario 92	3	ES (5)	0	MYJ (2)	ERA5	
Scenario 93	9	WSM6 (6)	GFES (3)	MYJ (2)	ERA5	47
Scenario 94	3	WSM6 (6)	0	MYJ (2)	ERA5	
Scenario 95	9	AATS (28)	GFES (3)	MYJ (2)	ERA5	48
Scenario 96	3	AATS (28)	0	MYJ (2)	ERA5	

PART II – Sea Surface Temperature (SST) Analysis

The interaction between the ocean and the atmosphere is a starting point of the climate patterns and their distribution through out the world. Since the atmosphere is a dynamic system, any change occured in it will be carried by the daily and annual rotations of the Earth, the ocean currents, the winds and the orographic factors so it will travel both on the vertical and horizontal distances which enables it to have power to influence the weather and the climate patterns where ever it goes (IPCC, 2014; Bigg et.al, 2003).

The radiation that can reach to the sea surface is called '***Sea Surface Temperature (SST)***'. The SST plays a critical role in the ocean – atmosphere interaction as the vertical fluxes such as the heat (latent heat, sensible heat), moisture and momentum are two way transmitted from the interface between the sea surface and the air above

(Bigg et.al, 2003). The surface winds, currents and waves are the main dynamics of this transfer (GHRSST, 2010).

As stated in 'Report on the Environment' by Environmental Protection Agency (EPA, 2008), the high temperature stored on the sea surface evaporates more, accelerates the atmospheric system and leads to heavy precipitation occurances onto both the seas and the inlands. Therefore, the terrain which has the complex topographic properties and high SSTs such as the Mediterranean region, carries great possibility for the SST triggered extreme weather events to be occured.

When the SST accelerates the flux exchanges through the ocean – atmosphere interface, the air circulates both in horizontal and vertical directions. In some cases, this circulation may impact larger regions. The tropical cyclones such as El Niño or La Niña, the summer mussons in India and the midlatitude storms near the Gulf Stream can be considered as the synoptic scale of extreme weather events due to this type of circulations. (Senatore et.al, 2014). Nevertheless, particularly the recent studies, claim that the some of mesoscale storms and extreme convective precipitation are also resulted by the abnormal changes in SST.

According to these studies, the SST is not the only reason underlies the extreme events, the orographic forcing which refers the reduction/exclusion of mountainbarriers (Hong and Lee 2009; Smith et al. 2010; Fleschand Reuter 2012) has also an undeniable contribution on the SST triggered extreme weather events.

The regions especially located at midlatitudes where the temperature is relatively high and has a complex coastal orography such as the Mediterranean (Rebora et al. 2013) can be influenced by the SST changes. Therefore, the mesoscale thunderstoms and hurricanes occured in these regions may likely be triggered by SST.

As the other mesoscale meteorological processes, the SST based weather events' impacts also can be observed from the coastal areas up to several hundred kilometers inlands (Senatore et.al, 2014). The aim of this part of the thesis is to observe the SST

effects on the heavy precipitation events occured in two regions of Turkey: Mediterranean and Eastern Black Sea. For Mediterranean region, Antalya basin, for Eastern Black Sea region like its name Eastern Black Sea basin are selected to work in the scope of this study.

3.4 Importance of SST on Mediterranean and Eastern Black Sea Regions

It has already known that the Mediterranean is one of the most vulnerable regions that is highly affected via the global warming (Cisneros et al., 2016) in the world. The rising temperature in air warms the seas as well as the lands which leads the SST has increased over the region. In regard to SST statics of GDM (GDM, 2019) average SST of Mediterranean Sea increased by 0.6 º C between two decades (from 1989 - 1998 to 1999 - 2008) whereas it continued to increase with 0.3 º C increment among 1999 - 2008 and 2009 - 2018 periods. These results show that the annual SST values has been rapidly rising in the last 20 years. While the average SST of Mediterranean Sea in December 2017 was 19.2 º C, it was estimated as 19.3 º C for the next year's December (GDM, 2019).

Therefore, the SST of the event year was higher than previous years and also it was observed the SSTs have been continued to rise by certain levels before and along the event period. Moreover, as stated in Senatore's article (Senatore et al., 2014), the complex coastal orography of Mediterranean region is quite suitable for the formation of SST caused precipitation. From all of these perspectives, Mediterranean was one of the essential regions to conduct SST analysis in Turkey.

Moreover to this, the impact of SST changes on precipitation has aimed to be study with Eastern Black Sea region, too. Since it is one of the most rainy basins in Turkey and the general rise in SSTs for all around the world has also observed on this region. Based on the archive dataset, the estimated average precipitation dropped was around 1.030,4 - 1.187,1 mm and the average SST on Black Sea had rised about 0.5º C from

2013 to 2015 then reached its maximum in 2018 by 16.5º C (Ministry of Forestry and Water Affairs & Directorate General for Water Management (GDWM), 2019). This is important for the study because it indicates the sea – atmosphere interaction valid for that year which draws a better picture to understand the event year's (2015) weather conditions. (GDM, 2019).

Similar to Mediterranean, Eastern Black Sea region is also surrounded with mountains at the coastal area so the orographical properties are complex on seaside of this basin. High air temperature heats the seas as well as the lands. The rapid and sharp increases in the SST accelerate the vertical flux exchanges among the sea and atmosphere. This dynamic cause the cloud formation and sometimes under the complex topographical effects, leads heavy precipitation to occur. Hence, Eastern Black Sea region also carries great potential for having SST triggered precipitation events.

3.5 SST Data Sources' Arrangement

There are many SST data sources to be used in the numerical weather prediction (NWP) models. The data of these sources can be obtained from the in – situ observation stations (ship, buoys), the satellites and also the model forecast results. In this thesis, three SST source datasets are planned to use. By this way, not only SST impacts on the selected heavy precipitation events are observed but also which SST dataset produces the most accurate prediction for these events can be investigated.

One of the selected SST source for this study is '***The Group for High Resolution Sea Surface Temperature Level 4 Ultra High Resolution (GHRSST)***' (GHRSST, 2010). GHRSST is a product of an international consortium which brings the research organizations, operational agencies, academic institutions and commercial enterprises together, (GHRSST, 2010). The SST is provided daily with a resolution 0.01°. The reason why this dataset has chosen as one of the sources, is because the

GHRSST offers the highest horizontal / spatial resolution among the other selected SST datasets. Thus, it is expected to the SST impacts on the events' precipitation are explicitly observed in this one.

Through Senatore and his colleagues' researches over the years (Senatore et al., 2014; Senatore et al., 2020), ***'Medspiration level 4 Ultra-High Resolution foundation SST'*** (MEDS) (with horizontal resolution of 0.022°) from the Medspiration Project is also included as the another SST source to analyse in this paper. The Medspiration project has been conducted by the cooperation of many institutions under the leadership of the Centre European Remote Sensing d'Archivage et de Traitement (CERSAT), Institut Français de Recherche pour L'Exploitation de la Mer (IFREMER) (Merchant et al., 2008; Robinson et al., 2012).

The third and final SST source is the '***real-time, global, sea surface temperature (RTG_SST_HR)'*** SST represented by the National Centers for Environmental Prediction (NCEP), National Oceanic and Atmospheric Administration (NOAA) and Marine Modeling and Analysis Branch (MMAB). This dataset, called NCEP SST, has relatively coarse horizontal resolution with 0.083° than the other two (NCEP, 2014).

The GHRSST and the Medspiration are the satellite derived SST datasets whereas the NCEP SST can be taken as the model derived dataset. However, it does not mean that the satellite derived dataset only contain satellite data or the model derived is just produced from the atmospheric model predictions. On the contrary, all of the three SST data sources utilize the satellites and the in-situ observations such as the ships, the buoys data together to provide a dataset. The only addition to this, is the NCEP SST dataset is obtained by combining the model forecasts with the satellite and in-situ observations. Therefore, it is distinguished from the others and that's why it is included in this study. Yet, no matter the source or how they obtained, all SST datasets are provided daily.

GHRSST ~ 1.1 km

MEDS ~ 2.2 km

NCEP ~ 9.2 km

Here, the format of the source dataset is critical as WRF model only reads the grib format whereas the satellite derived datasets like the GHRSST and the Medspiration are offered in 'nc' format. Hence, these SST datasets should be externally arranged before putting into the model.

Through the directives in "Sensitivity of Modeled Precipitation to Sea Surface Temperature in Regions with Complex Topography and Coastlines: A Case Study for the Mediterranean" paper (Senatore et al., 2014), the external pre-processing steps are applied on GHRSST and the Medspiration datasets by the GIS based techniques. Taken steps are listed as follows:

First, "nc" format daily SST datasets are opened on the QGIS for each day and reprojected to the WRF projection (e.g. converting WGS84 to Lambert projection). Second, the grids of reprojected datasets are resampled by using the nearest neighbour method, where the values are assigned to the closest grids without changing. It should not be forgotten that the domain extents and their horizontal resolutions are need to be specified during resampling process. The meteorological data is fed into the model to update the boundary conditions for every 6 hours, but the SST datasets are produced daily. To be able to adjust the interval of these external SSTs are fed into the model, each dataset is repeated 4 times in a day. For this task, the R programming is used. Lastly, the resampled and intervally adjusted SST datasets are merged with land SSTs of the model. Hence, like in the reference paper (Senatore et al., 2014), the SST data of model on the seas is changed with the new source datasets SSTs while the original model SST values such as GFS or ECMWF provided, on the land remains the same with the model data.

To be able to make the changes and insert the new SST datasets, the lower boundary condition files of each domains (e.g. wrflowinp_d01 for domain 1, wrflowinp_d02 for domain 2) should be provided by the WRF model. Therefore, two relevant options should be activated via the WRF model's input namelist options: ***sst_update*** and ***sst_skin***. The sst_update option is used so that the model updates the SSTs for each time steps otherwise the model does not make time-varying prediction on SST, the sst_skin option is turned into open to make the model calculates the skin SSTs (Zeng and Beljaars, 2005). When the SST dynamics of the model is permitted via these options, the lower boundary condition files are produced on each domains. The current SST is replaced with the new source SST dataset by means of ncks commands.

3.6 WRF ARW Model Set Up for SST Analysis

While **Table 3.6.1** represents the event dates to be studied by SST Analysis, **Table 3.6.2** shows the scenarios and their model configuration options on each region.

According to the observation data taken from GDM, it was accepted that the event occured in between 15 - 17 December of 2018. Based on the archive database, this case was considered as one of the biggest catastrophic event that has ever happened over the entire country since the total precipitation amount dropped in just one station on December 16, was calculated as 654.4 mm which is quite a lot comparing to the montly average precipitation on December for the whole Antalya city was estimated as 265.3 mm (Forestry and Water Affairs and General Directorate of Meteorology, 2019).

The second heavy precipitation event included into this SST analysis, happened on Eastern Black Sea region of Turkey. Once again, the observation station dataset were provided from GDM. With 32.4 mm maximum precipitation production, the event date had been defined for 23 – 24 August of 2015.

Table 3.6.1 Selected event dates and determined model run periods for SST Analysis

Region	Event Season	Event Date	Main Station	Peak Precipitation Amount (mm)	Model Run Period
Mediterranean	Winter	16.12.2018	Ovacık / Antalya	53.1	10.12.2018 – 20.12.2018
Eastern Black Sea	Summer	24.08.2015	Arhavi / Artvin	32.4	17.08.2015 – 27.08.2015

Table 3.6.2 The model configurations determined to be tried in the SST Analysis

Events	Scenario	Grid Sizes or Resolution (km)	SST Data Source	Input Dataset Type	Simulation No
MED - Winter	**Scenario 1**	9	WRF - GFS	GFS	1
	Scenario 2	3	WRF - GFS	GFS	
	Scenario 3	9	GHRSST	GFS	2
	Scenario 4	3	GHRSST	GFS	
	Scenario 5	9	Medspiration	GFS	3
	Scenario 6	3	Medspiration	GFS	
	Scenario 7	9	NCEP	GFS	4
	Scenario 8	3	NCEP	GFS	
EBLS - Summer	**Scenario 1**	9	WRF - ERA5	ERA5	1
	Scenario 2	3	WRF - ERA5	ERA5	
	Scenario 3	9	GHRSST	ERA5	2
	Scenario 4	3	GHRSST	ERA5	
	Scenario 5	9	Medspiration	ERA5	3
	Scenario 6	3	Medspiration	ERA5	
	Scenario 7	9	NCEP	ERA5	4
	Scenario 8	3	NCEP	ERA5	

Model configurations in order to use in the SST study, are determined by the outcomes obtained from the sensitivity analysis (Chapter 4 – PART I). The physical parameters and input data sources are selected based on their forecasting accuracies. Of course, it has also considered for the better options in the sensitivity event seasons match or at least be similar with the SST event seasons. Since it has already known, specific approach in physics can not suit to build up all of the seasonal atmospheric conditions. According to this information, the selected schemes to be used in model configurations of SST events on each basin are shown at **Table 3.6.3.**

Table 3.6.3 Physical Schemes Selected to be Used in SST Analysis

Selected Physical Schemes	**Mediterranean**	**Eastern Black Sea**
Microphysics (mp)	Eta (Ferrier) Scheme (5)	Aerosol–aware Thompson Scheme (28)
Cumulus (cu)	Grell–Freitas Ensemble Scheme (3)	Grell–Freitas Ensemble Scheme (3)
Planetary Boundary Layer (bl_pbl)	Mellor–Yamada–Janjic Scheme (MYJ) (2)	Mellor–Yamada–Janjic Scheme (MYJ) (2)
Shortwave Radiation (ra_sw)	Dudhia Shortwave Scheme (1)	Dudhia Shortwave Scheme (1)
Longwave Radiation (ra_lw)	RRTM Longwave Scheme (1)	RRTM Longwave Scheme (1)
Surface Layer (sf_sfclay)	Eta Similarity Scheme (2)	Eta Similarity Scheme (2)
Land Surface (sf_surface)	Unified Noah Land Surface Model (2)	Unified Noah Land Surface Model (2)

CHAPTER 4

RESULTS OF EVENT CASE STUDIES

PART I - Sensitivity Analysis Event Cases

4.1 TOPSIS Analysis

As a part of the sensitivity study, to be able to rank the overall performance of each scenario, the 'Technique for Order of Preference by Similarity to Ideal Solution (TOPSIS)' analysis has been planned to use. TOPSIS is one of the multi-criteria decision tools that ranks the alternatives according to have the shortest distance from the positive ideal solution to the farther distance from negative ideal solution. This kind of analysis' working mechanism is usually shaped by the data type, the normalization process and the decision maker preferences about the used parameters, the value range, the weightage of parameters. Since based on these factors, the final decisions of TOPSIS can easily change.

By this analysis, each of 96 scenarios has been measured for various statistical parameters such Mean Bias Error (MBE), Standard Deviation (SD), Root Mean Square Error (RMSE). Addition to those, some commonly used forecast verification indicators (e.g. Probably of Detection, False Alarm Ratio, Critical Success …) are also included into TOPSIS calculations. All of the used parameters are shown under the name of 'TOPSIS Parameters' in **Table 4.1.1**. Since TOPSIS has its own normalization algorithm to be used on each scenario, the weightage is determined as 1 for all the parameters. The value range for the rankings has been decided from 0 to 1. To be able to make all parameters' values fit in this range, some specific conditions

are determined for the Frequency Bias Index (FBI), MBE and SD. These conditions are also displayed under 'Method Used in Re-arranged Range' column of **Table 4.1.1**.

By appling TOPSIS on the Sensitivity Analysis, it is aimed to find possible best scenarios and also make comparisons for their differences from the worst scenarios. It, at least, can give an idea about the average performances of 96 scenarios and create a ranking system based on multiple criteria.

Table 4.1.1 The Algorithms of TOPSIS Analysis (Nurmi, 2007)

TOPSIS Parameters	**Group**	**Value Range**	**Best Performance**	**Re-arranged Range**	**Method Used in Re-arranged Range**
Probability of Detection (POD) = $\frac{A}{A+C}$	Categoric	0 to 1	1	-	-
False Alarm Ratio (FAR)= $\frac{B}{A+B}$	Categoric	0 to 1	0	-	-
Critical Success Index (CSI)= $\frac{A}{A+B+C}$	Categoric	0 to 1	1	-	-
Percent Correct (PC)= $\frac{A+D}{E}$	Categoric	0 to 1	1	-	-
Frequency Bias Index (FBI)= $\frac{A+B}{A+C}$	Categoric	0 to ∞	1	0 to 1	**A)** If FBI[i]>2, => FBI[i]=0 **B)** If 2>FBI[i]>1, => FBI[i]=2-FBI[i] **C)** If FBI[i]<1, => FBI[i]= FBI[i]

Table 4.1.1 (cont'd) The Algorithms of TOPSIS Analysis (Nurmi, 2007)

Root Mean Square Error (RMSE) = $\sqrt{[\ \Sigma(P_i - O_i)^2 / n\ ]}$	Statistical	0 to ∞	0	-	-
Mean Bias Error (MBE) = $\Sigma\ \|(P_i - O_i)\| / n$	Statistical	-∞ to ∞	0	0 to ∞	MBE[i]=|MBE[i]|
Standard Deviation (SD) = $\sqrt{[\ \Sigma(P_i - \bar{P}_i)^2 / \Sigma(O_i - \bar{O}_i)^2\ ]}$	Statistical	-∞ to ∞	1	0 to 1	**A)** If SD[i]>2, => SD[i]=0 **B)** If 2>SD[i]>1, => SD[i]=2-SD[i] **C)** If SD[i]<1, => SD[i]= SD[i]
Correlation Coefficient (R) = $[\Sigma\ (P_i - \bar{P}_i) * (O_i - \bar{O}_i)] / \sqrt{[\Sigma(P_i - \bar{P}_i)^2]} * \sqrt{[\Sigma(O_i - \bar{O}_i)^2\ ]}$	Statistical	-1 to 1	1	-	-

n = the total number of comparisons, P = the model predictions, $\bar{P}$ = the average of model predictions, O = the observations, $\bar{O}$ = the average of observations

The A,B,C,D and E symbols in the TOPSIS forecast verification parameters' (POD, FAR, CSI, PC, FBI) formulas refer different relations between the model and the observation. The algorithms of these parameters are given in **Table 4.1.2**.

Table 4.1.2 The Algorithms of Categorical Forecasts

Forecast Precipitation	**Observation Precipitation**		
	Yes	No	Marginal Total
Yes	A	B	A+B
No	C	D	C+D
Marginal Total	A+C	B+D	A+B+C+D = E

Through the evalution of TOPSIS analysis, the top 10 scenarios in the rankings are shown for each event case in **Table 4.1.3**. The '9 km' column refers the top performance model configurations of the parent domain (domain 1) whereas the '3 km' column indicates the best performances of configurations for only the nest (domain 2). Even though the TOPSIS analysis or the top 5 of rankings can not offer the actual results, it may be helpful to draw general picture of prediction performances among 96 scenarios. As comparing with the rest, the common schemes of parameters used in the best configurations can be differenciated from the others and this can be useful for the researcher to focus on those mutual points while trying to find the schemes and parameters that the WRF model tends to be more sensitive.

For instance, in Mediterranean autumn event, Eta (Ferrier, ES) dominates the higher rankings for both domains which means it has a certain effect on enhancing the forecast accuracy. On the other hand, Eastern Black Sea autumn event, as expected and mentioned in Chapter 3.2.2, Aerosol Aware Thompson (AATS) and WRF Single 6 (WSM6) microphysics are really good at predictions among both 9 and 3 km scenarios.

For cumulus performances, there is only one column to look at because the cumulus parameterization in domain 2 (3 km) model configurations has been closed for this

study. From the overall list of the four events, it can be noticed that Kain Friscth (KFS) and Grell Freitas (GFES) performed better for autumn events while KFS gives its place to Betts Miller Janjic (BMJ) for summer events of the regions. This might be related with the event characteristics (synoptic or convective) in terms of precipitation period and its impact area.

In PBL, however, the two schemes are not exactly differenciated from each other as the options are too limited and almost every event has a couple of both PBL approach in their top 5. Yet, it does not be wrong to consider, MYJ approach usually corresponds good to autumun and summer seasons' precipitation events on both regions.

Lastly, the input data source effect on model predictions represented in 'Source Type' column of

Table 4.1.4 and **Table 4.1.5**, seems mostly depending on the regional features, not seasons. From, this column depicts that ERA5 is more appropiate for Eastern Black Sea region whereas GFS is more suitable to use in Mediterranean regional forecasts.

Table 4.1.3 Top 10 of model configurations in each event case through TOPSIS Analysis Results

Events	Topsis Rankings	Scenario Number	Domains	Microphysics	Cumulus	PBL	Input Dataset Type
MED - Autumn	1st	Scenario 43	Domain 1 (9 km)	ES (5)	GFES (3)	MYJ (2)	GFS
	2nd	Scenario 27	Domain 1 (9 km)	ES (5)	KFS (1)	MYJ (2)	GFS
	3rd	Scenario 3	Domain 1 (9 km)	ES (5)	KFS (1)	YSU (1)	GFS
	4th	Scenario 44	Domain 2 (3 km)	ES (5)	0	MYJ (2)	GFS
	5th	Scenario 47	Domain 1 (9 km)	AATS (28)	GFES (3)	MYJ (2)	GFS
	6th	Scenario 19	Domain 1 (9 km)	ES (5)	GFES (3)	YSU (1)	GFS
	7th	Scenario 4	Domain 2 (3 km)	ES (5)	0	YSU (1)	GFS
	8th	Scenario 20	Domain 2 (3 km)	ES (5)	0	YSU (1)	GFS
	9th	Scenario 35	Domain 1 (9 km)	ES (5)	BMJ (2)	MYJ (2)	GFS

Table 4.1.3 (cont'd) Top 10 of model configurations in each event case through TOPSIS Analysis Results

	10th	Scenario 36	Domain 2 (3 km)	ES (5)	0	MYJ (2)	GFS
MED - Summer	1st	Scenario 48	Domain 2 (3 km)	AATS (28)	0	MYJ (2)	GFS
	2nd	Scenario 1	Domain 1 (9 km)	KS (1)	KFS (1)	YSU (1)	GFS
	3rd	Scenario 95	Domain 1 (9 km)	AATS (28)	GFES (3)	MYJ (2)	ERA5
	4th	Scenario 9	Domain 1 (9 km)	KS (1)	BMJ (2)	YSU (1)	GFS
	5th	Scenario 25	Domain 1 (9 km)	KS (1)	KFS (1)	MYJ (2)	GFS
	6th	Scenario 7	Domain 1 (9 km)	AATS (28)	KFS (1)	YSU (1)	GFS
	7th	Scenario 15	Domain 1 (9 km)	AATS (28)	BMJ (2)	YSU (1)	GFS
	8th	Scenario 41	Domain 1 (9 km)	KS (1)	GFES (3)	MYJ (2)	GFS
	9th	Scenario 43	Domain 1 (9 km)	ES (5)	GFES (3)	MYJ (2)	GFS
	10th	Scenario 45	Domain 1 (9 km)	WSM6 (6)	GFES (3)	MYJ (2)	GFS
EBLS - Autumn	1st	Scenario 77	Domain 1 (9 km)	WSM6 (6)	KFS (1)	MYJ (2)	ERA5
	2nd	Scenario 69	Domain 1 (9 km)	WSM6 (6)	GFES (3)	YSU (1)	ERA5
	3rd	Scenario 21	Domain 1 (9 km)	WSM6 (6)	GFES (3)	YSU (1)	GFS
	4th	Scenario 93	Domain 1 (9 km)	WSM6 (6)	GFES (3)	MYJ (2)	ERA5
	5th	Scenario 78	Domain 2 (3 km)	WSM6 (6)	0	MYJ (2)	ERA5
	6th	Scenario 79	Domain 1 (9 km)	AATS (28)	KFS (1)	MYJ (2)	ERA5
	7th	Scenario 45	Domain 1 (9 km)	WSM6 (6)	GFES (3)	MYJ (2)	GFS
	8th	Scenario 49	Domain 1 (9 km)	KS (1)	KFS (1)	YSU (1)	ERA5
	9th	Scenario 19	Domain 1 (9 km)	ES (5)	GFES (3)	YSU (1)	GFS
	10th	Scenario 71	Domain 1 (9 km)	AATS (28)	GFES (3)	YSU (1)	ERA5
EBLS - Summer	1st	Scenario 87	Domain 1 (9 km)	AATS (28)	BMJ (2)	MYJ (2)	ERA5
	2nd	Scenario 88	Domain 2 (3 km)	AATS (28)	0	MYJ (2)	ERA5
	3rd	Scenario 91	Domain 1 (9 km)	ES (5)	GFES (3)	MYJ (2)	ERA5
	4th	Scenario 85	Domain 1 (9 km)	WSM6 (6)	BMJ (2)	MYJ (2)	ERA5
	5th	Scenario 96	Domain 2 (3 km)	AATS (28)	0	MYJ (2)	ERA5

Table 4.1.3 (cont'd) Top 10 of model configurations in each event case through TOPSIS Analysis Results

	6th	Scenario 81	Domain 1 (9 km)	KS (1)	BMJ (2)	MYJ (2)	ERA5
	7th	Scenario 95	Domain 1 (9 km)	AATS (28)	GFES (3)	MYJ (2)	ERA5
	8th	Scenario 93	Domain 1 (9 km)	WSM6 (6)	GFES (3)	MYJ (2)	ERA5
	9th	Scenario 71	Domain 1 (9 km)	AATS (28)	GFES (3)	YSU (1)	ERA5
	10th	Scenario 41	Domain 1 (9 km)	KS (1)	GFES (3)	MYJ (2)	GFS

Since the TOPSIS Analysis can create a ranking system among 96 scenarios based on various statistical aspects, it can also offer to make a comparison between the general performances of meteorological input sources for each domain. This helps to researcher to differenciate mainly which input source type (GFS or ERA5) achieved to generate more realistic predictions for every event period. That's why, the highest and lowest rankings in GFS and ERA5 scenarios are determined in each of four events. They are named as 'GFS - Best', 'ERA5 - Best' and 'GFS - Worst', 'ERA5 - Worst', respectively. Similarly, this kind of classification can also be useful to observe how the shemes used in physical parameters have changed or remained same between the best and the worst performed configurations or GFS and ERA5 scenarios.

The best and the worst scenarios of two sources for the conducted sensitivity analysis are represented by **Table 4.1.4** and **Table 4.1.5**.

Table 4.1.4 Best and worst scenarios of GFS and ERA5 datasets for domain 1 (9 km)

Performances based on Topsis Analysis			**9 km**			
Events	***Among Domain 1 Scenarios***	***Scenario Number***	***Microphysics***	***Cumulus***	***PBL***	***Source Type***
MED - Autumn	GFS - Best	Scenario **43**	ES	GFES	MYJ	GFS
	GFS - Worst	Scenario **25**	KS	KFS	MYJ	GFS
	ERA5 -Best	Scenario **67**	ES	GFES	YSU	ERA5
	ERA5 - Worst	Scenario **65**	KS	GFES	YSU	ERA5
MED - Summer	GFS - Best	Scenario **1**	KS	KFS	YSU	GFS
	GFS - Worst	Scenario **35**	ES	BMJ	MYJ	GFS
	ERA5 -Best	Scenario **95**	AATS	GFES	MYJ	ERA5
	ERA5 - Worst	Scenario **65**	KS	GFES	YSU	ERA5
EBLS - Autumn	GFS - Best	Scenario **21**	WSM6	GFES	YSU	GFS
	GFS - Worst	Scenario **43**	ES	GFES	MYJ	GFS
	ERA5 -Best	Scenario **77**	WSM6	KFS	MYJ	ERA5
	ERA5 - Worst	Scenario **83**	ES	BMJ	MYJ	ERA5

Table 4.1.4 (cont'd) Best and worst scenarios of GFS and ERA5 datasets for domain 1 (9 km)

EBLS - Summer	GFS - Best	Scenario **41**	KS	GFES	MYJ	GFS
	GFS - Worst	Scenario **39**	AATS	BMJ	MYJ	GFS
	ERA5 -Best	Scenario **87**	AATS	BMJ	MYJ	ERA5
	ERA5 - Worst	Scenario **53**	WSM6	KFS	YSU	ERA5

Table 4.1.5 Best and worst scenarios of GFS and ERA5 datasets for domain 2 (3 km)

Performances based on Topsis Analysis			**3 km**		
Events	***Among Domain 2 Scenarios***	***Scenario Number***	***Microphysics***	***PBL***	***Source Type***
MED - Autumn	GFS - Best	Scenario **44**	ES	MYJ	GFS
	GFS - Worst	Scenario **26**	KS	MYJ	GFS
	ERA5 -Best	Scenario **68**	ES	YSU	ERA5
	ERA5 - Worst	Scenario **54**	WSM6	YSU	ERA5
MED - Summer	GFS - Best	Scenario **48**	AATS	MYJ	GFS
	GFS - Worst	Scenario **4**	ES	YSU	GFS
	ERA5 -Best	Scenario **96**	AATS	MYJ	ERA5
	ERA5 - Worst	Scenario **58**	KS	YSU	ERA5
EBLS - Autumn	GFS - Best	Scenario **22**	WSM6	YSU	GFS
	GFS - Worst	Scenario **28**	ES	MYJ	GFS
	ERA5 -Best	Scenario **78**	WSM6	MYJ	ERA5
	ERA5 - Worst	Scenario **84**	ES	MYJ	ERA5

Table 4.1.5 (cont'd) Best and worst scenarios of GFS and ERA5 datasets for domain 2 (3 km)

EBLS - Summer	GFS - Best	Scenario **42**	KS	MYJ	GFS
	GFS - Worst	Scenario **40**	AATS	MYJ	GFS
	ERA5 -Best	Scenario **88**	AATS	MYJ	ERA5
	ERA5 - Worst	Scenario **54**	WSM6	YSU	ERA5

TOPSIS Analysis has also applied to rank the performances among the SST scenarios. **Table 4.1.6** represents the prediction performances rankings of data sources with their domain resolutions on both regions.

Table 4.1.6 Rankings among SST model configurations in each event case through TOPSIS Analysis Results

Events	Topsis Rankings	Scenario Number	Domains	SST Data Source	Input Dataset Type
MED - Winter	1st	Scenario **8**	Domain 2 (3 km)	NCEP	GFS
	2nd	Scenario **6**	Domain 2 (3 km)	Medspiration	GFS
	3rd	Scenario **4**	Domain 2 (3 km)	GHRSST	GFS
	4th	Scenario **2**	Domain 2 (3 km)	WRF - GFS	GFS
	5th	Scenario **7**	Domain 1 (9 km)	NCEP	GFS
	6th	Scenario **5**	Domain 1 (9 km)	Medspiration	GFS
	7th	Scenario **3**	Domain 1 (9 km)	GHRSST	GFS
	8th	Scenario **1**	Domain 1 (9 km)	WRF - GFS	GFS
EBLS - Summer	1st	Scenario **2**	Domain 2 (3 km)	WRF - ERA5	ERA5
	2nd	Scenario **4**	Domain 2 (3 km)	GHRSST	ERA5
	3rd	Scenario **6**	Domain 2 (3 km)	Medspiration	ERA5
	4th	Scenario **3**	Domain 1 (9 km)	GHRSST	ERA5
	5th	Scenario **8**	Domain 2 (3 km)	NCEP	ERA5
	6th	Scenario **5**	Domain 1 (9 km)	Medspiration	ERA5

Table 4.1.6 (cont'd) Rankings among SST model configurations in each event case through TOPSIS Analysis Results

	7th	Scenario **1**	Domain 1 (9 km)	WRF - ERA5	ERA5
	8th	Scenario **7**	Domain 1 (9 km)	NCEP	ERA5

4.2 Mediterranean – Autumn Event (2017/11/26 - 2017/11/29)

The first case to be investigated under the sensitivity analysis of WRF model on predictions, is the autumn event of the Mediterranean region. According to recorded data, the actual date of the event is 28 of November 2017. However, because the model needs to some spin up time to build an active atmospheric system on the study area during the actual event hour, all four of the events' periods are considered with one before the event date. That's why, the model run time of each case, has determined as 73 hours in total.

In **Figure 4.2.1**, precipitation and temperature changes of the main station of this event where the highest rainfall was recorded, has shown. As it can be seen from this graph, the peak rain amount dropped on the region is approximately 30 mm (29.6 mm precisely) and that occured almost at the end of 73 hours period. From the observation dataset that is taken from GDM, the main station of this event is Manavgat / Antalya station and like in **Figure 4.2.1**, the event occured around the surrondings of this station on November 28 at 19:00 UTC.

Sudden and sharp changes in air temperatures seem very effective on precipitation formation over the region. Since most of the time, temperature usually drops while it is raining and then it rises again when there is no or not much rain formation. Especially, from the dramatic decrease in temperature at the peak precipitation hour indicates a convective system. The cumulative precipitation also proves that the actual change in total, created by the rain amount at the peak hour.

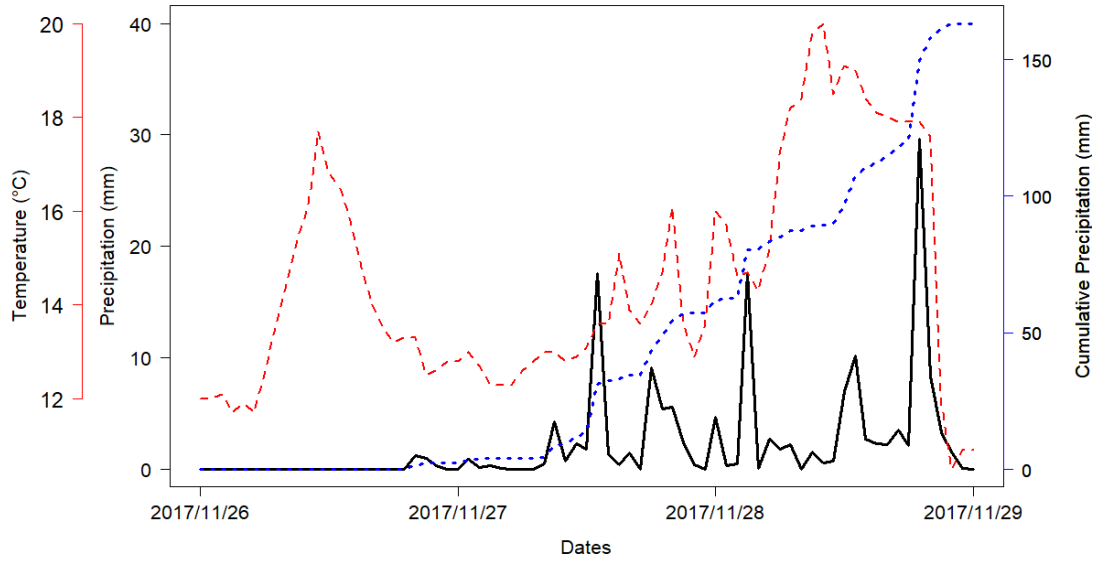

Figure 4.2.1 Precipitation and Temperature time series of the main station (Manavgat - Antalya) for Mediterranean – Autumn event through the model run period between 2017/11/26 – 2017/11/29. Black solid line refer precipitation amounts dropped over the station while the dashed red line indicates recorded temperature of the station. Dashed blue line represents the cumulative precipitation amounts through the time

As mentioned before, through the scope of sensitivity analysis, 96 configurations / scenarios are run by the WRF model in each case of this thesis. The performances of these scenarios and their overall prediction powers during this event period are shown on the graphs in **Figure 4.2.2**. One of them includes only the configurations which take the boundary conditions from GFS dataset whereas the other one represents the scenarios worked with ERA5 dataset. By this way, the time series graphs offer a general idea about the sensitivity analysis of the WRF model on the performances of input meteorological datasets for the specific event case. Of course, to be able to do this comparison between GFS and ERA5, mean of observation stations' data (solid black line) is also represented onto these graphs.

The raster time series which are placed at the bottom of **Figure 4.2.2**, depict the bias variance among the configurations. It can be observed from **Table 3.3.4**, the first 48

scenarios are run by the GFS while for the rest of them, 49 – 96, ERA5 dataset is prefered to use.

Through the light of this aspect, the timeseries and the bias graphs on **Figure 4.2.2**, demonstrate that ERA5 used scenarios performed better than GFS used ones since the gap among the means of model and observation (black and red solid lines) is much more smaller especially at the peak hour when the means reachs maximum value (in this case at 2018.11.28 _ 00:00), on its graphs. It is apparent that the most of GFS dataset used scenarios made huge overestimations to predict the maximum rain amount, although they were enable to build most unstable atmospheric conditions at the peak hour. That is the reason why the precipitation bias of many GFS configurations has estimated more than 3 mm (red colored rasters at hour 48) although it is around 0 - 1 for most of ERA5 configurations (rasters colored with white at hour 48) in the bias raster representations at the bottom.

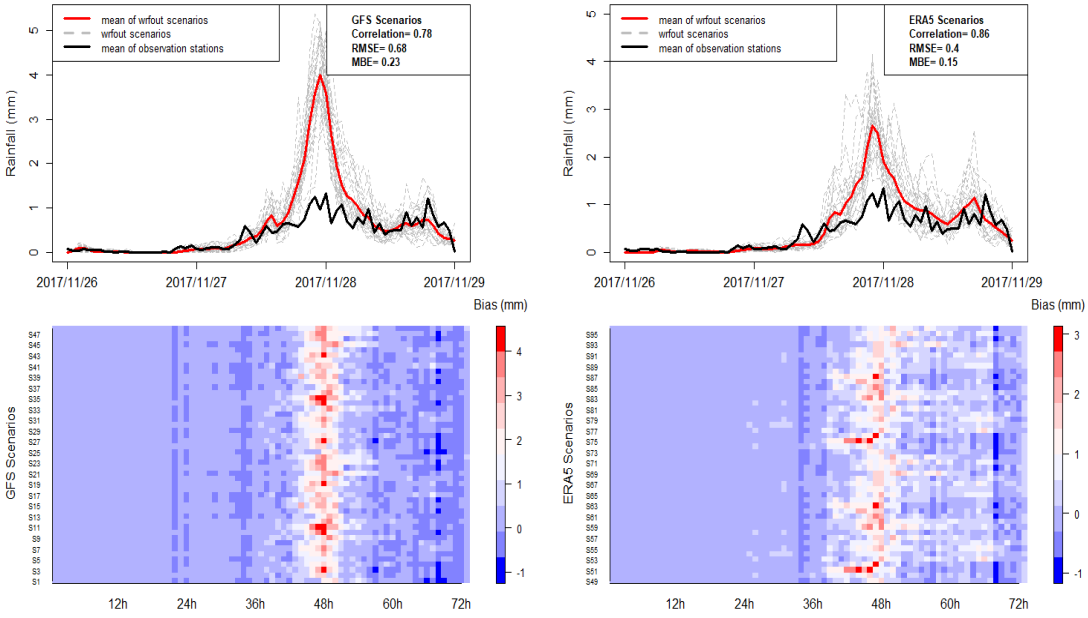

Figure 4.2.2 Average precipitation and bias raster plots of observation and model forecasts throughout the run period. The dashed gray lines represent the each model prediction scenario while the red line indicates the mean of these model scenarios and the solid black line shows the mean of observed precipitation regime in 3 days. The left column illustrates the results for GFS source used model predictions, the right column demonstrates the ERA5 source used model predictions

The performances of 96 scenarios are also wished to be compared by some common statistical parameters for each event examination. In **Figure 4.2.3**, mean bias (MBE), root mean square (RMSE) and standard deviation (SD) errors with correlation coefficient (R) of the model predictions are shown as the bar plot type. While the y axis on these graphs indicates the statistical parameter, the x axis represents the scenario numbers. As mentioned on the previous chapter (on **Table 3.3.4**) , the first 48 of scenarios are run by GFS input dataset whereas the rest 48 used ERA5 dataset to generate their forecasts. Hence, from the graphs in **Figure 4.2.3**, both general and specific performances of each type of configuration can be obtained. Additionally, again by looking at **Table 3.3.4**, it can be observed that odd numbered scenarios refer the domain 1 (with 9 km horizontal resolution) and even numbers depict the model configurations are run over domain 2 (with 3 km horizontal resolution) among the total numbers of scenarios. This is also stated on the colored domain legends of every graphs in **Figure 4.2.3**. All in all, this kind of panel plots can be considered as a beneficial tool to be able to see the overall performances of scenarios based on their grid sizes and meteorological input sources that they have used.

Through the light of this information, the black bars on MBE graph, which means second domain configurations, produce small errors comparing to the red bars of parent domain. Similar outcome can be said for other error parameters like RMSE and SD. In terms of input source types, the model mostly generates lower errors and relatively higher correlations when it is run by ERA5 dataset rather than GFS. Yet, according to the first 10 scenarios ranked by TOPSIS analysis **Table 4.1.3**), the scenarios take the boundary conditions from GFS source usually perform better than ERA5 source scenarios. That means if the aspect numbers to look for in an examination of this study increases, the overall picture of performances of scenarios can change a lot.

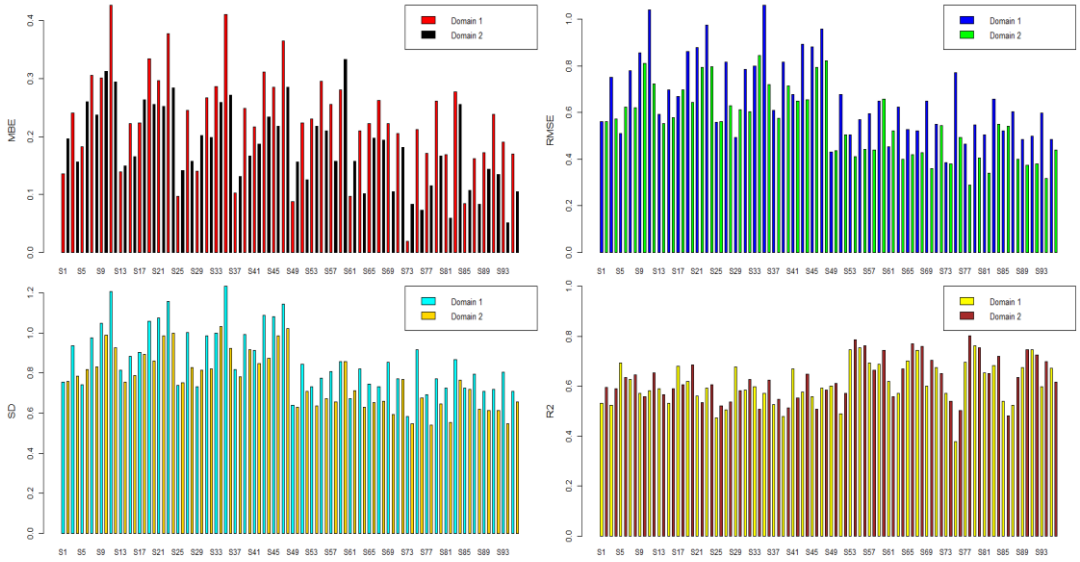

Figure 4.2.3 The performance comparison among 96 scenarios based on some statistical parameters. Mean bias error ('MBE') , Root Mean Square Error (RMSE), Standard Deviation (SD), Correlation Coefficient (R)

Additionally, the best and worst scenarios (based on the TOPSIS results and shown by **Table 4.1.4** and **Table 4.1.5**) of these datasets' performances over the region are also essential to look at. According to this, both the observed data and the model outcomes are illustrated on **Figure 4.2.4, Figure 4.2.5** and **Figure 4.2.6.** The map at the top on these figures refers the real conditions while the four maps at the bottom, picture the best and worst model performances through the TOPSIS Analysis. Here, only 3 km scenarios are included into these graphs as with their higher resolutions, these type of configurations give most accurate results for the model prediction performances. The lower resolution like 9 km of parent domain in this study, usually produce less bias and high correlation but this does not prove its real success because by the coarse grid sizes of parent domain may lead the model to miss or miscalculate the actual event formation which occurs on relatively smaller area such as the basins. Hence, the best and worst configurations' maps represented in the event cases are only taken from **Table 4.1.5**, for the domain 2 (3 km) scenarios.

Precipitation contours on real condition map has prepared from the interpolation (based on nearest neighbour methods) of observation stations data over the region. Besides, each black circle represents a valid station which was actively recording rainfall during the event period. These station circles are filled with the colors according to their precipitation values. The scale of 'Station Precipitation' has arranged to show both the stations and the interpolated area's precipitation values on the same labelbar.

With **Figure 4.2.4**, the best and worst model configurations are analysed for their ability of catching the right spot and producing enough rain on the peak hour. This is important to see as it shows the model prediction sensitivities for excess precipitation cases. Therefore, the maps on **Figure 4.2.4** are drawn for the peak hour when the maximum precipitation is recorded, for this event. Based on the station data provided by GDM, the peak rain amount dropped over the region in three days period, is found out as 29.6 mm on November 28 at 19:00 UTC. Even though, they are ranked as 'the bests and worsts' through the TOPSIS analysis, actually none of the models can able to predict maximum precipitation (around 30 mm) and catch the hotspot near to main station. Therefore, although the four of models could generate the overall pattern of precipitation (< 10 mm) on the region because they miss the sudden heavy rainfall formation, their predictions are far more away then the reality. Still, there is an order among them since TOPSIS Analysis tells the best and worst by looking at the differences and similarities between the model and observation for whole region along 73 hours.

Yet, since the model performances at the peak time are not very successful and it only offers 'main station focused' aspect of the event, the highest mean precipitation hour is also included into this analysis by **Figure 4.2.5**. The aim here, is to observe how the model forecasts' accuracies have changed when the precipitation was recorded by most the stations so the larger area of region is wet.

As it can be obtained from **Figure 4.2.1**, the average rain amount of stations reachs its peak at midnight of November 28. From the models' maps in **Figure 4.2.5**, it can be said that different from previous figure, all of the models rather best or worst, GFS or ERA5, overestimate the rain amounts on very larger portion of the region. This indicates that, the model could notice the atmospheric instability over multiple distant spots. However, it could not produce enough amount and distribute accordingly. They all are able to find the hot spot of this hour (red colored point with 10 – 12 mm) but their general patterns do not fit into the reality. Though they are not successful, by looking at only this hour performances, it can be obtained 'best ERA5' model offers the closest forecast since the level of overestimation is little bit smaller here and additionally, it is able to catch and drop correct rain amounts on darker colored stations at the upper parts of inland area. In last two maps for instance (**Figure 4.2.5c,d**) , excess rainfall (red colored area) occupies large spaces and gathered onto irrelevant places. The best models, on the other hand, distributes the precipitation amounts on the region by this way, they are able to catch closer prediction to the actual conditions. Probably, that is the usual behaviour of those for 73 hours and that's why the errors are calculated much more smaller so they are selected as 'best' configurations among all GFS and ERA5 scenarios by TOPSIS Analysis.

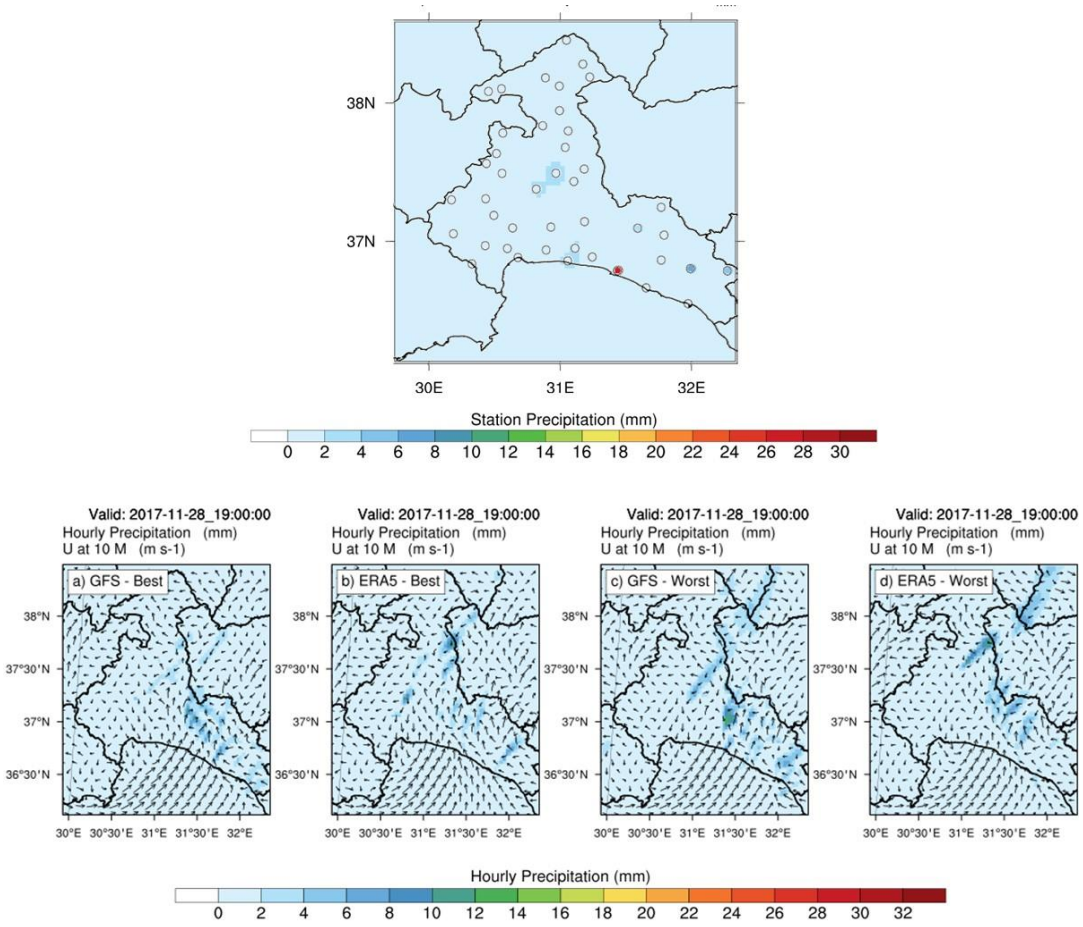

Figure 4.2.4 Precipitation maps of observation and model predictions at the peak hour of Mediterranean autumn event (2017.11.28_19:00:00). The map at top illustrates the interpolated station precipitation contours whereas the black circles refer the locations of these stations. The graphs at bottom represent the forecasted precipitation contours and wind speed vectors at 10 m for both best and worst performances of GFS and ERA5 source used scenarios (These scenarios are determined from **Table 4.1.4)**

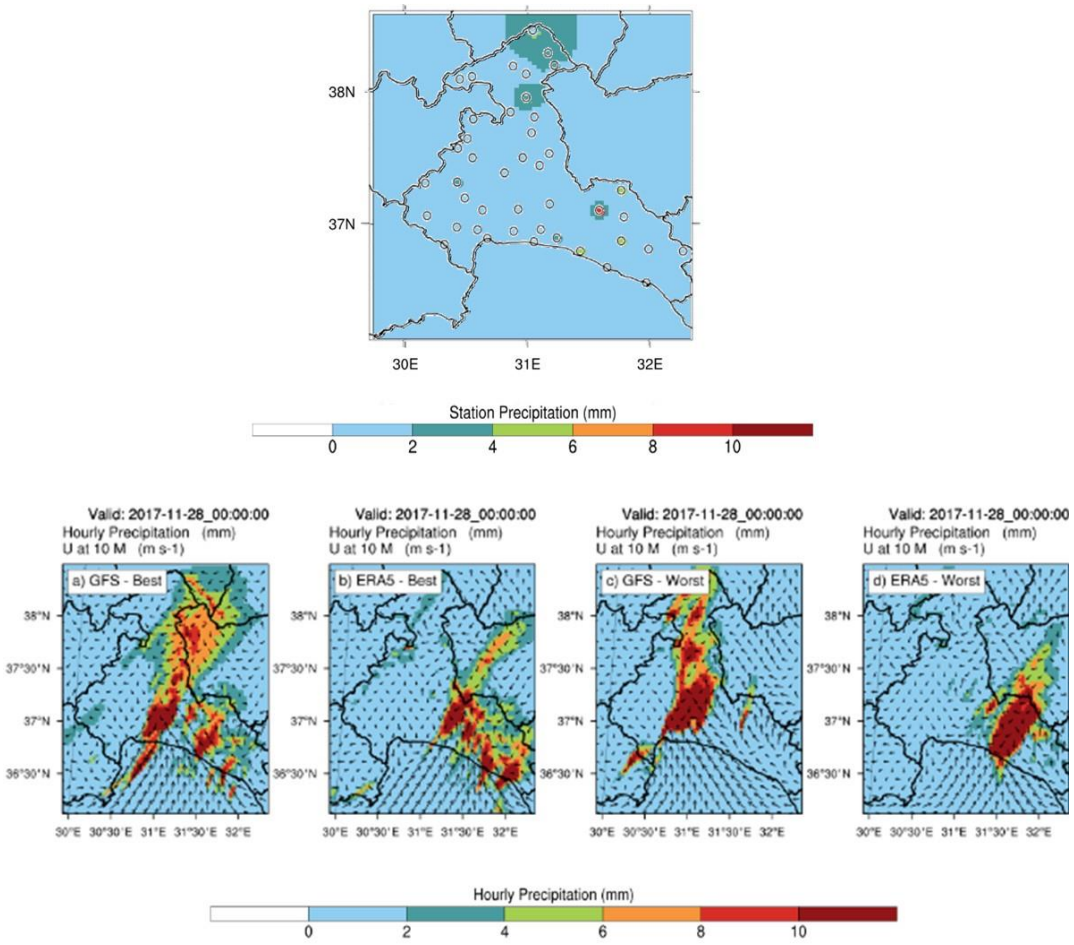

Figure 4.2.5 Precipitation maps of observation and model predictions at the maximum mean precipitation hour of Mediterranean autumn event (2017.11.28_00:00:00). The map at top illustrates the interpolated station precipitation contours whereas the black circles refer the locations of these stations. The graphs at bottom represent the forecasted precipitation contours and wind speed vectors at 10 m for both best and worst performances of GFS and ERA5 source used scenarios (These scenarios are determined from **Table 4.1.4)**

The overall results of best and worst configurations for this event period are represented on **Figure 4.2.6**. Here, again the map at the top illustrates the total precipitation amount distribution which has estimated by the interpolation of observation stations data, throughout the region. The four maps pictured **Figure 4.2.6**, show the best and worst GFS and ERA5 scenarios' (according to TOPSIS Analysis) performances at the end of 73 hour model run period. In this case, it is November

29th of 2017 at 00:00 UTC. They also demonstrate the cumulative rain amounts dropped over the Mediterranean region.

Based on this information, it can be easily identified that the most of the precipitation (both yellow with 120 – 140 and orange with 140 - 160 mm colored grids on **Figure 4.2.6**) during the event period fell around the main station, where also receives the peak precipitation in **Figure 4.2.6**. When the model outcomes are examined, comparing to 'best' scenarios, there is an accumulation of precipitation in 'worst' configurations (whether GFS or ERA5). The worst option of GFS (**Figure 4.2.6c**) has already missed the activity surronding main station and moved towards to the center inlands of region. On the other hand, 'ERA5 – Worst' option actually catches the hot spot but it makes huge overestimation there which leads to damage on its prediction accuracy. Probably, that's why it has ranked at the end by TOPSIS. Although they have some overestimations, both of the best configurations offer closer picture of the overall precipitation distribution to the station map at the top, especially 'GFS – Best'. Still, their grid based performances around main station are poor since the rain dropped over there can not 80 – 100 mm whereas it should be somewhere between 120 – 160 mm.

Additionally, the direction of wind vectors at 10 m indicate that the precipitation has carried from sea to the right handside of region in all four model configurations.

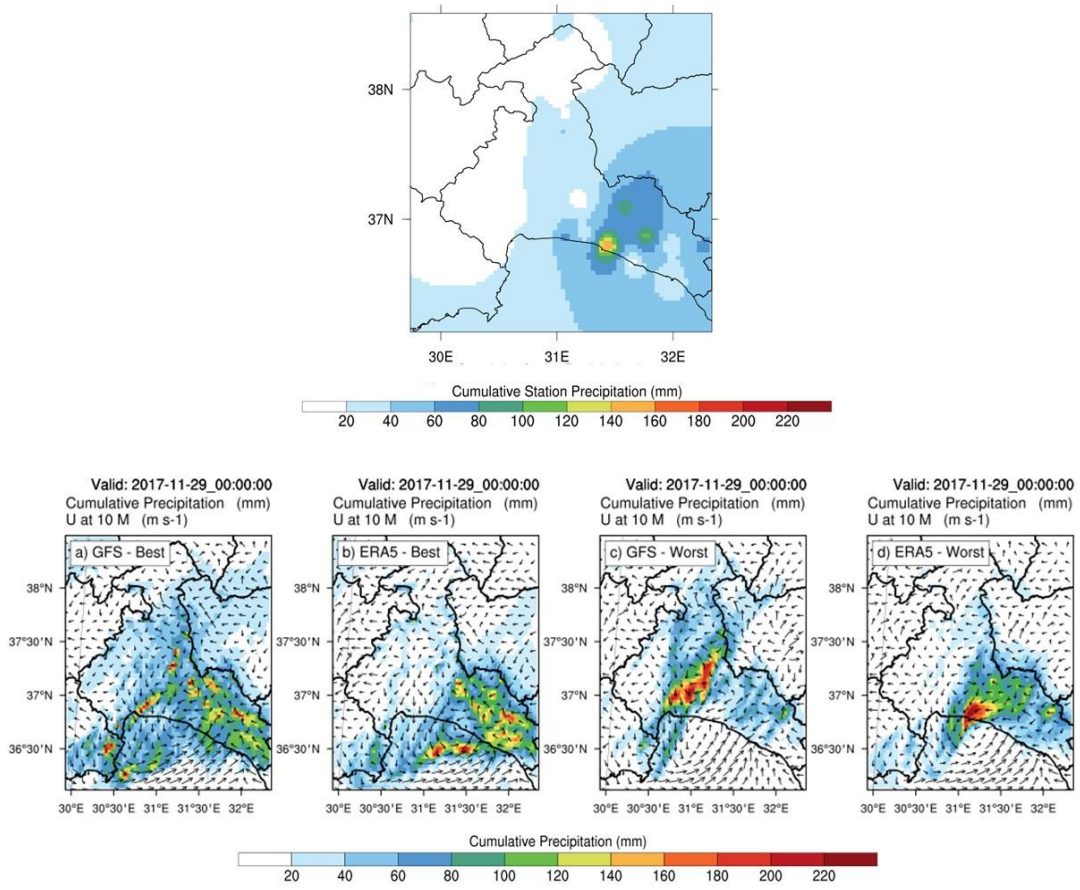

Figure 4.2.6 Precipitation maps of observation and model predictions at the end of Mediterranean autumn event model run period (2017.11.29_00:00:00). The map at top illustrates the interpolated station precipitation contours. The graphs at bottom represent the forecasted precipitation contours and wind speed vectors at 10 m for both best and worst performances of GFS and ERA5 source used scenarios (These scenarios are determined from **Table 4.1.4)**

So far the model scenarios are evaluated for various statistical analyses as well as the peak and highest mean hour performances to observe precipitation amount and distribution over the region. Those comparisons are helpful to have an idea about the successful configurations and the common schemes used in them. Yet, one of the main aims of sensitivity analysis is also determining most vulnerable side of the model which the model responds quickly when that thing has changed. Since in this study, the physical parameters and input data sources are the variables which were not kept constant and provided various combinations to try by the model, it can be said the current sensitivity analysis has been conducted to examine their impacts on the WRF model predictions. This type of analysis represents more general aspect of model sensitivity rather than which scheme mechanism achieved to mimic real conditions best.

To be able to find the impacts of parameters into WRF model, the variance between each physical parameter such as microphysic, cumulus and planet boundary layer, are investigated. For this purpose, as it can be seen from the graphs in **Figure 4.2.7**, the mean precipitation amounts of parameters are illustrated through the event period and each of them are divided based on the used schemes of scenarios in **Table 3.3.4**. That means every colored line shown on these graphs, refers the average precipitation prediction of scenarios worked with that physical scheme in their configurations whereas the dash black line indicates the mean of observed precipitation as the reference profile.

For instance the graph at top, depicts the means of rainfall produced by Kessler scheme (KS) used scenarios with blue color, Eta scheme (ES) used ones with green, WRF Single Moment 6 (WSM6) with orange and lastly Aerosol Aware Thompson (AATS) with dark red. Since the microphysics parameterization option has been opened for both domain 1 (9 km) and domain 2 (3 km), the configurations that are used to calculate the mean of precipitation lines on this plot include 96 scenarios in total.

This condition is also valid for PBL graph at the bottom. However, because the cumulus parameterization has only applied on domain 1 configurations (odd numbers on **Table 3.3.4**), the total scenario number of three cumulus schemes on that plot is 48. Normally, the input data source is another varible that is changing through the 96 of model configurations in this sensitivity analysis. Yet, as they have already showed multiple times on previous analyses of this event, here they are not preferred to drawn again.

First of all, just like the evaluations had done before, this kind of representation of scenarios can make the performances of physical schemes on model clear to differenciate. But still, in all plots, it also can be easily noticed that there is an overestimation without depending on scheme type or physical parameter. Besides, this current analysis is mainly done to find which physical component establishs superiority on which event forecasts. Therefore, the variance ,with another word the gap, between the lines can be considered as a good indicator via showing the impact of each parameter on WRF model. For the current event case (Mediterranean autumn event), the variance (the gap) between the microphysical scheme lines (**Figure 4.2.7a**) is relatively bigger than the gap in two PBL schemes (**Figure 4.2.7c**) which means PBL component of the atmospheric system builded by the model, does not create great difference on the predictions of this event like microphysics does. Since, even though the lines are close to each other at topmost graph, there are still visible gaps among them. Hence, using different microphysical scheme affects the model process very much for the current event predictions. Similar interpretation can be done for cumulus schemes, too. Because the variance between each approach's average is quite obvious. For example, Grell Freitas (GFES) cumulus scheme used models tend to produce excess rain during the peak hour, this leads them to have a wider range of values bigger than the mean of observed data whereas Kain Fristch scenarios (KFS) draw the same patter with less overestimation around peak hour. That's why, the variance among these two lines grows for this period that proves the cumulus scheme impacts on WRF model during intense precipitation occurence.

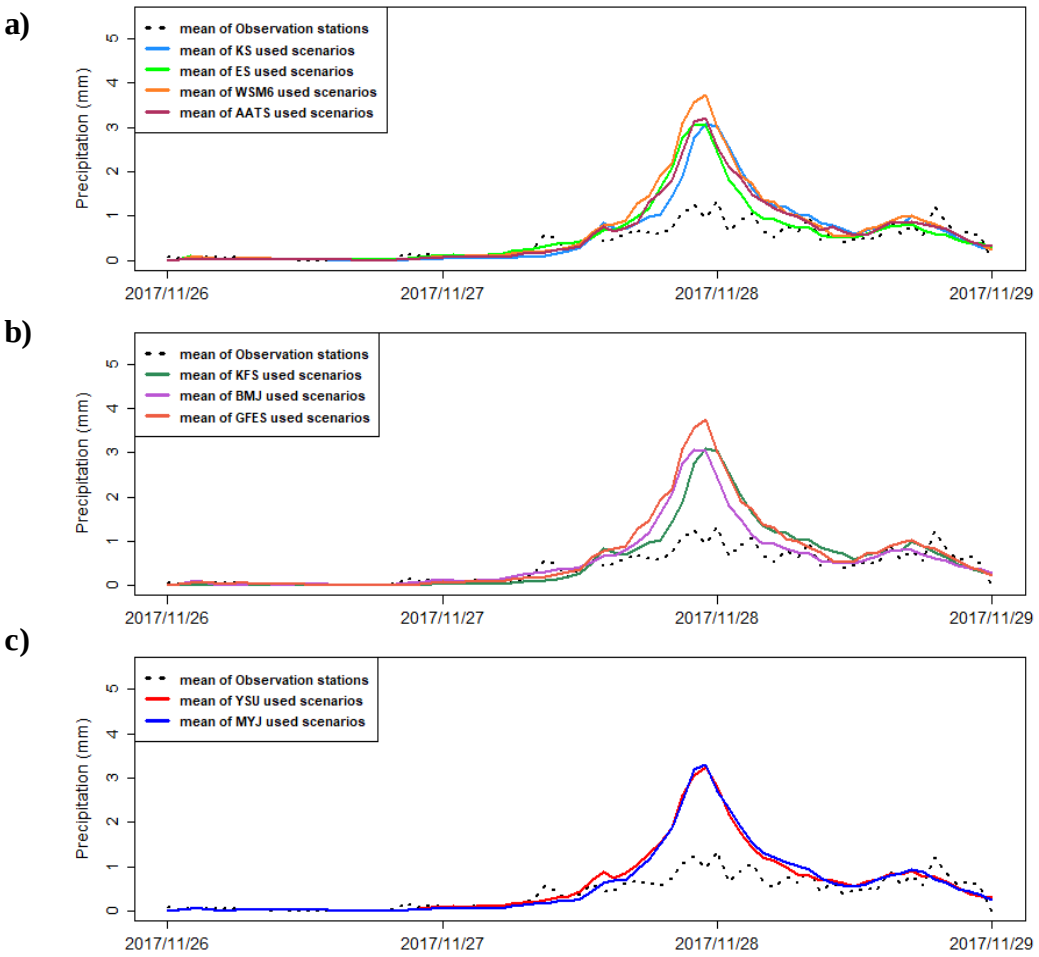

Figure 4.2.7 Variance analysis of the physical parameter schemes based on the observation stations' and model scenarios' precipitation data through the run period of autumn event of Mediterranean region. The dashed black line indicates the observed data. The colorful lines in each plot, refer the model precipitation patterns according to the schemes they used. The plots: a,b and c are prepared to represent the scenario performances on microphysics, cumulus and PBL physics, respectively

4.3 Mediterranean – Summer Event (2017/08/29 - 2017/09/01)

Second event is a summer seasonal heavy precipitation recorded on Mediterranean region. Likewise the other three cases, here too, the model has run for 73 hours even though the actual event happened on 30th of August 2017.

The main station of this event is determined as Sutculer station in Isparta province with 59.2 mm. The precipitation – temperature time series of the main station has shown at the graph **Figure 4.3.1**. One more time, the solid black line refers the precipitation amount whereas the dashed red line indicates air temperature fluctuation of the current event. The dashed blue line, on the other hand, depicts the changes in cumulative precipitation through three days event period. By this way, the event occurence can be observed much clearly because as it can be seen from **Figure 4.3.1**, before and after the peak hour, there is no rain on this portion of the region. Therefore, the only change in cumulative precipitation occurs at the peak and only rainy hour of the event which is August 30 at 14:00 UTC. Since this is a summer time event, the temperatures are high in daytime and usually drops little at nights. From this perspective, the main station recordings offers a typical summer time precipitation event.

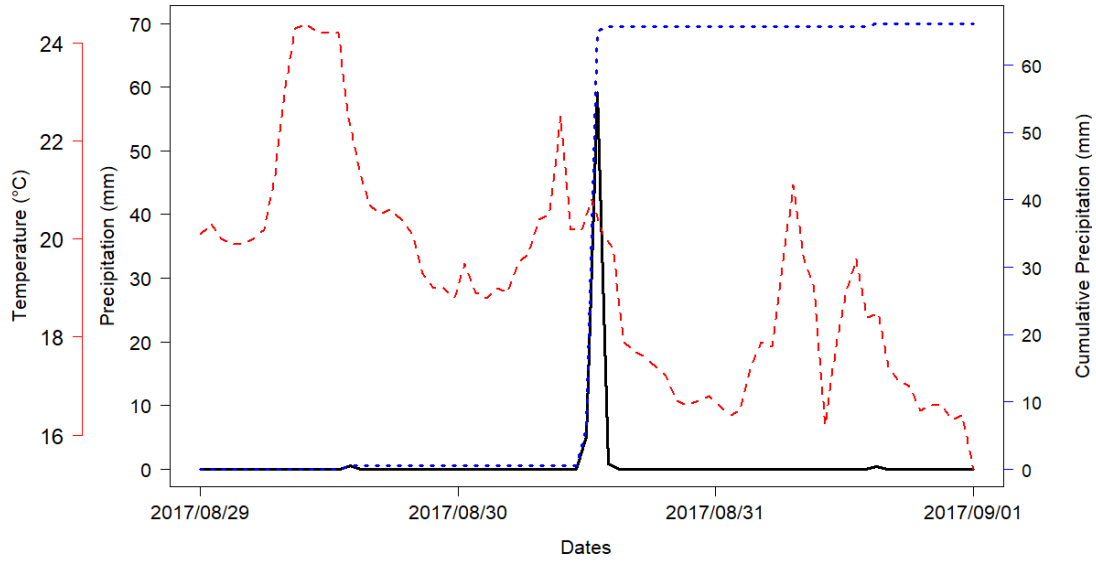

Figure 4.3.1 Precipitation and Temperature time series of the main station (Sutculer – Isparta) for Mediterranean – Summer event through the model run period between 2017/08/29 – 2017/09/01. Black solid line refer precipitation amounts dropped over the station while the dashed red line indicates recorded temperature of the station. Dashed blue line represents the cumulative precipitation amounts through the time

From the average of model scenarios on **Figure 4.3.2**, neither GFS nor ERA5 dataset used configurations are achieved to draw a similar profile to the station data. Since, even though they could catch the two peak times during the period, the general rainfall dropped on the region is much less than the real conditions (see the gap between the black and red solid lines on the graphs). Still, because the characteristic of this event is not very suitable with the events which bring enourmous amount of rain and take wide areas under their impacts, the mean of observation stations also does not pass over 2.5 mm. That's why, the bias values shown underneath via the rasters are quite small.

Although there are not huge differences between two meteorological sources' bias graphs, the numbers of negative bias rasters which indicates the underestimation, at the peak recorded precipitation hour are fewer for GFS scenarios comparing to ERA5. However, a couple of hours before and after the peak hour, GFS scenarios represent more positive biases (red colored rasters) than ERA5. Yet, because the range of bias values are quite small, the over and underestimations onto this event can be neglected to compare. As it can be seen from the timeseries at the top, both GFS and ERA5 scenarios provide very similar average predictions, they are far more away to generate real maximum rain amount dropped over the region.

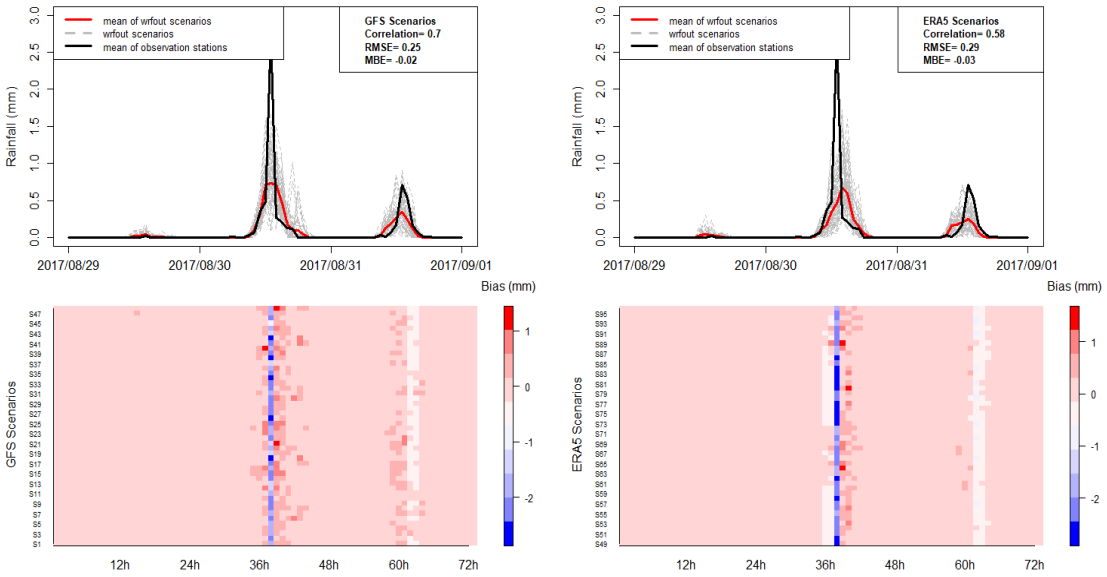

Figure 4.3.2 Average precipitation and bias raster plots of observation and model forecasts throughout the run period. The dashed gray lines represent the each model prediction scenario while the red line indicates the mean of these model scenarios and the solid black line shows the mean of observed precipitation regime in 3 days. The left column illustrates the results for GFS source used model predictions, the right column demonstrates the ERA5 source used model predictions

As in autumn event of Mediterranean region, the scenarios of its summer event are also compared through some statistical parameters. However, the low performances of 96 scenarios can be easily seen by looking at the overall display of four graphs in **Figure 4.3.3**. From the negative MBEs, almost all of the scenarios underestimate real precipitation amounts, especially in nest or domain 2 (3 km) scenarios. Actually, this condition is valid for all three error plots because the errors of domain 1 (9 km) configurations are relatively smaller and their correlations seem much more higher than the domain 2. Different from previous case, the bars of plots here, tell that the first 48 scenarios produce more accurate forecasts to the reality than the rests. Thus, GFS used models perform slightly better comparing to ERA5 for this event and TOPSIS Analysis results (from **Table 4.1.3**) also verify this comment.

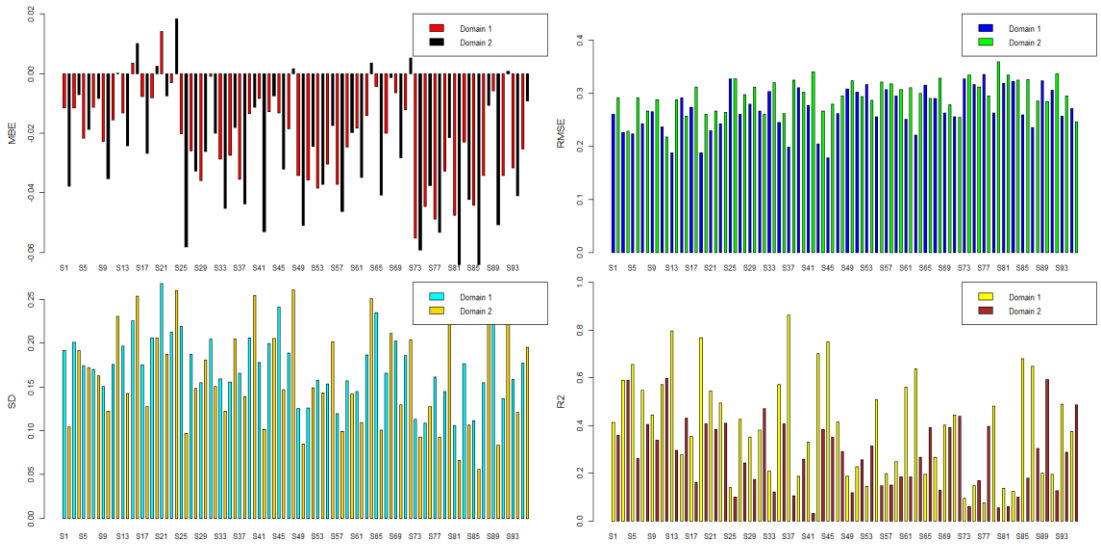

Figure 4.3.3 The performance comparison among 96 scenarios based on some statistical parameters. Mean bias error ('MBE') , Root Mean Square Error (RMSE), Standard Deviation (SD), Correlation Coefficient (R)

Likewise the previous case, again both peak precipitation and maximum mean precipitation hours are wanted investigate in the scope of this event. However, because the rainy time of region is same with the time when the highest rain drops, only this hour has been drawn on the figure.

Based on the maps in **Figure 4.3.4**, without depending on the rankings of model configurations (best or worst, GFS or ERA5), they all could not achieve to find the hotspot (around main station) ,which is the red colored point in Station graph on the top, of this event. Normally, the model forecasts should form approximately 60 mm rain on a single point; however, none of them even excess 20 mm all over the region. In fact, this failure is not special only to four configurations on the figure but it has already observed from all of 96 scenarios average precipitation amounts through grey lines on the time series graphs in **Figure 4.3.2**.

Hence, by looking at the maps on this hour, it is not much possible to decide the best and the worst performance among the four predictions.

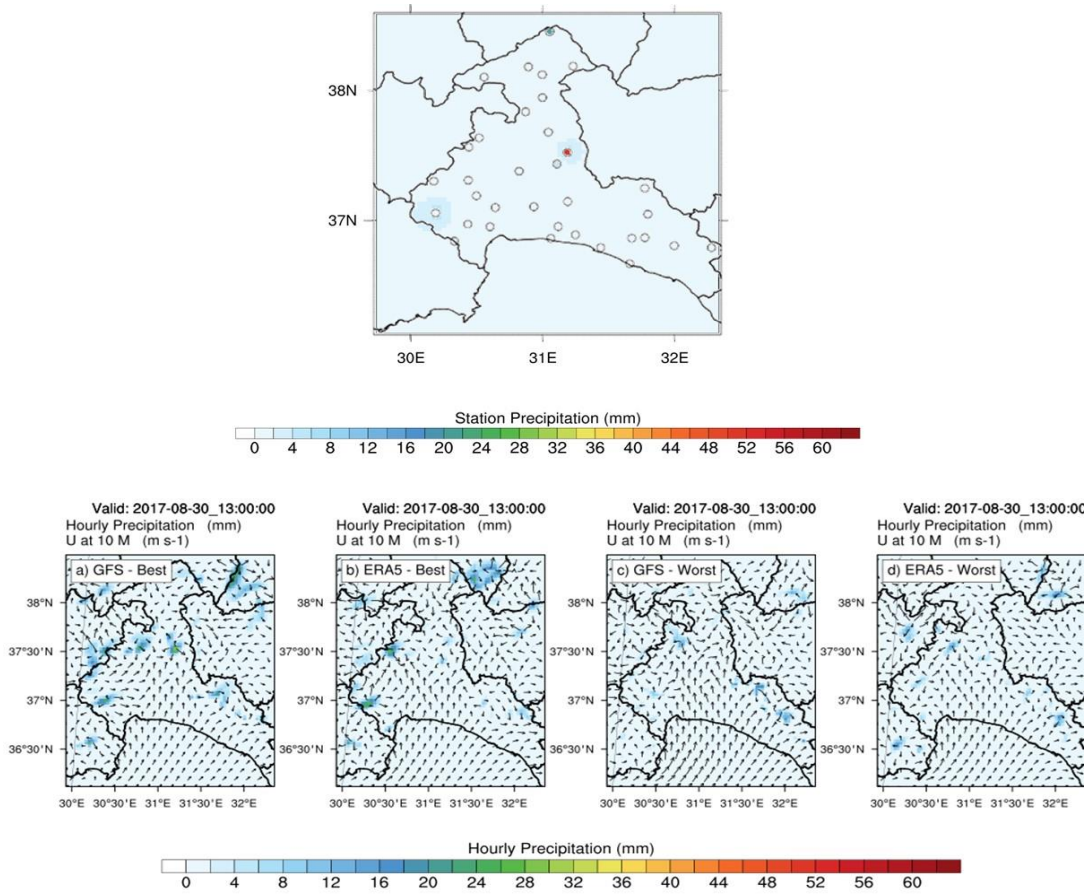

Figure 4.3.4 Precipitation maps of observation and model predictions at peak hour (and also the maximum mean precipitation hour) of Mediterranean summer event (2017.08.30_13:00:00). The map at top illustrates the interpolated station precipitation contours whereas the black circles refer the locations of these stations. The graphs at bottom represent the forecasted precipitation contours and wind speed vectors at 10 m for both best and worst performances of GFS and ERA5 source used scenarios (These scenarios are determined from **Table 4.1.4)**

The prediction performances of the model configurations at the end of the run period are represented in **Figure 4.3.5**. Based on the event information and determined model run period (73 hours), the final hour of WRF has run for Mediterranean summer event is at the midnight (00:00 UTC) of September 1st of 2017.

As mentioned before, this event shows a typical convective system characteristics. That's why, the interpolated precipitation on the Station map at top of **Figure 4.3.5** only points out couple of grids. With maximum cumulative precipitation (60 – 70 mm), one of the these grids indicate the same location of the main station determined for this event. Considering the highest amount dropped over this station in **Figure 4.3.4** and the total amount here in **Figure 4.3.5** it is also clear that almost all portion of the precipitation during this event fell on August 30 of 2017 at 13:00 UTC.

Yet, likewise the peak and highest mean map illustrations, because the event is so specific to one location (around main station only) and there is not much rain obtained overall the region, the general model performances for this event period are quite poor. Since the data to conduct various analyses is too limited. This causes that all of the analyses' aspects, somehow should be related with the configuration performances on the grid based accuracy, not the whole region. Through this approach, the slight yellow colored grids (60 - 70 mm) in the 'GFS – Best' scenario was able to catch the instability around main station, performed relatively better than others whereas the 'ERA5 – Best' option could still produced closer amounts but missed the actual spot. The TOPSIS Analysis ranked the configurations which could not generate enough amount of precipitation near to the main station, as the 'worst' for both GFS and ERA5.

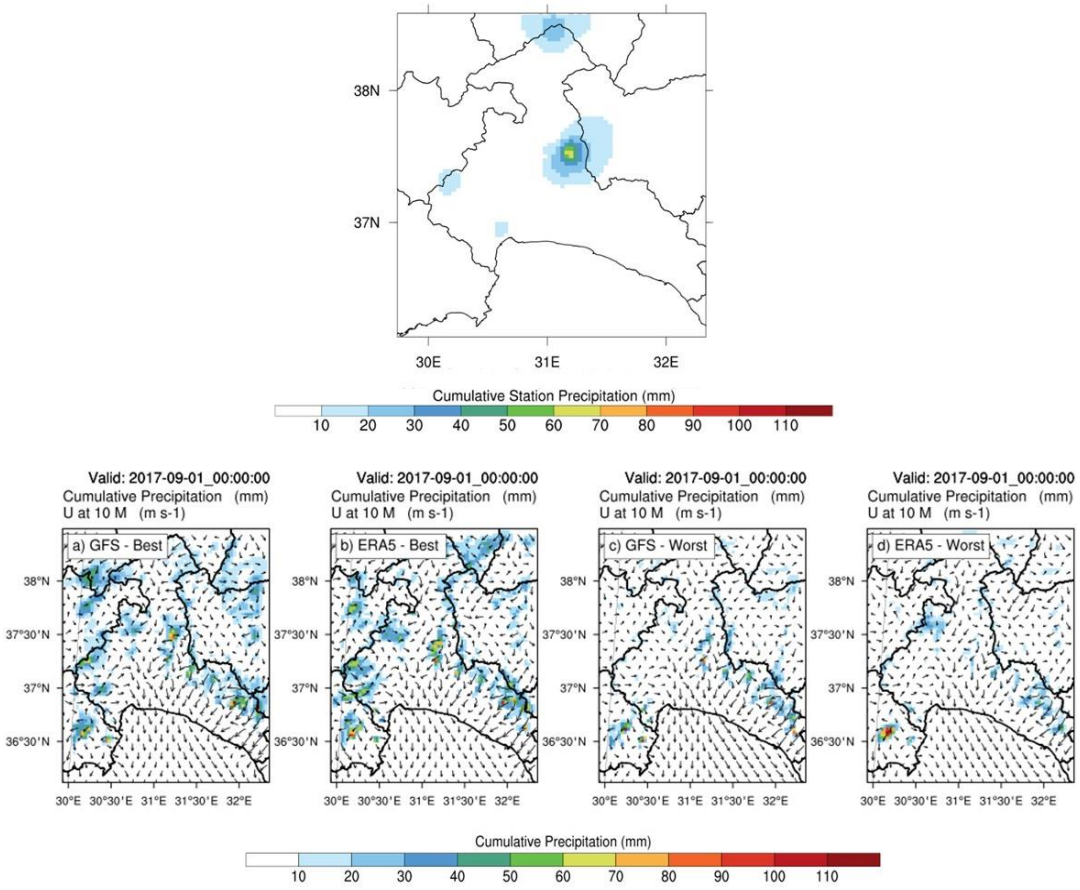

Figure 4.3.5 Precipitation maps of observation and model predictions at the end of Mediterranean summer event model run period (2017.09.01_00:00:00). The map at top illustrates the interpolated station precipitation contours. The graphs at bottom represent the forecasted precipitation contours and wind speed vectors at 10 m for both best and worst performances of GFS and ERA5 source used scenarios (These scenarios are determined from **Table 4.1.4)**

Justlike the many other analyses, the physical parameter comparison of this event also shows lack of sharp differences among the scenarios as the overall accuracy of them is small. That's why, neither depending on the scheme or paramater type, every model predictions make underestimation the rain amount of the current event.

Because of the poor performances of 96 configurations, all three mean precipitation regimes of different schemes and parameters such as microphysics, cumulus and planet boundary layer, in **Figure 4.3.6** look very similar to each other. Hence, the variances or the gaps among the shemes on each plot are quite low, almost '0'. Additionally, because the average rainfall lines draw almost the same patterns for each parameter graphs, the variances between the physical components are also close. This leads the researcher to think none of these three physical components of atmosphere has remarkable effect on the WRF model forecasts for the current event. That's why, changing the schemes used in these parameters does not create a difference in model's results for the current event case.

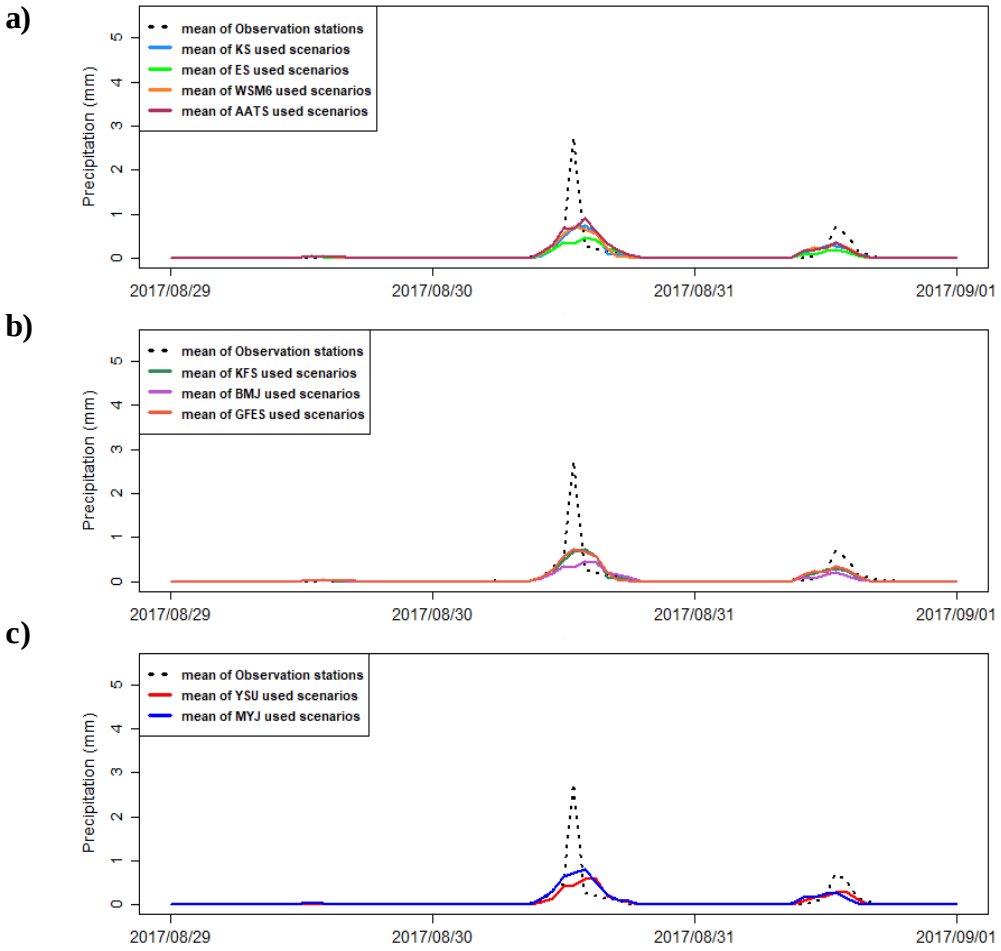

Figure 4.3.6 Variance analysis of the physical parameter schemes based on the observation stations' and model scenarios' precipitation data through the run period of autumn event of Mediterranean region. The dashed black line indicates the observed data. The colorful lines in each plot, refer the model precipitation patterns according to the schemes they used. Theplots: a,b and c are prepared to represent the scenario performances on microphysics, cumulus and PBL physics, respectively

4.4 Eastern Black Sea – Autumn Event (2016/11/13 - 2016/11/16)

Although Eastern Black Sea region generally receives rain throughout the year, the autumn event selected on the behalf of this study, occured on November 14 of 2016 at 06:00 UTC in the morning. Through the observed data, the peak amount of rain was recorded as 40.1 mm by Camlıhemsin / Rize station.

Just comparing this case with the previous two events' graphs, the climatic difference between the regions can be easily seen. For instance, in **Figure 4.4.1**, the total rain amounts at the end of event period, could reached around 400 mm whereas in Mediterranean cases this number could not exceed 150 mm. Additionally, temperature may not be taken as the actual trigger of high amounts of rainfalls in Eastern Black Sea region as it may on Mediterranean. Since most of the time, there is not much sudden fluctuations observed in temperature patterns of this region. Therefore, the intense precipitations do not usually start and end in a short period of time. They generally drop by small amounts and continue along many days which indicates that they tend to show synoptic precipitation event characteristics. Slow and smooth increments in cumulative precipitation regime in **Figure 4.4.1**, again demonstrate the same characteristics' pattern.

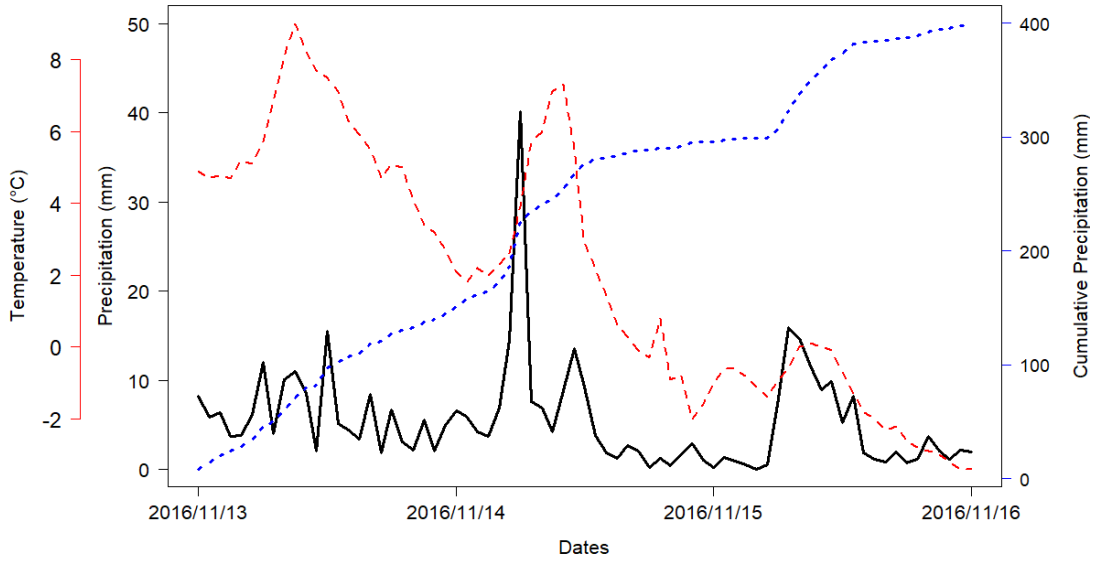

Figure 4.4.1 Precipitation and Temperature time series of the main station (Camlıhemsin – Rize) for Eastern Black Sea – Autumn event through the model run period between 2016/11/13 – 2016/11/16. Black solid line refer precipitation amounts dropped over the station while the dashed red line indicates recorded temperature of the station. Dashed blue line represents the cumulative precipitation amounts through the time

As mentioned multiple times, in Eastern Black Sea region, due to its climatic and orographic features, generally synoptic precipitation system are observed. According to this type of system, the atmospheric instability lasts for many days but the dropped amount of rain is small. Therefore, the precipitation pattern of Eastern Black Sea region does not usually fit the convective systems' profile, where quick heavy rainfall events are mostly seen. This condition can also be verified from the value of peak point of average observed data (black solid line on the time series in **Figure 4.4.2**) as even in the most rainy hour of the region, the mean could not pass 1.2 mm.

According to the illustrations in **Figure 4.4.2**, the overall performances of GFS and ERA5 scenarios are quite similar to each other. In this case graphs, it can be clearly seen that because of the model spin up time, none of the configurations could produce any rainfall before the midday of November 14 of the event period.

Therefore, the model misses the small amounts of precipitation during the first 2 days and again may be that's why, the average of these model configurations were also not successful to provide enough rain amounts at the peak hour.

The bias raster representations at the bottom of **Figure 4.4.2**, again refer the same conclusion and the value ranges of both datasets' scenarios are quite small to make a comparison between them. However, there are still minor differences among two graphs within the last two days of event period. This can point out that GFS configurated models usually perform relatively better than ERA5, as the gap between the predictions and observation is represented lower on the GFS bias raster graph.

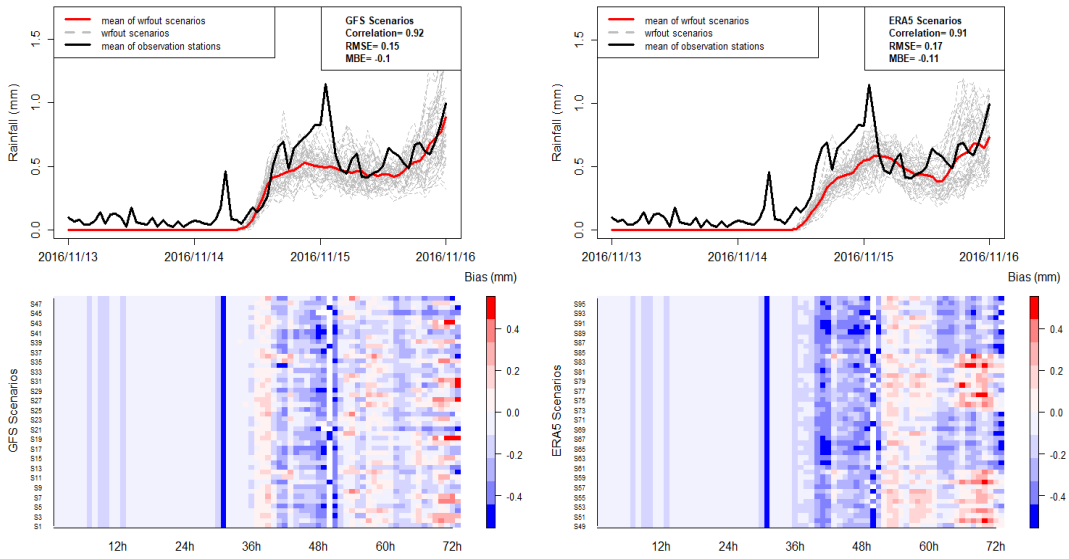

Figure 4.4.2 Average precipitation and bias raster plots of observation and model forecasts throughout the run period. The dashed gray lines represent the each model prediction scenario while the red line indicates the mean of these model scenarios and the solid black line shows the mean of observed precipitation regime in 3 days. The left column illustrates the results for GFS source used model predictions, the right column demonstrates the ERA5 source used model predictions

The statistical performance of scenarios for this event are shown by **Figure 4.4.3**. In this case, the mean bias (MBE), root mean square (RMSE), standard deviation (SD) and finally the correlation coefficient (R) are compared among the 96 different scenarios. From the general values of four graphs represented in **Figure 4.4.4**, it can be said that most of model configurations were able to produce successful predictions as the data range on y axis which has been prepared from the model outcomes, are very small for error parameters. Moreover, without creating any distinction, parent or nested domain (9 km / domain 1 or 3 km / domain 2), GFS or ERA5; the majority of scenarios' correlation values also confirm the general accuracies of these forecasts. According to top 10 best performances list of TOPSIS Analysis (**Table 4.1.3**), on the other hand, the ERA5 dataset used scenarios have come a step forward than GFS.

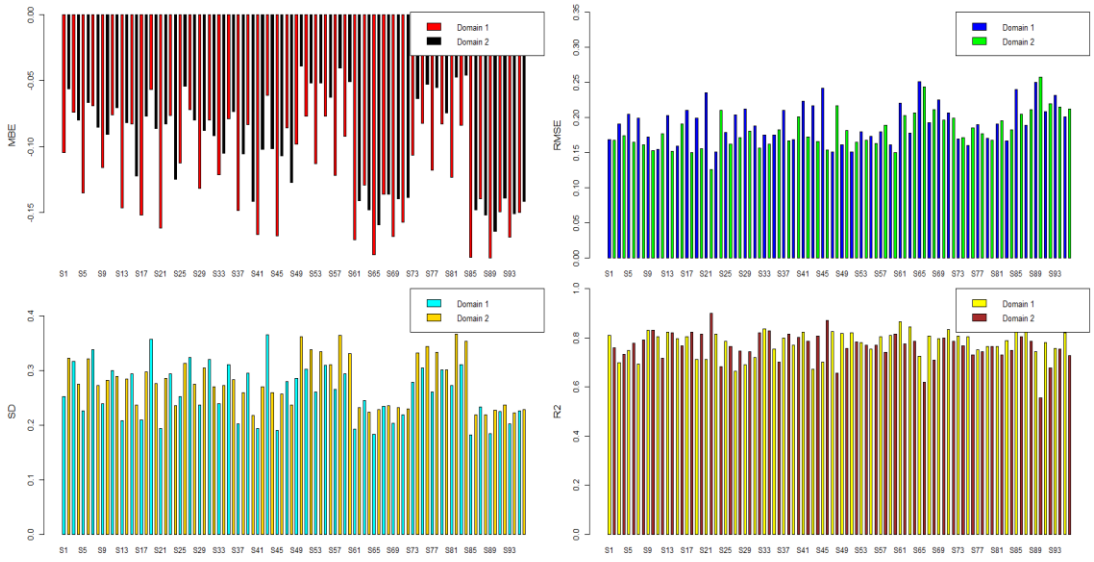

Figure 4.4.3 The performance comparison among 96 scenarios based on some statistical parameters. Mean bias error ('MBE') , Root Mean Square Error (RMSE), Standard Deviation (SD), Correlation Coefficient (R)

The outcomes from the time series graphs represented above, become more visible to observe on the maps by **Figure 4.4.4**. Likewise the previous cases, the map at top illustrates the interpolated station precipitation contours whereas the black circles refer the locations of valid stations at the peak hour. The four maps in **Figure 4.4.4**; however, represent the forecasted precipitation contours and wind speed vectors at 10 m for both the best and worst performances of GFS and ERA5 source used scenarios (**Table 4.1.4).**

Based on the provided stations data through the 3 days run period, the highest rain is recorded in 14 of November 2016 at 6 am with 40.1 mm. Additionally, from 'Station map', the main station (colored in red) where this amount had been recorded, is located at southern east portion of the region and it is not near to the coast. Yet, the common forecast labelbar that has shown at the bottom of the same figure, indicates that none of four configurations achieved to produce even more than 6 mm rain all over the region. Hence, whether it is defined as the 'best or worst of performances' by TOPSIS Analysis, actually none of these four configurations showed an accurate prediction for the peak hour. As in the Mediterranean events, this situation depicts that the WRF model can not create a sensitivity difference on the highest rainfalls if that much amount had only observed for specific locations but not for the larger portion of region. The model can not catch the right points. Of course, here it should be also reminded that the spin up time, which the model uses to build the system before generating a dynamic atmosphere (Yilmaz, 2015; Bonekamp et al., 2018), had cut off from the most of 73 hours run period. In this perspective, the event periods in the model could have been started little bit earlier so that the model may build up the actual instability on the real event time and enhance its accuracy.

Likewise the previous event cases, the maps are again drawn for the highest mean precipitation hour. As it can be seen from **Figure 4.4.2**, almost 1.2 average precipitation amount, the time when most of stations received rain over the region, has determined as 02:00 UTC of 15th November 2016.

In **Figure 4.4.5**, the labelscales of interpolated observed and four model prediction data show that once again the WRF model forecast accuracy has enhanced. Since both of them have exactly the same rain amount range and the overall distribution of observed precipitation has matched with model maps. This result may prove the claim about the effect of impact area size on WRF model prediction success. Because by considering the same type of maps of the previous events, it can be said, the model scenarios mainly catch the general atmosperic activity on the region and perform beter at highest mean precipitation observed hour than the peak precipitation observed hour. The reason underlies this, may be related with the input meteorological dataset. Since if that much rain has recorded by many stations, their data eventually affect the meteorological dataset provided to use in WRF model. That's why, more rain data obtained for that hour means more realistic forecast the model can give. Still, in this case, among the best and worst scenarios shown on **Figure 4.4.5**, ERA5 – Best option (**Figure 4.4.5b**) was able to generate the closest prediction around the most active area in this hour. It could catch the right location (near to the yellow point on observation map) to build up relatively unstable atmosphere comparing to the rest of region. Similar things can be also said about GFS – Best option performance. Yet, here the underestimation on the eastern north point at the coast (the hotspot of this hour) can be easily identified. The performances of these four scenarios on **Figure 4.4.5**, also fit the performance rankings of TOPSIS Analysis for this event period (**Table 4.1.4).**

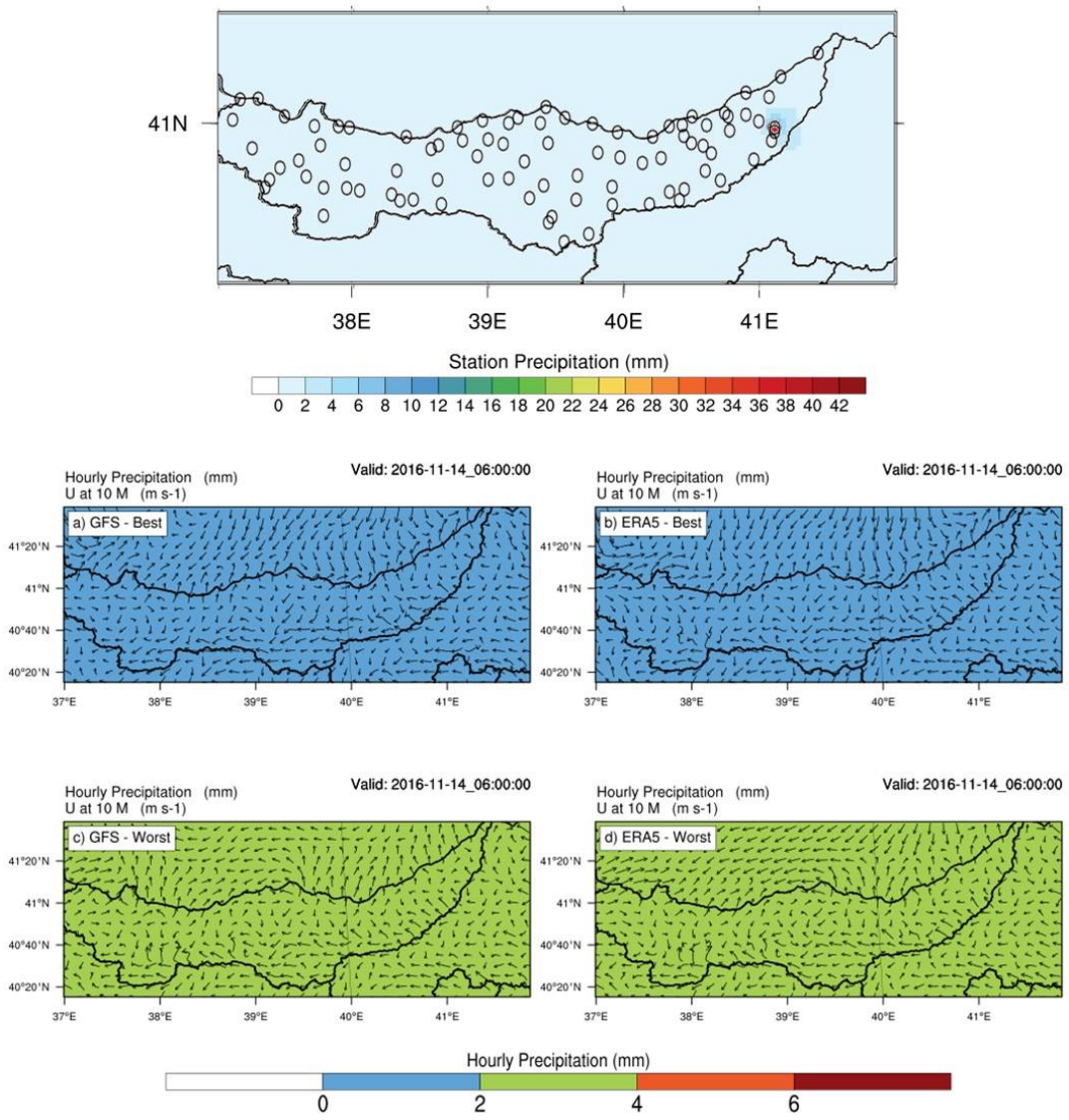

Figure 4.4.4 Precipitation maps of observation and model predictions at the peak hour of Eastern Black Sea autumn event (2016.11.14_06:00:00). The map at top illustrates the interpolated station precipitation contours whereas the black circles refer the locations of these stations. The graphs at bottom represent the forecasted precipitation contours and wind speed vectors at 10 m for both best and worst performances of GFS and ERA5 source used scenarios (These scenarios are determined from **Table 4.1.4)**

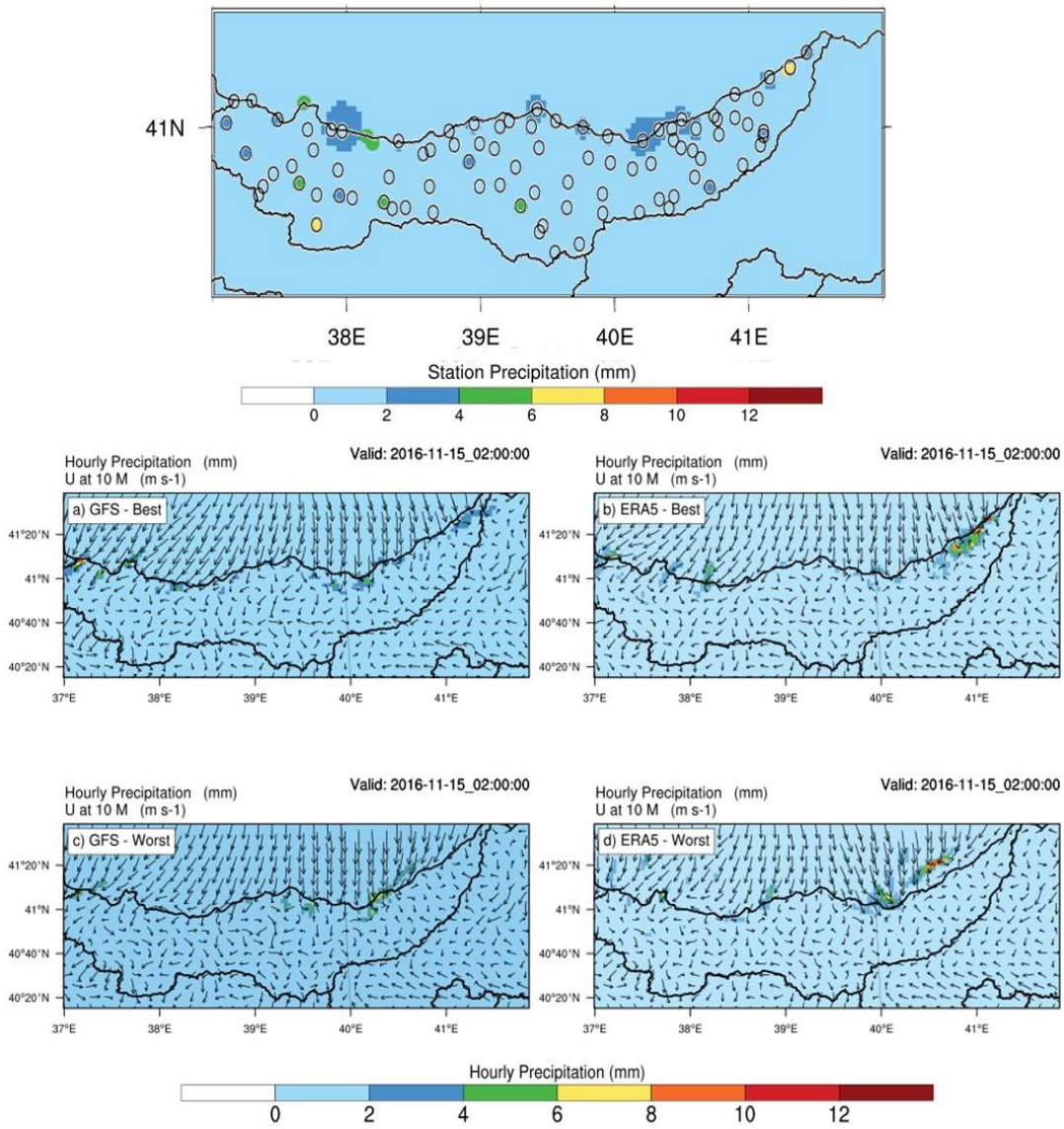

Figure 4.4.5 Precipitation maps of observation and model predictions at the maximum mean precipitation hour of Eastern Black Sea autumn event (2016.11.15_11:00:00). The map at top illustrates the interpolated station precipitation contours whereas the black circles refer the locations of these stations. The graphs at bottom represent the forecasted precipitation contours and wind speed vectors at 10 m for both best and worst performances of GFS and ERA5 source used scenarios (These scenarios are determined from **Table 4.1.4)**

Figure 4.4.6 shows the cumulative precipitation distribution among the station and model data for this event period. After 73 hours run time, model stops at November 16 of 2016 for 00:00 UTC. Here similar to the previous cases, the majority of rain dropped over the main station (100 – 110 mm) that has already represented in **Figure 4.4.4**. Additionally, there is also a single point which is colored into red at the coastal side, has received large amount of precipitation. However, beside that the coastal area of region has already generally dominated by the unstable atmospheric conditions. At this point of view, the four of model configurations at the bottom, perform well enough to differentiate the rain amounts along the coastal line. Comparing to the GFS scenarios (best or worst), the ERA5 ones generate closer predictions to the reality shown by 'Station map'. Since in those two maps, over and underestimations are much more less than GFS, especially as regards the 'GFS – Worst' configuration (**Figure 4.4.6c**). TOPSIS Analysis also verifies this interpretation as it can be seen from **Table 4.1.3**, most of the configurations in top 10 prediction rankings of 3 km are selected among the ERA5 scenarios.

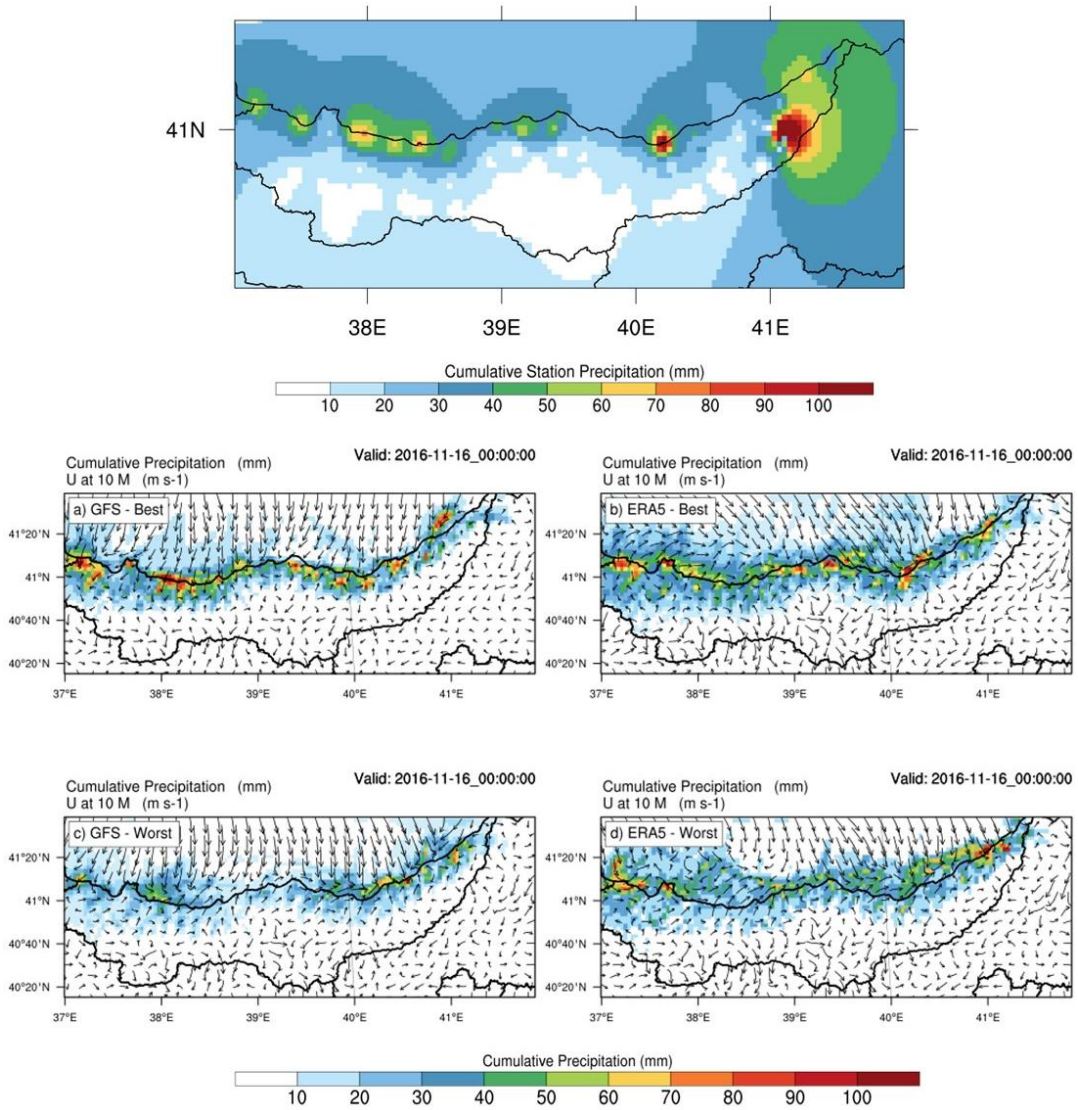

Figure 4.4.6 Precipitation maps of observation and model predictions at the end of Eastern Black Sea autumn event model run period (2016.11.16_00:00:00). The map at top illustrates the interpolated station precipitation contours. The graphs at bottom represent the forecasted precipitation contours and wind speed vectors at 10 m for both best and worst performances of GFS and ERA5 source used scenarios (These scenarios are determined from **Table 4.1.4)**

Up to now, there has been many analyses conducted to find the best performer approach of each parameter that enhances the prediction accuracy. Yet in the case, the focus is not just the schemes that are used in configurations but the physical components of atmosphere, too. Since by conducting a sensitivity analysis, it was also aimed to find the most critical parameter which can affect the model forecasts a lot, for each event period.

The physical parameter impacts on this event can be obtained by looking at how the average precipitation pattern varies from one scheme to another at the plots of Variance Analysis in **Figure 4.4.7**. For instance, in this case, from **Table 4.1.3**, WRF Single Moment 6 (WSM6) and Aerosol Aware Thompson (AATS) microphysics schemes seem more promising than Kessler (KS) and Eta / Ferrier (ES) whereas both Yonsei University (YSU) and Mellor Yamada Janjic (MYJ) offer similar results for the their performances on the predictions of this event.

However, the plots in **Figure 4.4.7**, draw different picture to observe. Since here, the variance or the gap between the schemes of every physical parameters is very small. Therefore, it indicates that there are not certain distinctions among any schemes and any physical parameter performances on the model predictions of the current event case. This means that it is nearly impossible to say that any of these physics (microphysics, cumulus and PBL) has great impact on the model forecasts in the scope of the autumn event period of Eastern Black Sea region, even the used approach in each parameter and their combined configurations with other physical components has changed through 96 scenarios.

Yet, that does not also mean all of the configurations show poor performances on the predictions. On the contrary, the average precipitation patterns of parameterization schemes are not only close to each others but also mainly overlap the observed rainfall regime throughout the event period, even though they underestimate the rain amounts at the peak precipitation hour. This may related with the frontal

precipitation system. Since the precipitation occurence in this type of systems, maintains for couple of days, the model usually provides better predictions.

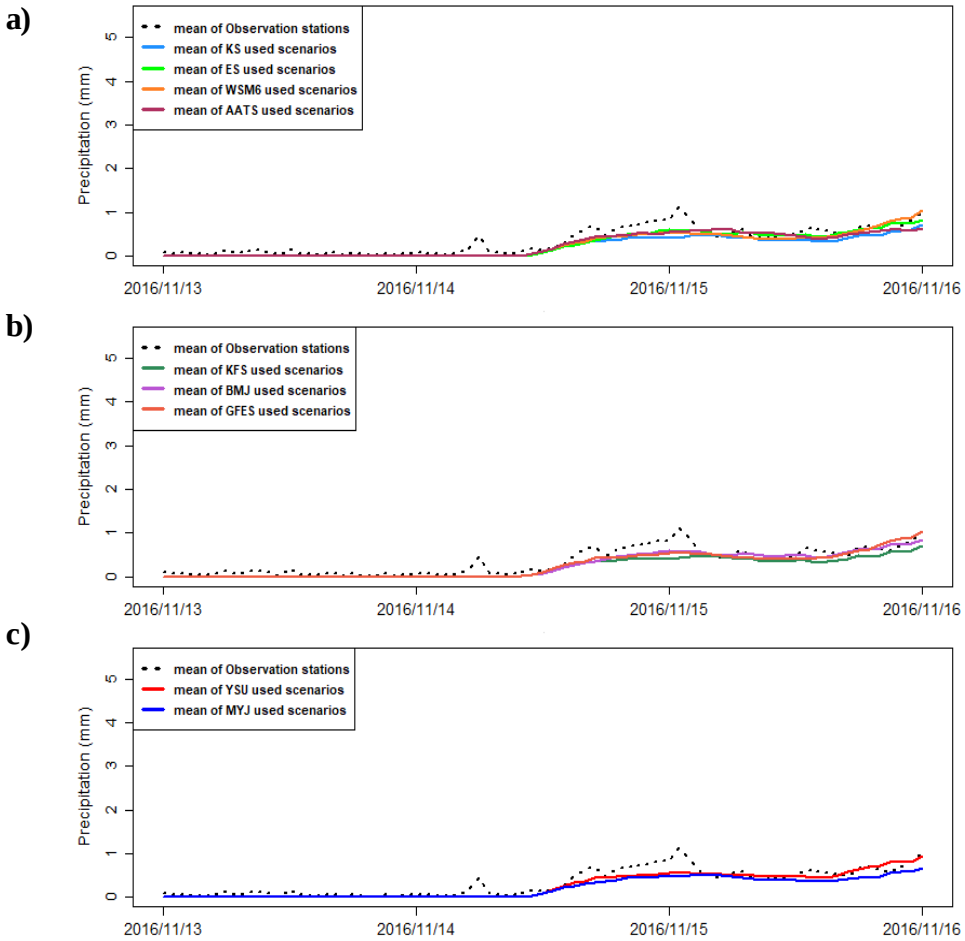

Figure 4.4.7 Variance analysis of the physical parameter schemes based on the observation stations' and model scenarios' precipitation data through the run period of autumn event of Eastern Black Sea region. The dashed black line indicates the observed data. The colorful lines in each plot, refer the model precipitation patterns according to the schemes they used. The plots: a,b and c are prepared to represent the scenario performances on microphysics, cumulus and PBL physics, respectively

4.5 Eastern Black Sea – Summer Event (2016/09/20 - 2016/09/23)

The last case is to examined under the sensitivity analysis of WRF model, is the summer event of Eastern Black Sea region. The maximum precipitation recorded during this event period is 81.1 mm and founded in Besikduzu / Trabzon station. This station is located at the center of coastal portion of the region. Therefore, it can be also considered that the event might be highly affected by the atmosphere over the sea surface. Once again, the model run period has estimated for 73 hours, starting from the day before and ends with the day after the event date.

The event period to be run by the model has chosen for 20 – 23 September of 2016. Although the event period indicates the autumn season in terms of its month because the dramatic drops in temperature seem triggering the sudden intense rainfall generation, the features of this event draw a typical summer convective precipitation. That's why, it has taken as one of the summer cases of the sensitivity analysis.

From **Figure 4.5.1**, the event time reveals itself as the peak amount of rain has obtained on September 21 at 09:00 UTC in the early hours of the day. By looking at both the current and the previous summer time event (in **Figure 4.3.1**), it can be seen that these events share some common seasonal characteristics. Likewise the other one, here in this event, almost only rainfall recorded by main station is the peak precipitation hour which also defines the event itself. The enourmous increase in total amount of rainfall is directly related with the same hour's precipitation. Yet, the major difference between these two events, is still the amounts that they have reached at the maximum.

As it can be observed from the temperature range on the graph, air temperature starts really high (30 º C) but then drops regularly and reachs to low levels (based on the obtained dataset of the stations, the minimum temperature of main station of this event in 3 days, is 10.5 º C).

This decreasement might trigger the cloud system to bring enourmous rain, in this case 81.1, all of a sudden. Through the whole, this event also seems convective type of precipitation system.

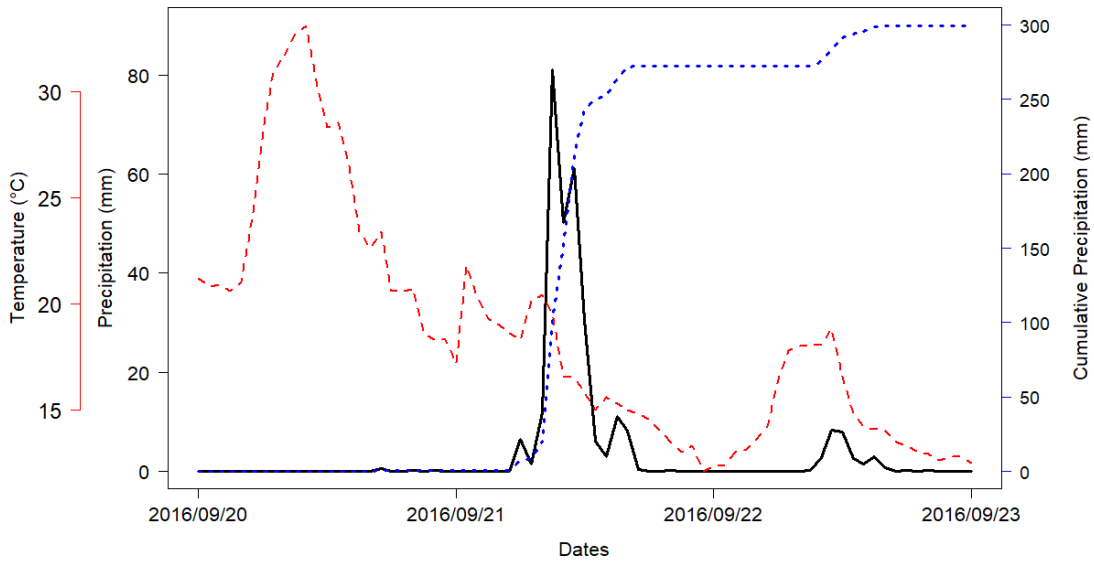

Figure 4.5.1 Precipitation and Temperature time series of the main station (Besikduzu – Trabzon) for Eastern Black Sea – Summer event through the model run period between 2016/09/20 – 2016/09/23. Black solid line refer precipitation amounts dropped over the station while the dashed red line indicates recorded temperature of the station. Dashed blue line represents the cumulative precipitation amounts through the time

Figure 4.5.2 represents the GFS and ERA5 configuration model predictions with the observed data through the run period. In both cases, some scenarios provide huge overestimations at the peak points of average precipitation (dashed grey lines on the graphs) and the same inference can be said for their means. Since the two of solid red lines that each of them, refer the average rain of GFS and ERA5 configurations and they draw similar precipitation patterns through the event period.

Yet, at the time when the maximum mean of recorded rainfall (4 mm) has reached (midday of September 21) from both time series and bias raster graphs, the general

correlation of GFS scenarios is little higher than ERA5 ones. Of course, this is valid for the first peak hour of the mean station data. For the second but relatively lower precipitation peak time, occured in the late hours of September 22, the result looks like quite the opposite. As in this hour, the average of ERA5 dataset used scenarios was able to catch the highest mean amount of rain that dropped over the region.

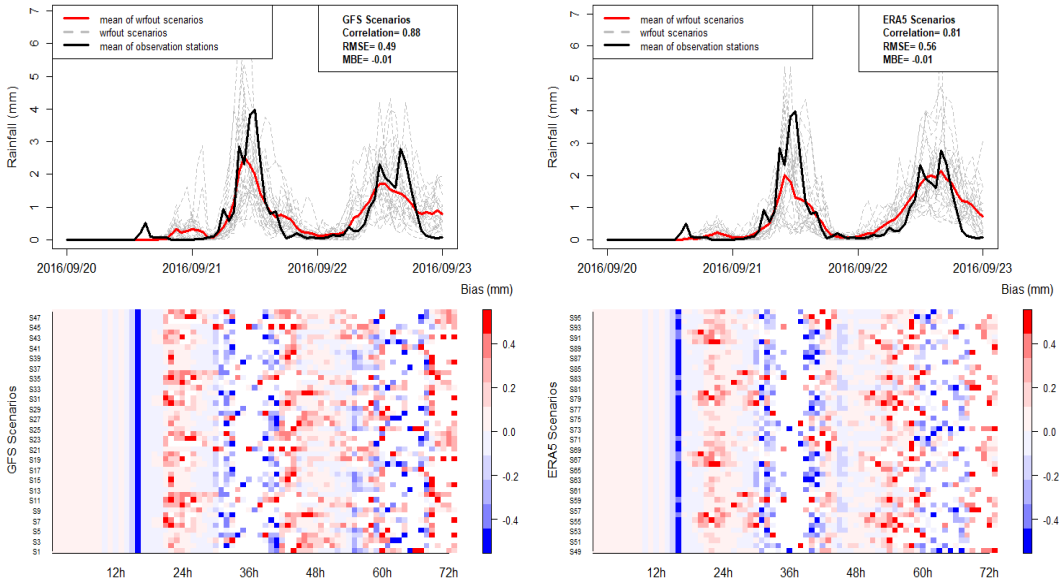

Figure 4.5.2 Average precipitation and bias raster plots of observation and model forecasts throughout the run period. The dashed gray lines represent the each model prediction scenario while the red line indicates the mean of these model scenarios and the solid black line shows the mean of observed precipitation regime in 3 days. The left column illustrates the results for GFS source used model predictions, the right column demonstrates the ERA5 source used model predictions

In terms of statistics performances, the summer event of Eastern Black Sea region in **Figure 4.5.3**, offers a complex layout to figure out which type of scenarios is the best. Based on the heights of bars and their values on y axis, it is clear that the forecasts do not often match with real event conditions because the average errors (MBE, RMSE and SD) estimated thoughout the event period is quite high.

Especially the configurations with ERA5 dataset on domain 2 (even numbered scenarios between 49 - 96), do not fit the best scenario profile. Overall, it seems like

domain 1 (9 km) scenarios do better job. However, apart from the superiority of underestimation in second and third events or the complete overestimation in the first event case, the excess or less amount of rain production here in this event, changes according to the scenario configurations. There is no certainty. This may indicate that, here, the WRF model shows extra sensitivity into their forecasts which can be also taken as the some of parameters have more impact power onto the model for this event period.

When the examination time comes to the input datasets, it can be seen the errors tend to rise with ERA5 configurations as the last 48 bars on the plots gets higher, except the SD graph. Since parallel to this outcome, the correlation bars of ERA5 scenarios become smaller, particularly for the nested domain (3 km / domain 2) configurations.

Even though the panel plots in **Figure 4.5.4** claim this way, once again TOPSIS Analysis ranks many ERA5 scenarios into the top 10 performers (**Table 4.1.3**) of this current event's forecasts.

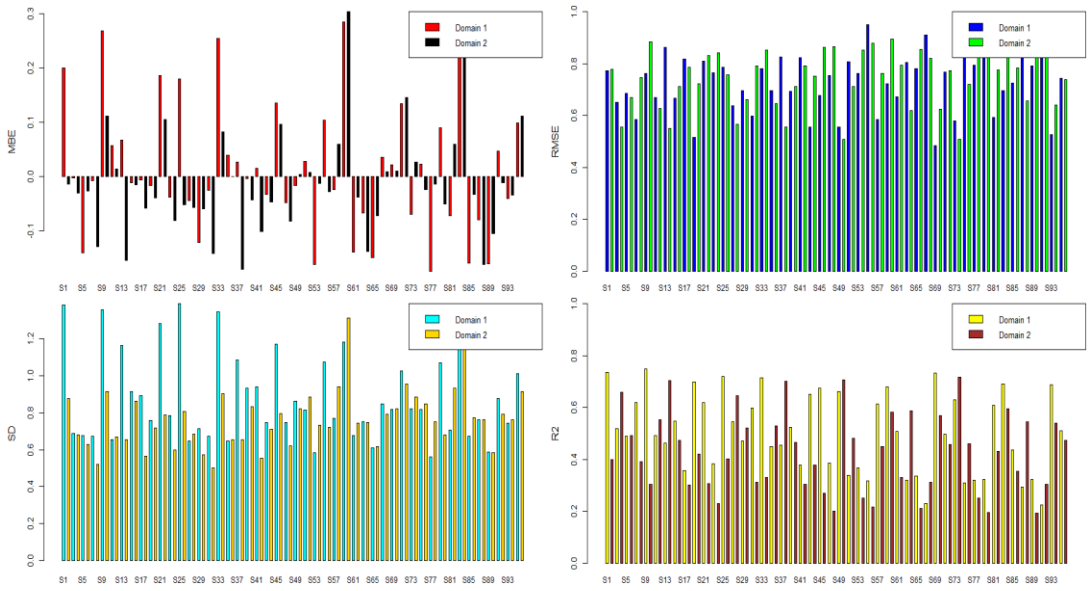

Figure 4.5.3 The performance comparison among 96 scenarios based on some statistical parameters. Mean bias error ('MBE') , Root Mean Square Error (RMSE), Standard Deviation (SD), Correlation Coefficient (R)

Different from the previous cases, the peak hour illustrations of this event have visible differences as they are shown in **Figure 4.5.4**. Yet again, without looking at the best or worst configurations (through TOPSIS analysis rankings), all the four of models could not achieve to generate maximum precipitation near the main station like in the real conditions represented on 'Station map' at the top.

In main station, located in the middle of coastal area, the rain was recorded as 81.1 mm on September 21 at 09:00 UTC whereas the model forecasts miss the complexity of atmospheric system upon this point for the same hour and because of that, they mainly underestimate the actual amount of dropped rain around this area. That's why, although some of the configurations could produce excess precipitation amounts that are closer to the peak rainfall in their predictions (**Figure 4.5.4a,c**), they were not able to build the unstable atmosphere over the right spot.

Yet still, 'GFS – Best' scenario can be considered as the most successful option among the four maps in **Figure 4.5.4**. Since even though, it caused huge overestimation on northern east part of the region, still it could estimate the high amounts of rainfall around the main station (up to 28 mm) and that increases its accuracy level in terms of the success for peak precipitation analysis. The similar things can also be said for the ERA5 – Best configuration (**Figure 4.5.4b**).

From the maps on **Figure 4.5.4**, the air builded is usually unstable enough to bring 20 - 24 mm (at small yellow point, it can reach 52 mm) precipitation over the main station whereas in the two worst ranked scenario's forecasts (**Figure 4.5.4c,d**), the excess precipitation has usually dropped on the sea. By looking at the wind vectors directions on them however, it may be possible to think, the unstable air is moving through the main station direction for GFS – Worst and upper northern portion for ERA5 – Worst (**Figure 4.5.4c,d**). Therefore, they may create the possible heavy rainfall system onto these areas in following hours but not the peak time.

For the peak mean precipitation performances in **Figure 4.5.5**, as mentioned before, most of observation stations record precipitation on the midday of 21 of September and the highest amounts are obtained again from main station and its surrondings. By looking at the maps of this figure, clearly 'GFS – Best' model configuration (**Figure 4.5.5a**) performed quite well for catching the hotspots and creating the unstable atmosphere that is enough to produce approximate rain to observed data, over them. Hence, the scenario performances have changed through the event time. Moreover, from both autumn and summer events of Eastern Black Sea region, it has also obtained that the model prediction accuracies for each hour have enhanced a lot as the number of stations which record rain in that hour, increases.

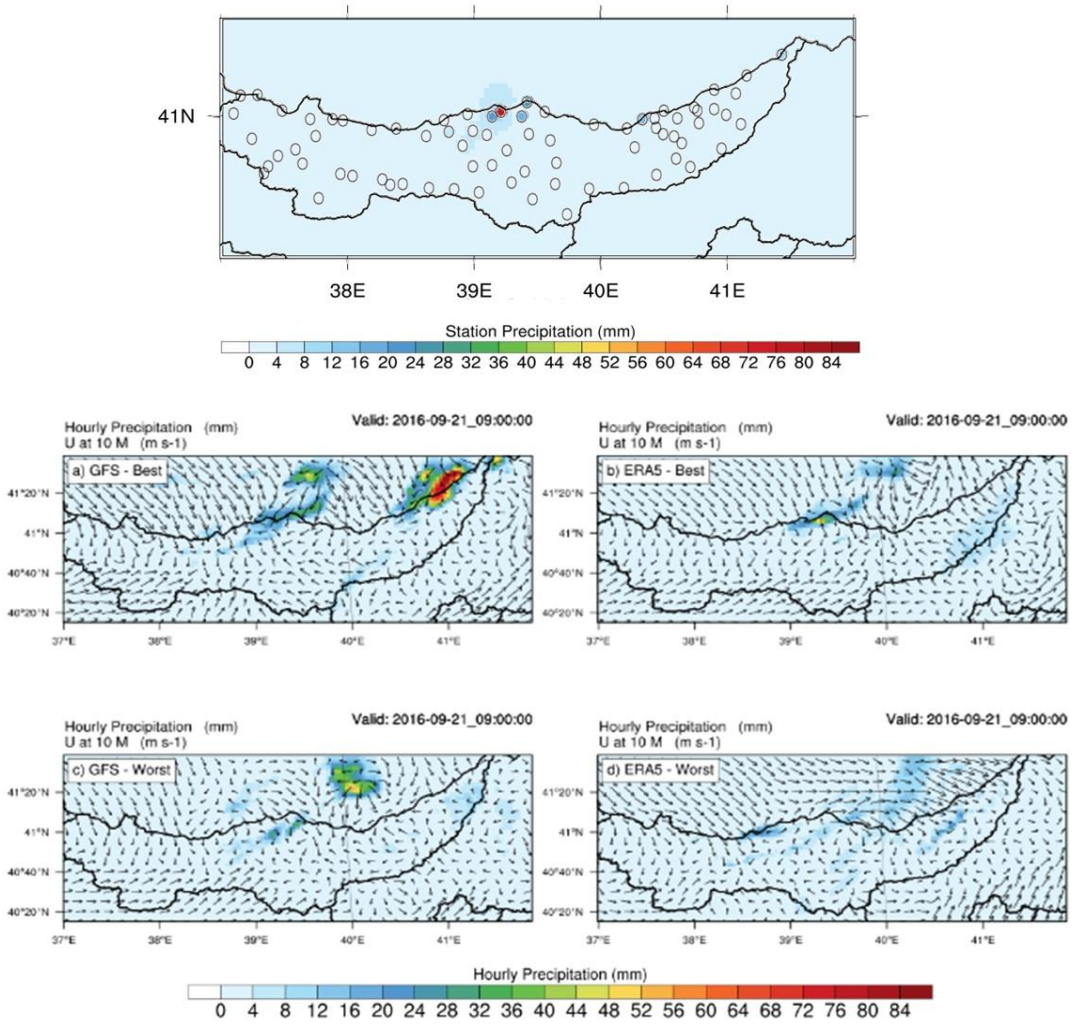

Figure 4.5.4 Precipitation maps of observation and model predictions at the peak hour of Eastern Black Sea summer event (2016.09.21_09:00:00). The map at top illustrates the interpolated station precipitation contours whereas the black circles refer the locations of these stations. The graphs at bottom represent the forecasted precipitation contours and wind speed vectors at 10 m for both best and worst performances of GFS and ERA5 source used scenarios (These scenarios are determined from **Table 4.1.4)**

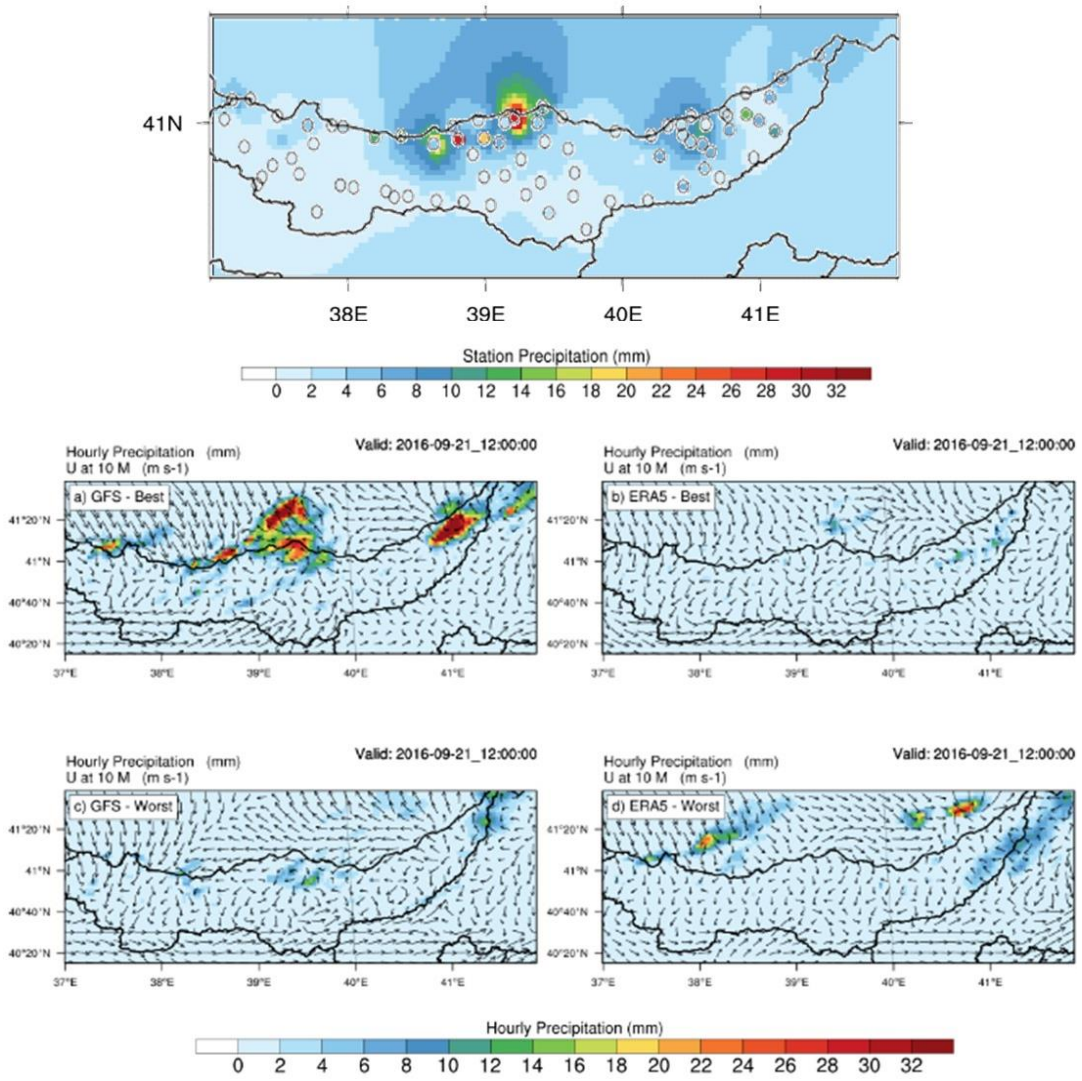

Figure 4.5.5 Precipitation maps of observation and model predictions at the maximum mean precipitation hour of Eastern Black Sea summer event (2016.09.21_12:00:00). The map at top illustrates the interpolated station precipitation contours whereas the black circles refer the locations of these stations. The graphs at bottom represent the forecasted precipitation contours and wind speed vectors at 10 m for both best and worst performances of GFS and ERA5 source used scenarios (These scenarios are determined from **Table 4.1.4)**

Lastly, the total precipitation collected by the stations between 20 – 23 of September 2016 has shown by **Figure 4.5.6**. By looking at the peak and highest mean precipitation observation maps, it is obvious that the most active area during this event period directly refers to the surrondings of main station. Just like the Mediterranean summer event, this also demonstrates a convective system where the majority of valid rain data belongs to specific grids, not the entire region. Therefore, due to lack of rain received by many observation stations, the dataset so the interpolation of this dataset, can not feed the model predictions. That's why, it is quite hard to find that local instability or the extreme amounts of precipitation via NWPs for this type of events.

The configurations in **Figure 4.5.6**, demonstrate this interpretation better since the weather, best or worst each of four, provide huge overestimations along the coast and sea surface, particularly 'GFS – Best' option. From this aspect, actually none of those is successful to collect realistic rain amounts throughout the region. Yet, if a comparison is still needed to make, 'ERA5 – Best' and 'GFS – Worst' configurations (**Figure 4.5.6b,c**) perform relatively better than other two. The excess amount of precipitation is much more less in these scenarios. Moreover, among these two, the ERA5 option was able to produce 140 - 180 mm rain around main station rather than GFS. Hence, based on grid accuracy near to the hotspot, it is a step forward. Even though, **Table 4.1.3** draws the ERA5 superiority among top 10 prediction performances by TOPSIS Analysis, it can be seen the GFS scenario which has chosen as 'worst' in **Figure 4.5.6** (**Figure 4.5.6c**) actually performed much more better than many of them, especially from 'GFS – Best' option for the total rain distribution at the end of event period.

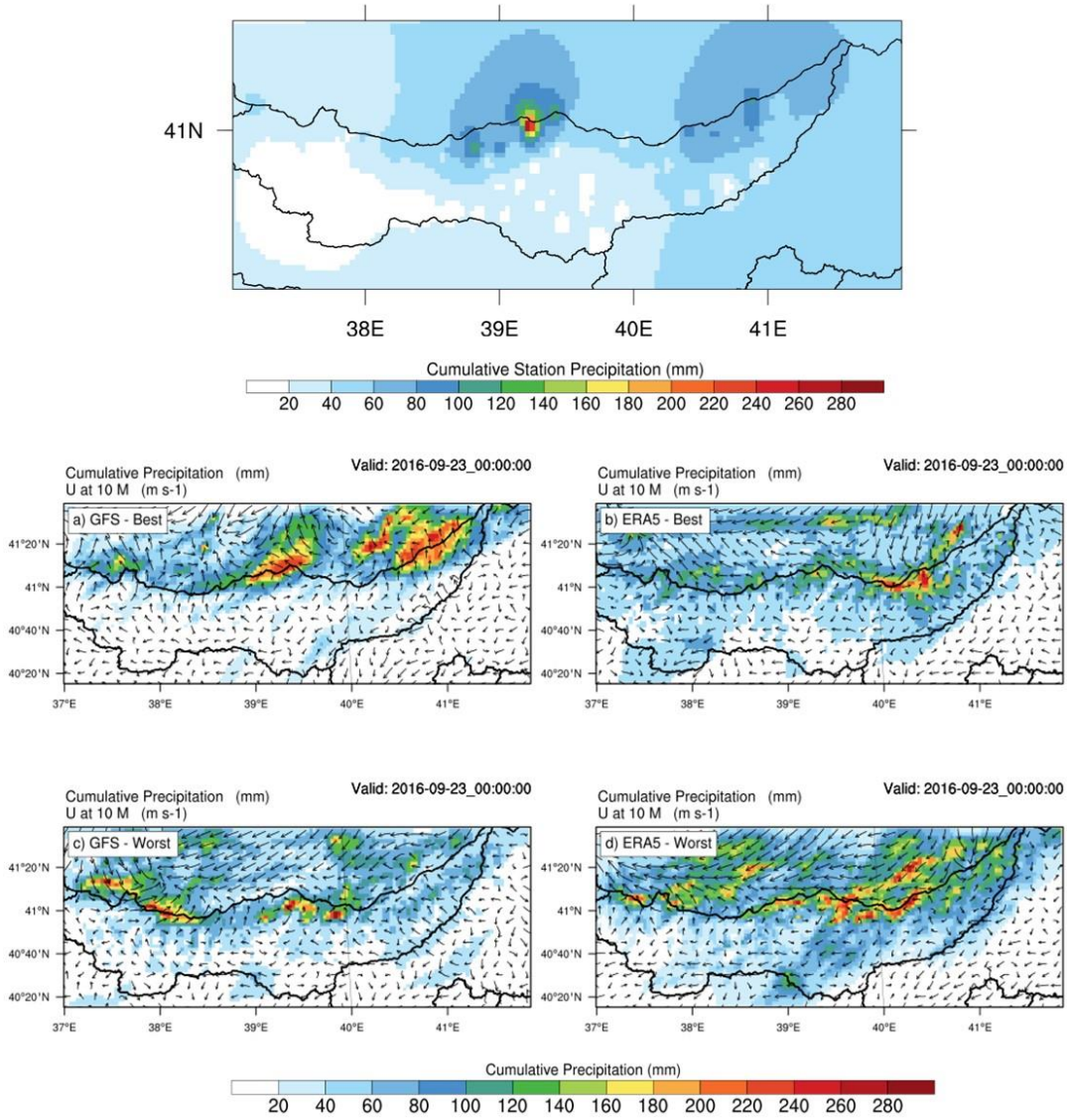

Figure 4.5.6 Precipitation maps of observation and model predictions at the end of Eastern Black Sea summer event model run period (2016.09.23_00:00:00). The map at top illustrates the interpolated station precipitation contours. The graphs at bottom represent the forecasted precipitation contours and wind speed vectors at 10 m for both best and worst performances of GFS and ERA5 source used scenarios (These scenarios are determined from **Table 4.1.4)**

As the final case of sensitivity analysis, the summer event occured in Eastern Black Sea region has received high amounts of rain during three days run period. This can be verified from both the mean precipitation of observation stations pattern shown by previous graphs and also by the Variance analysis offered in **Figure 4.5.7**.

Similar to previous three event studies, here again the plots in **Figure 4.5.7**, depict the model prediction accuracies among the determined scenarios (from **Table 3.3.4**) according to their physical configuration options.

For this event, it is obvious that the schemes or the approachs used in both microphysics, cumulus and PBL; create differences into WRF model operation since they directly alter the outcomes of the average rain dropped over the region. Moreover, the differences among these schemes are actually the good indicator of the model sensitivity to the physical components, too. The variance (the gap) between the plots indicates that the microphysics and cumulus both have great power onto weather predictions because as the used sheme has changed for these parameters, the model provides a new forecast that does not follow the same path with others for these two physical components (**Figure 4.5.7a,b**). However, the scheme lines of PBL do not offer the same difference between their prediction patterns. Their variance is much more smaller than what has been observed from the first two physics' plots.

For instance, the variance gets higher from blue (Kessler, KS) to green (Eta / Ferrier, ES) line in microphysics graph at topmost. As the KS approach with blue line could generate higher precipitation and become closer to the observed conditions more while the ES approach with green line, mostly underestimated the actual amount of rain during the event period which enables it to decrease its forecast accuracy.

Or the cumulus sheme performances in **Figure 4.5.7**, show the increasing variance or the gap between dark green (Kain Fritsch – KFS) and purple (Grell Freitas – GFES) lines as the performance gets poorer from top to bottom of lines order in the graph.

This indicates the great impact of cumulus physics on the predictions of parent domain (9 km) since any scheme approach of it can directly affect the cumulus cloud system builded in the model.

Nevertheless, considering the same PBL plots of both the autumn and summer events of this region with Mediterranean events, it is clear that planetary boundary layer is more powerful atmospheric component for Eastern Black Sea regional weather system. Since the variance on the current region is relatively higher comparing to first two event cases (**Figure 4.2.7c and Figure 4.3.6c**), which means the WRF model responds to the change made in used PBL scheme more for Eastern Black Sea region events rather than Mediterranean's, especially during heavy rainfall occurrences.

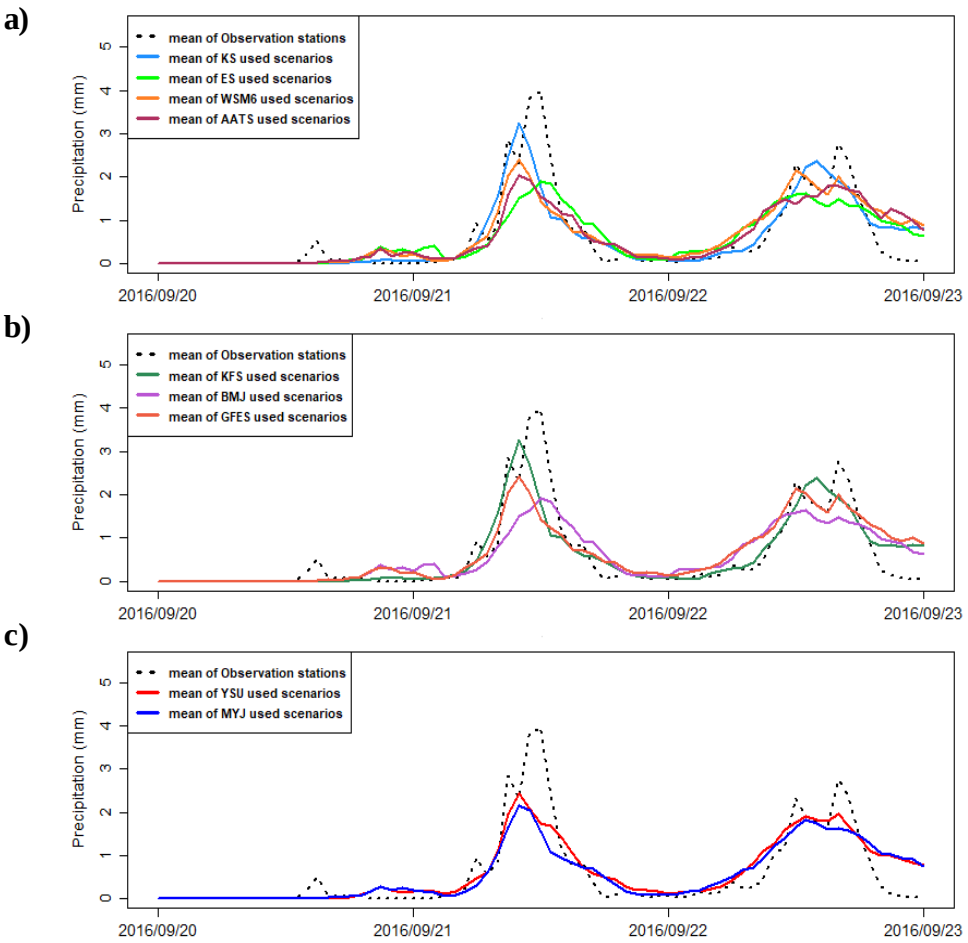

Figure 4.5.7 Variance analysis of the physical parameter schemes based on the observation stations' and model scenarios' precipitation data through the run period of autumn event of Eastern Black Sea region. The dashed black line indicates the observed data. The colorful lines in each plot, refer the model precipitation patterns according to the schemes they used. The plots: a,b and c are prepared to represent the scenario performances on microphysics, cumulus and PBL physics, respectively

4.6 Taylor Diagram Analysis

So far, the physical parameters and input datasets' performances are investigated by various aspects such as Topsis, GFS – ERA5 time series, multiple statistical variables, visual illustrations on maps for both peak and highest mean hours. All of these analyses are conducted as the parts of sensitivity analysis of WRF model on heavy precipitation forecasts. Although not all of them support the same results, they are sufficient to draw a general aspect of the best configuration options for each event case. Now, as the last step of this analysis, each parameter were further examined using Taylor diagrams.

The important thing to keep in mind for these diagrams, is the scenario numbers used to create them. That means, every parameter's diagram, except cumulus, is drawn for 96 scenarios (combining domain1 and domain 2). On the other hand, since the cumulus parameterization in the model has deactivated for all domain 2 (3 km) scenarios, the diagrams in **Figure 4.6.2** are created by only using the domain 1 configurations' statistics which are 48 scenarios in total.

Even though Taylor diagrams represented on each figure are provided for different parameters, the overall distribution of the configuration points (colored dots) seems similar for each event graphs.

As already mentioned in map illustrations before, the correlations of model configurations for Mediterranean events are not very successful even for the best scenarios. The same results can also be observed in **Figure 4.6.1.** The correlations of this region's Taylor diagrams are generally located between 0.1 - 0.3 and almost all of their standard deviations are already greater than 1. Yet again, from the two diagrams at the top, the most appropiate microphysic option to use in Mediterranean region looks like Eta / Ferrier scheme (ES). Since the configurations run with Eta scheme, provide the closest results to the observation curve comparing the others.

Especially, in summer case, there are couple of scenarios located near to this curve. If the approach behind Eta is considered well, it can be said these remarks are convenient as it can work for both convective and non-convective precipitation types. However, still it does not include some of precipitation forms like snow, graupel or hail into its calculations so it is not very successful to provide fully complex atmospheric system.

From the cumulus diagrams of Mediterranean event cases, shown on **Figure 4.6.2**, mostly Grell Freitas (GFES) and Kain Fritsch (KFS) schemes perform better comparing to Betts Miller Jancij (BMJ). This also makes sense because GFES and KFS use similar approachs into their calculations and can form a convective system easily whereas the mechanism of the BMJ is more suitable to adapt into synoptic rain systems like in Black Sea region.

When it comes to the PBL diagrams in **Figure 4.6.3,** it seems red colored Yonsei University (YSU) scenarios are prominent for both cases since they are the options that generally stand closest to the observation curve. However, from the TOPSIS (**Table 4.1.3**) and Variance analyses, it is known that PBL does not have a huge impact on WRF model predictions of precipitation. Therefore, it is not possible to come up with a certain best option for this parameter.

Similarly, through the TOPSIS Analysis results for Mediterranean event cases, GFS configurations are usually ranked at higher places than ERA5 scenarios. Yet, this can change depending on the type of analysis. For instance, on the last Taylor diagram **(Figure 4.6.4)** of Mediterranean events, ERA5 dataset used scenarios looks like they perform better than GFS. Hence, when the number of options to compare, have decreased such as PBL and initial boundary conditions, both have 2 options, selecting the best option among them is not much possible because their performances are quite similar. This makes them so hard to differenciate for each event case.

For Eastern Black Sea cases, it is obvious that autumn event does not show a certain variety among the parameterization schemes. As almost all the points of the schemes used for each physical parameter of this event, are gathered around the observation curve on every Taylor diagram.

From this aspect, it can be said that all of model configurations achieve to generate realistic simulations over the region which means the model does not behave sensible for its forecasts in this event period because the scenarios' performances do not change by using different physical approachs in the model configuration.

However, the summer event between 20 – 23 of September 2016, offers an order among the scheme performances in their diagrams. Through those, again Eta (ES) microphysics seems one step ahead from the others, and closer to the 'OBS' curve. Aerosol Aware Thompson (AATS) comes next as most of their scenarios are accumulated near to the same curve. Yet, from the knowledge that mentioned in Chapter 3.2 'Selection of Parameterization Schemes' because of the complex dynamics they use in atmospheric calculations, it was expected that AATS and WSM6 perform better to mimic the Black Sea events which are mostly dominated by synoptic or non-convective precipitation systems. Topsis results can also verify this interpretation because due to the overall performance according to many statistical parameters in Topsis Analysis, the model configurations run by AATS or WSM6 microphysics prevail the top places in the rankings (**Table 4.1.4)**

For cumulus parameterization, still there is no best to fit on the curve; however, different from Mediterranean cases, it can be observed the Grell Freitas (GFES) scheme scenarios' performances are highly diminished in this event. Moreover, as expected before in Chapter 3.2.2, the Betts Miller Janjic (BMJ) used configurations show some improvements in predictions of this region.

By looking at the common points between the two events occured in Black Sea region, Mellor Yamada Janjic (MYJ) PBL scheme in **Figure 4.6.3** and Global Forecast System (GFS) dataset in **Figure 4.6.4** seems like providing an advantage to the model by increasing their forecast accuracies. Since the TOPSIS Analysis refers the similar outcome for MYJ configurations (**Table 4.1.3**), it may be considered, as comparing to Mediterranean events, the PBL is more sensitive parameter for weather forecasting model when non-convective precipitation system are dominant in the events like occured over Black Sea region. However, on the contrary to **Figure 4.6.4**, TOPSIS Analysis and the visual illustrations of last two events demonstrate that ERA5 dataset is much suitable choice to build initial boundary conditions onto Black Sea regional events.

a) Mediterranean – Autumn **b)** Mediterranean – Summer

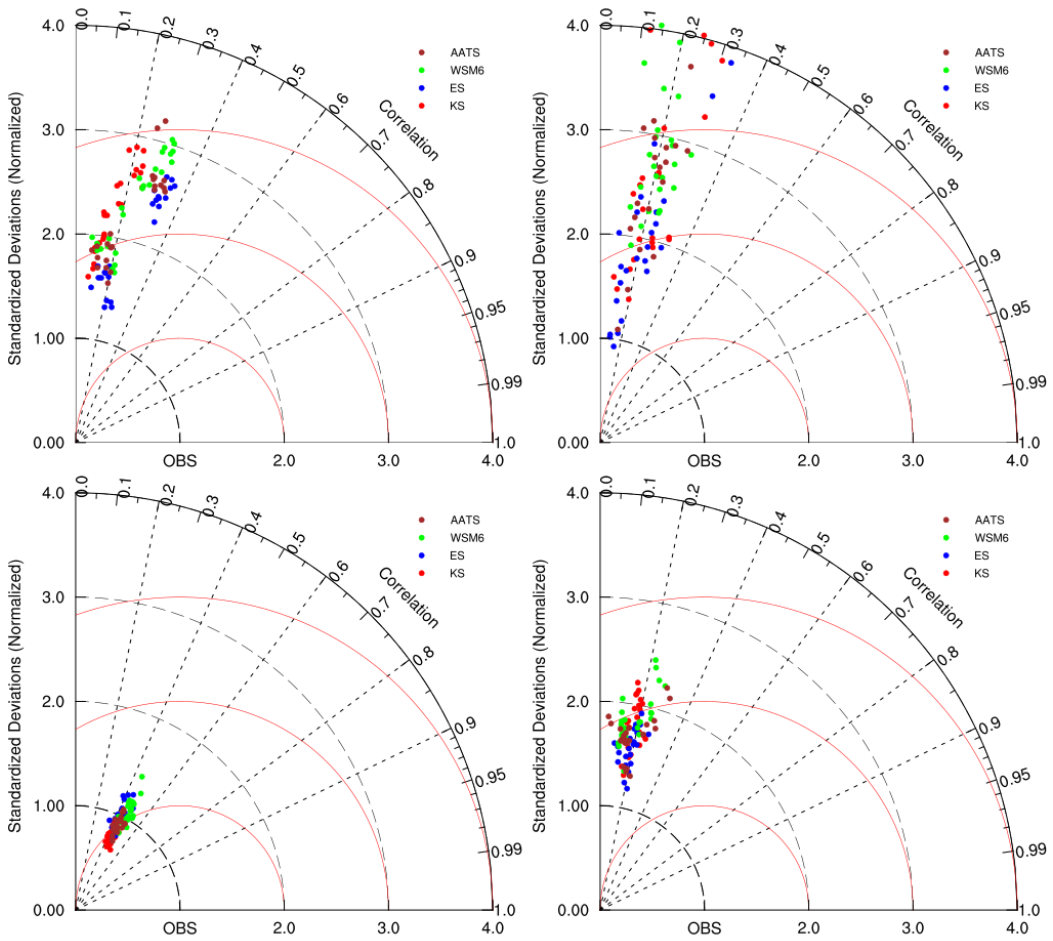

c) Eastern Black Sea – Autumn **d)** Eastern Black Sea – Summer

Figure 4.6.1 Taylor Diagrams of the model scenarios according to the microphysics schemes they use in each event case. The scenarios worked with the schemes: Aerosol Aware Thompson (AATS) by burgundy, WRF Single Moment 6 by green, Eta / Ferrier (ES) by blue and lastly Kessler (KS) by red dots, have shown on the graphs

a) Mediterranean – Autumn **b)** Mediterranean – Summer

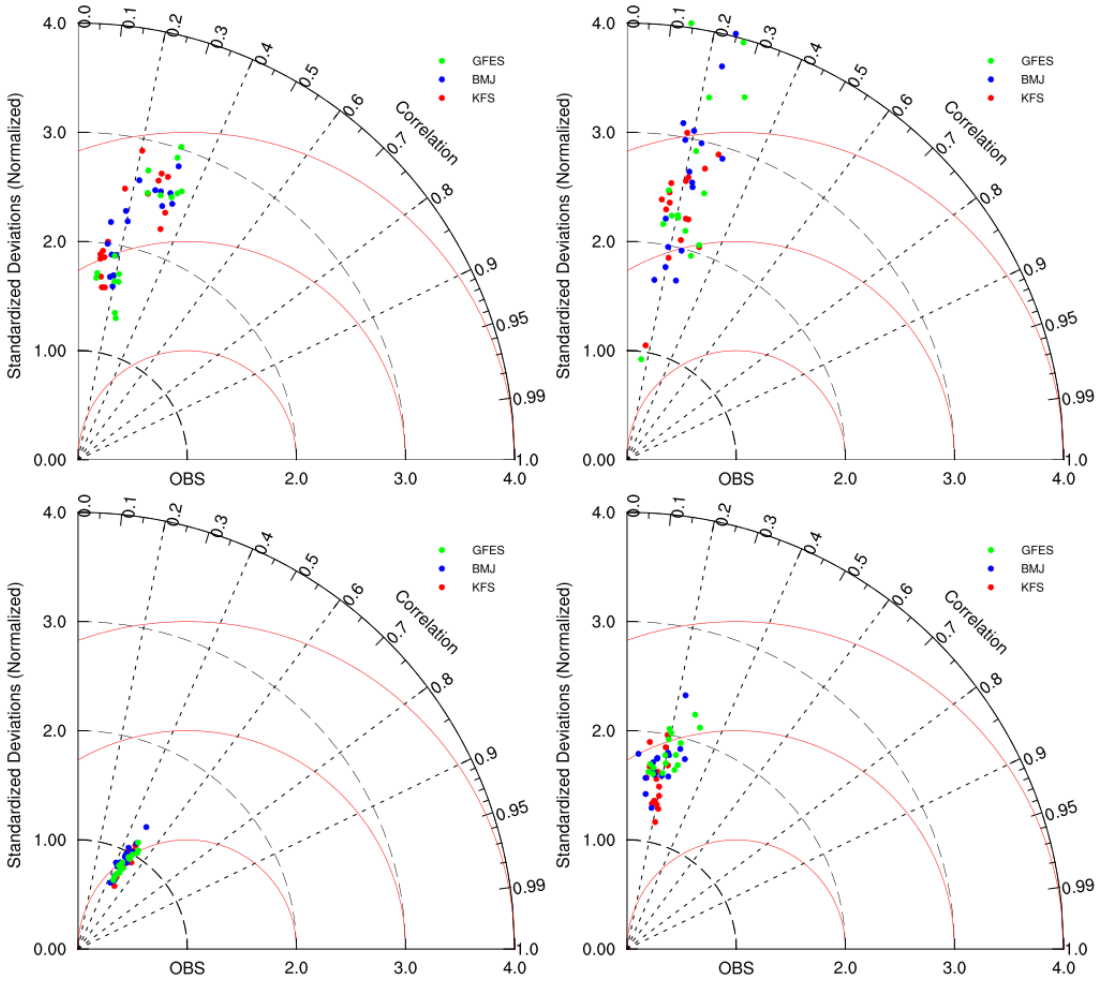

c) Eastern Black Sea – Autumn **d)** Eastern Black Sea – Summer

Figure 4.6.2 Taylor Diagrams of the model scenarios according to the cumulus schemes they use in each event case. The scenarios worked with the schemes: Grell Freitas (GFES) by green, Betts Miller Janjic (BMJ) by blue, Kain Fritsch (KFS) by red dots, have shown on the graphs

a) Mediterranean – Autumn **b)** Mediterranean – Summer

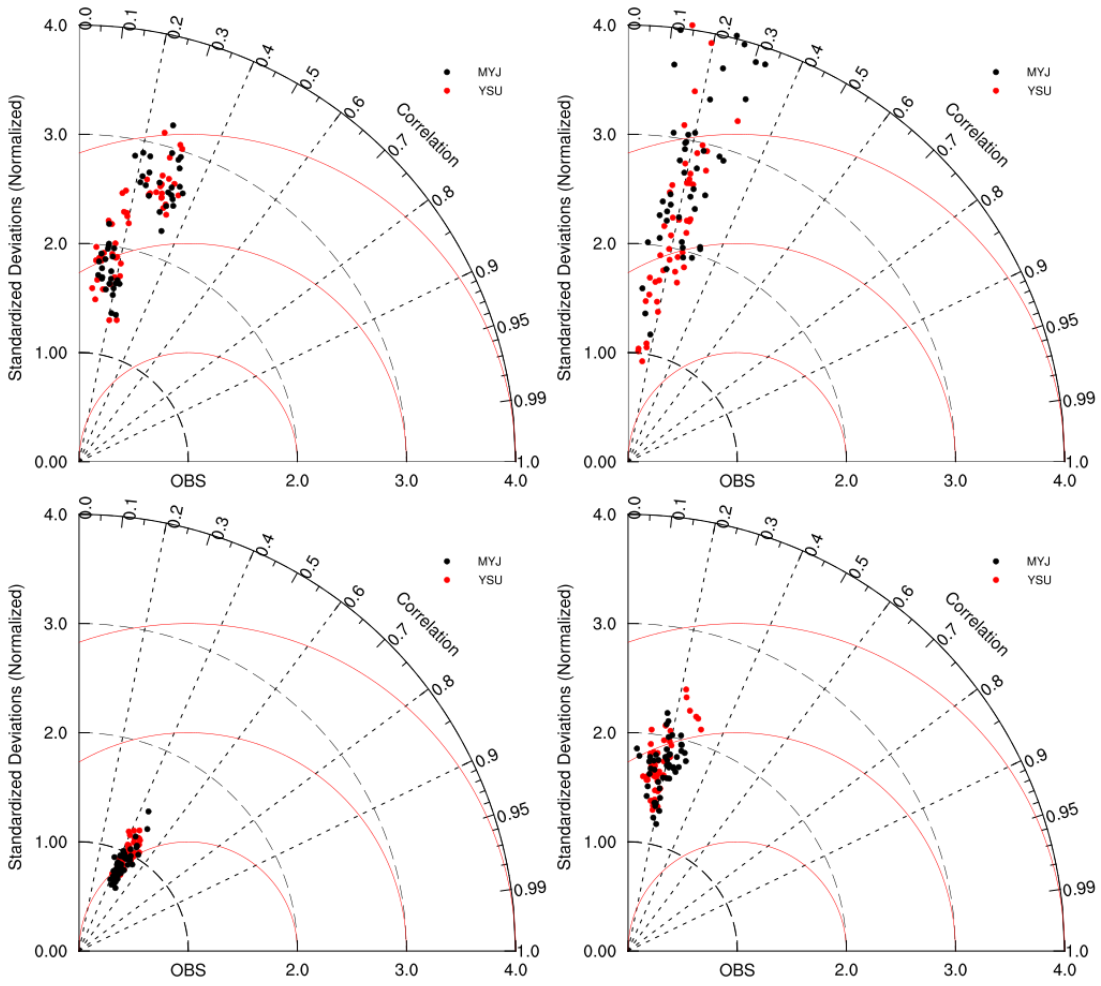

c) Eastern Black Sea – Autumn **d)** Eastern Black Sea – Summer

Figure 4.6.3 Taylor Diagrams of the model scenarios according to the PBL schemes they use in each event case. The scenarios worked with the schemes: Mellor Yamada Janjic (MYJ) by black and Yonsei University (YSU) by red dots, have shown on the graphs

a) Mediterranean – Autumn **b)** Mediterranean – Summer

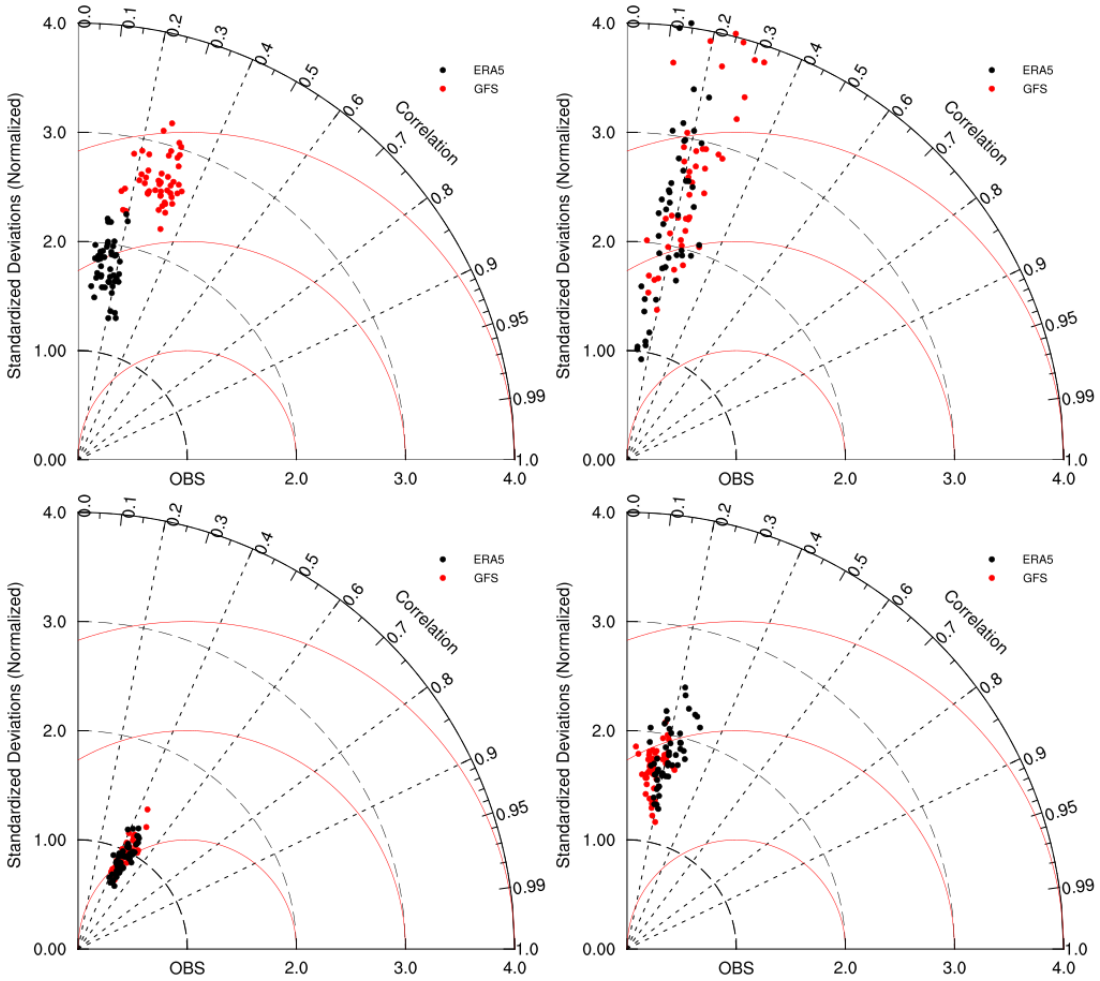

c) Eastern Black Sea – Autumn **d)** Eastern Black Sea – Summer

Figure 4.6.4 Taylor Diagrams of the model scenarios according to the input meteorological sources they use in each event case. The scenarios worked with the datasets: ERA5 Reanalysis by black and GFS by red dots, have shown on the graphs

PART II – SST Analysis Event Cases

4.7 Mediterranean – Winter Event (2018/12/10 - 2018/12/20)

The first case that is taken under this part of the thesis, is the extreme precipitation event occured in the Antalya basin, Mediterranean region of Turkey. According to the observation data taken from the General Directorate of Meteorology of Turkey (GDM), it is accepted that the event occured in between 15 - 17 December of 2018. The model run period starts from a couple days before the event day and ends three days after so in total, the run time has determined as 10 days. Thus, the model is worked between 2018.12.10_00:00:00 – 2018.12.20_00:00:00. Here, the longer simulation period enables enough time to the model to build up the atmospheric system for the event dates. Therefore, the SST impacts on precipitation occurrence can be investigated effectively.

Figure 4.7.1 shows the precipitation – temperature time series of the main station where the peak and maximum total precipitation in 10 days were received. However, this graph has prepared for only 3 days (14 – 17 December) out of 10 days model period is because the actual impacts of event has started to observe in station from the fourth day. While the black solid line represents precipitation amounts, the red dash line indicates temperature and the blue dash line on the right side depicts the change in cumulative rainfall recorded of main station during the time period. In this case, with hourly 53.1 mm on December 16 17:00 UTC and at the end of period, nearly 700 mm rain collected in total, Antalya – Ovacık is selected as 'the main station' to be examined in the case analysis.

By looking at the graph on **Figure 4.7.1**, sudden temperature changes (sharply increasing and decreasing between 0 – 10 °C) during the period can be easily distinguished. These changes indicate how actually the atmosphere gets unstable around the main station as the time flows to event hour. There is no rain recorded in main station when first two critical drops in temperature happen, the reason behind this, may be the precipitation for these days falls over somewhere else on region. However, third one is observed during event and trigger the rain production (as it can be seen from the sharp slope in black and blue lines on the graph) before couple of hours from the peak time. The same changes also occur at December 16 17:00 UTC when precipitation reachs the maximum.

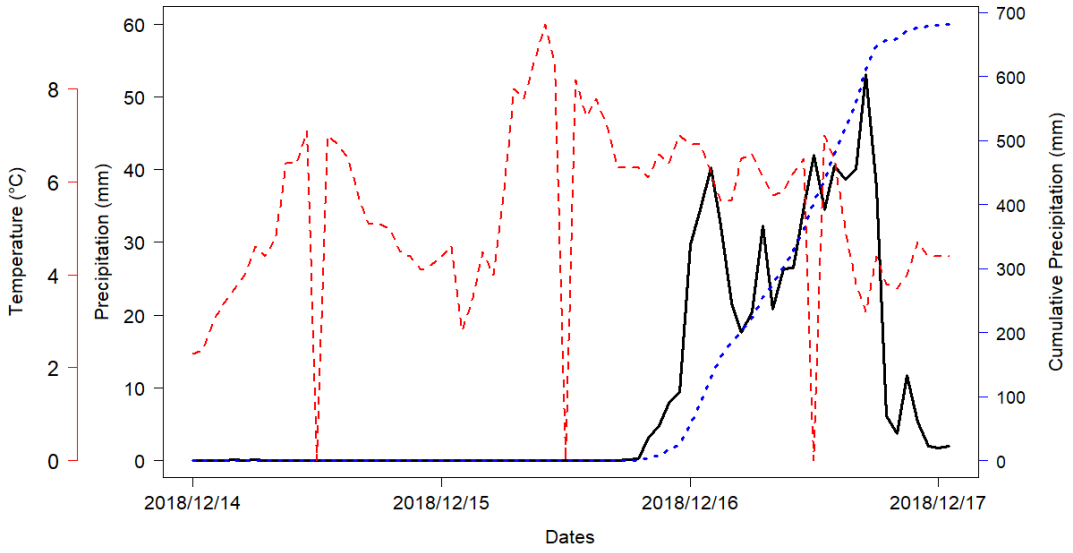

Figure 4.7.1 Precipitation and Temperature time series of the main station (Ovacık – Antalya) for Mediterranean – Winter event between 2018/12/14 – 2018/12/17. Black solid line refer precipitation amounts dropped over the station while the dashed red line indicates recorded temperature of the station. Dashed blue line represents the cumulative precipitation amounts through 3 days from total event period

Together with **Figure 4.7.2** and **Table 4.7.1**, some of the critical components of precipitation systems are compared among the various SST dataset models. On **Figure 4.7.2**, the pattern of models and the observation in terms of precipitation, temperature, wind and relative humidity, are shown through the event period. Yet, because the WRF model needs some spin up time to shape the right atmospheric system to generate future forecasts (Yilmaz, 2015; Bonekamp et al., 2018), it usually can not form much precipitation during this period.

For the current case, the first two days of run period are considered as the 'spin up time' of the models. That's why, to be able to diminish the errors between the predictions and observed data, these days are excluded from the representation of time series on **Figure 4.7.2** and calculation of statistical parameters such as Root Mean Square, Mean Bias, Standard Deviation and Correlation on **Table 4.7.1.**

Based on the relation between the graphs and statistics, all of the four components indicate the overestimation for the model forecasts. Since, particularly on temperature graph, it is obvious that the models tends to create hot and more humid atmosphere near the ground comparing to the real condition. Due to that, evaporation may lead the flux exchanges to accelerate, increase the wind speed on both horizontal and vertical axes which will eventually bring heavy precipitation over the region. Especially from the peaks between December 16 – 17 and 18 -19, the excess rainfall formation in the models may be caused by high temperature estimations. Again, through the data showed in **Table 4.7.1**, none of the models could generate a successful forecast. Enormous standard deviations and very small correlations (< 1) are good indicators of this result.

Even though, it is not much possible to differenciate the model performances with each other by looking at these analyses, still one thing has become prominent which is using the updated SST source in WRF model, increases the accuracy of the forecast rather than using SST from the meteorological input dataset, in this case GFS.

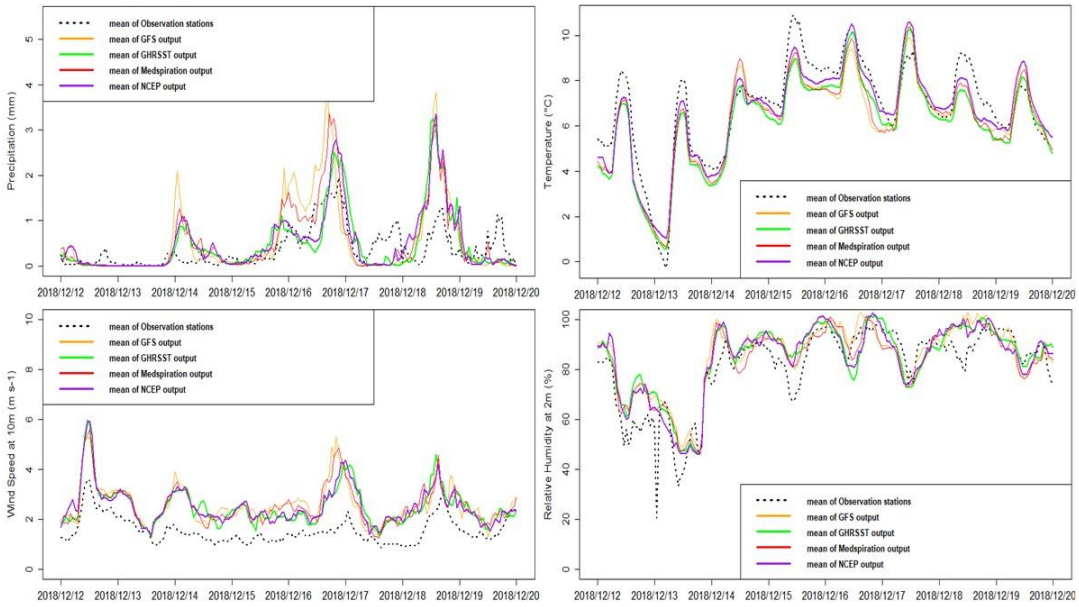

Figure 4.7.2 2018.12.12_00:00:00 – 2018.12.20_00:00:00 run period. The timeseries graphs of observation and SST model forecasts in terms of precipitation (mm), temperature (°C) , wind speed (m/s) and relative humidity (%). The solid colorful lines represent the each model prediction scenario while the dashed black line indicates the mean of observed precipitation regime in 10 days

Table 4.7.1 Statistical analysis of SST scenarios for 2018/12/12– 2018/12/20 event period

Mediterranean Region	RMSE	MBE	Standard Deviation	Correlation
Precipitation				
GFS	0.664	0.179	1.948	0.675
GHRSST	0.546	0.098	1.575	0.619
Medspiration	0.556	0.144	1.726	0.710
NCEP	0.541	0.125	1.565	0.633
Temperature				
GFS	0.869	-0.028	0.865	0.925
GHRSST	0.748	-0.107	0.898	0.946
Medspiration	0.825	0.017	0.897	0.932
NCEP	0.829	0.309	0.908	0.941
Combined Wind Speed				
GFS	1.193	1.041	1.478	0.667
GHRSST	1.088	0.961	1.462	0.754
Medspiration	1.162	1.019	1.459	0.691
NCEP	1.113	0.984	1.435	0.730
Relative Humidity				
GFS	8.805	4.277	0.843	0.871
GHRSST	8.751	3.614	0.870	0.860
Medspiration	8.319	2.683	0.854	0.864
NCEP	8.293	3.195	0.923	0.873

While **Table 4.7.1** represents some statistical parameters between the observation stations and SST model predictions, the hourly bias of precipitation along 10 days is also shown on the graph by **Figure 4.7.3**. To be able to calculate the bias, 'model – observation' formula has been used. Therefore, the red colored raster hours indicate the overprediction whereas for the portions where blue color gets darker, the model forecasts underestimate the real precipitation amount. The mean precipitation time series of model and observation stations graph on the top in **Figure 4.7.3**; however, prove these bias differences.

As it can be observed from **Figure 4.7.3,**usually most of models produce more rainfall than the reality (the precipitation patterns of colorful solid lines are higher than black dashed line of observation pattern), except some points. For peak hour at 17:00 UTC of December 16, GFS and Medspiration SST dataset used models (orange and red colored lines) make overestimations while the other GHRSST and NCEP models provide predictions closer to the stations data. The bias near to this hour also support this interpretation since the color here is red for GFS and Medspiration and with closest precipitation forecast, bias of GHRSST model is smallest (from 0 to - 2 mm). However, when all models produce more than actual as in the late hours of December 18, the four of bias rasters are painted in dark red. By only looking at the graphs on **Figure 4.7.3**, GHRSST and NCEP datasets used models perform little better to form accurate precipitation pattern than the others.

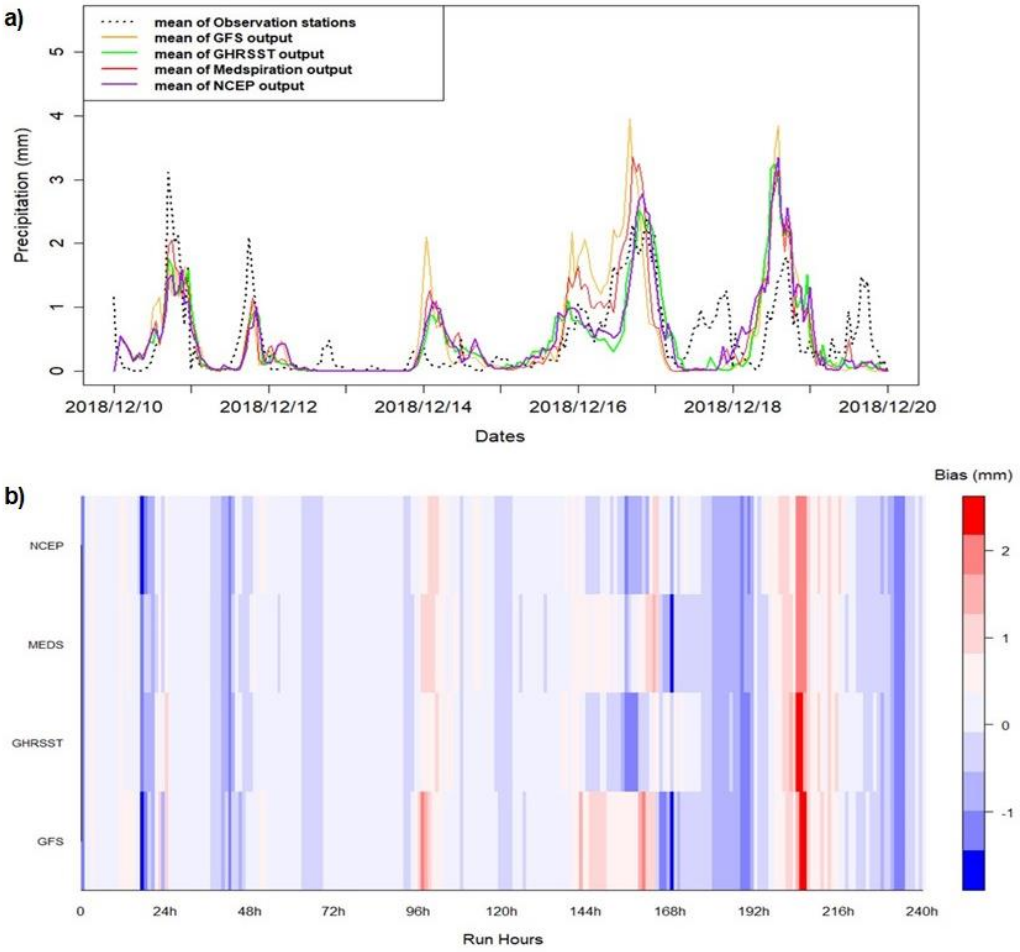

Figure 4.7.3 a) The average precipitation and b) bias raster plots of observation and SST model forecasts throughout the model run period. The dashed gray lines represent the each model prediction scenario while the red line indicates the mean of these model scenarios and the solid black line shows the mean of observed precipitation regime in 10 days

In addition to the analyses that has been conducted to examine the SST model performances so far; this time, the comparison among the observation and the WRF forecasts has illustrated, in terms of regional distribution for the peak precipitation hour (December 16 17:00 UTC) by **Figure 4.7.4**. Here, the graph at the top represents the observation stations' locations by small black circles on the map. These station circles are filled with the various colors upon their precipitation values at the peak hour. The precipitation spread over the rest of map had estimated from the interpolation (based on nearest neighbour methods) of the stations recorded data. The scale of 'Station Precipitation' had been arranged to show both the stations and the interpolated area's precipitation values on the same labelbar.

It should be stated that some of stations which were included into this analysis (the black circles at left side of the graph in **Figure 4.7.4**) are not located in the Antalya basin boundaries. However, because the event has mainly occured on the border (Ovacık Station, represented in red circle station on the graph), to be able to enhance the illustration accuracy of reality and statistic analysis, it was decided adding also these stations into the study.

The four graphs beneath this station map, however, display the WRF model outputs produced from using different SST datasets. This kind of illustration is important to analyse how well the models could catch the local precipitation amounts dropped in reality. Therefore, it can be said that, all graphs shown on **Figure 4.7.4** represent a grid based efficiency comparison among various SST data sources at the peak hour.

In **Figure 4.7.4**, the red colored point that strikes the eyes remarks the Ovacık – Antalya station which is defined as the 'main station' for this event. With 53.1 mm received at December 16 17:00 UTC, this station provides the maximum precipitation in 10 days period. As it can easily be observed, all four model outputs are successful to predict the heavy precipitation of the main station and its surroundings. By looking at the wind vectors 10 m, it is also clear that the cumulus

clouds which brings rain over the region, are carried from the sea towards near the main station.

Yet, when the model runs with GFS provided SST dataset (**Figure 4.7.4a**), the high amount of rain has produced over the sea whereas by the external SST source datasets such as GHRSST, Medspiration and NCEP model forecasts, the maximum precipitation has formed on the same portion of land which also matchs the peak precipitation received area on the station map at top. Once again, this condition verifies the importance of SST impact on precipitation as well as using special daily SST sources in weather prediction models to be able to obtain more realistic forecast.

Still, these three SST sources can be investigated based on their performances at the peak time shown by this figure. The model working with GHRSST satellite derived SST dataset (**Figure 4.7.4b**) has failed to generate enough amount precipitation in contrast to the other external SST source predictions (**Figure 4.7.4c, d**). The maximum rain produced in GHRSST graph is colored in blue – green range (20 – 24 mm) while it is painted as reddish orange color ($\geq$ 44 mm) in Medspiration and NCEP graphs which gives much closer prediction to the observed precipitation on same area. Therefore, these configurations, especially Medspiration, step forward in terms of catching hotspots and generate similar rain amounts around the main station.

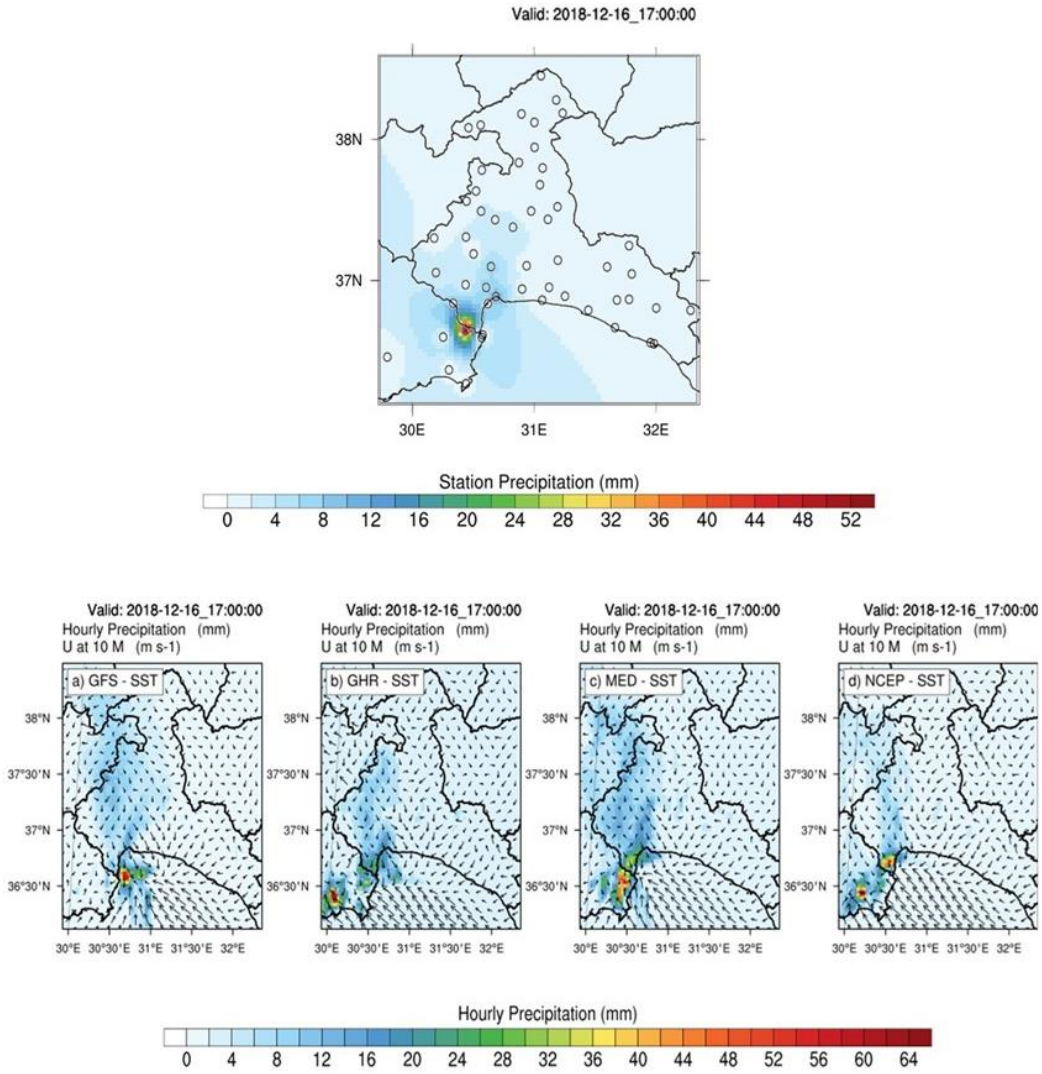

Figure 4.7.4 2018.12.10_00:00:00 – 2018.12.20_00:00:00 run period. The precipitation maps with 3 km horizontal resolution at the peak hour when the highest rain dropped over the Mediterranean region. The map at the top shows the stations' precipitation data (m) and their interpolation throughout the whole domain once again for the peak time (17:00 UTC of December 16). The black circles indicate the locations of observation stations and the color scale of label bar determined according to the stations and their interpolated rain data together). The four maps at the bottom refer the WRF model precipitation forecasts (m) for the peak hour by working with different SST data sources: **a)** GFS, **b)** GHRSST, **c)** Medspiration and **d)** NCEP, respectively. Black colored vectors on each of these maps, demonstrate the wind speed (m/s) vector at 10 m above the ground

The reflectivity and SST graphs on **Figure 4.7.5** actually support the precipitation graphs shown in **Figure 4.7.4**. These maps are drawn for both peak and 6 hours before the peak time to observe how the atmospheric conditions has altered within the six hours for the whole region. Apart from the model outcomes, the radar reflectivity (provided from Yousefi, 2020) is also wished include into this figure as an another perspective and it has shown at upmost visualisation in **Figure 4.7.5** but it has prepared only for the peak hour (2018.12.16_17:00 UTC).

Since the radar data offers only 360 degree of visibility, the current region can not be completely contoured by reflectivity data. Yet still, there are some common areas where the SST model scenarios on the second row and the radar reflecitivity contours overlap on the region such as the inlands and surrondings of main station. As it can be observed from the map at top, the radar estimate the reflectivity mainly on the inner portion. However, the cloud activity around main station can be still obtained from the orange reflectivity contours (15 – 20 dBZ) draw like a skew line at the left handside coastal area. Just all of the four model scenarios spread more and make some overestimations for predicting the reflective parts of these areas.

Likewise the radar data, the reflectivity of model predictions has also spread more through the inlands as the time goes by. Nevertheless, based on event center, the external SST source forecasts such as GHRSST, Medspiration and NCEP become more reflective (up to 40 - 45 dBZ) around the main station at the peak hour, since it is known the reflectivity increases as the number and the depth of cumulus clouds (responsible to form heavy precipitation) grow. Especially the blue colored (30 - 45 dBZ) portions of these maps refer the exact areas where relatively higher rain has dropped. On the other hand, GFS source forecast reflectivity path, turns toward to the sea as the time reachs to the peak hour. That's why, it misses the high reflectivity near to main station at this hour.

The SST has also increased on both coastal and inner areas in three models' forecasts as the time passes, except GFS. Since the SST contour lines and magnitudes seem exactly the same in each hour of GFS model predictions. Even this difference

indicates the importance of using daily updated dataset for SST to run in weather prediction models. As higher SST means more evaporation and acceleration in the air circulation which makes the atmosphere much unstable that will pave the way to form heavy precipitation. Therefore, the external source SST models comparing to unchanged data can build more dynamic atmospheric system and may catch the right spots during the event.

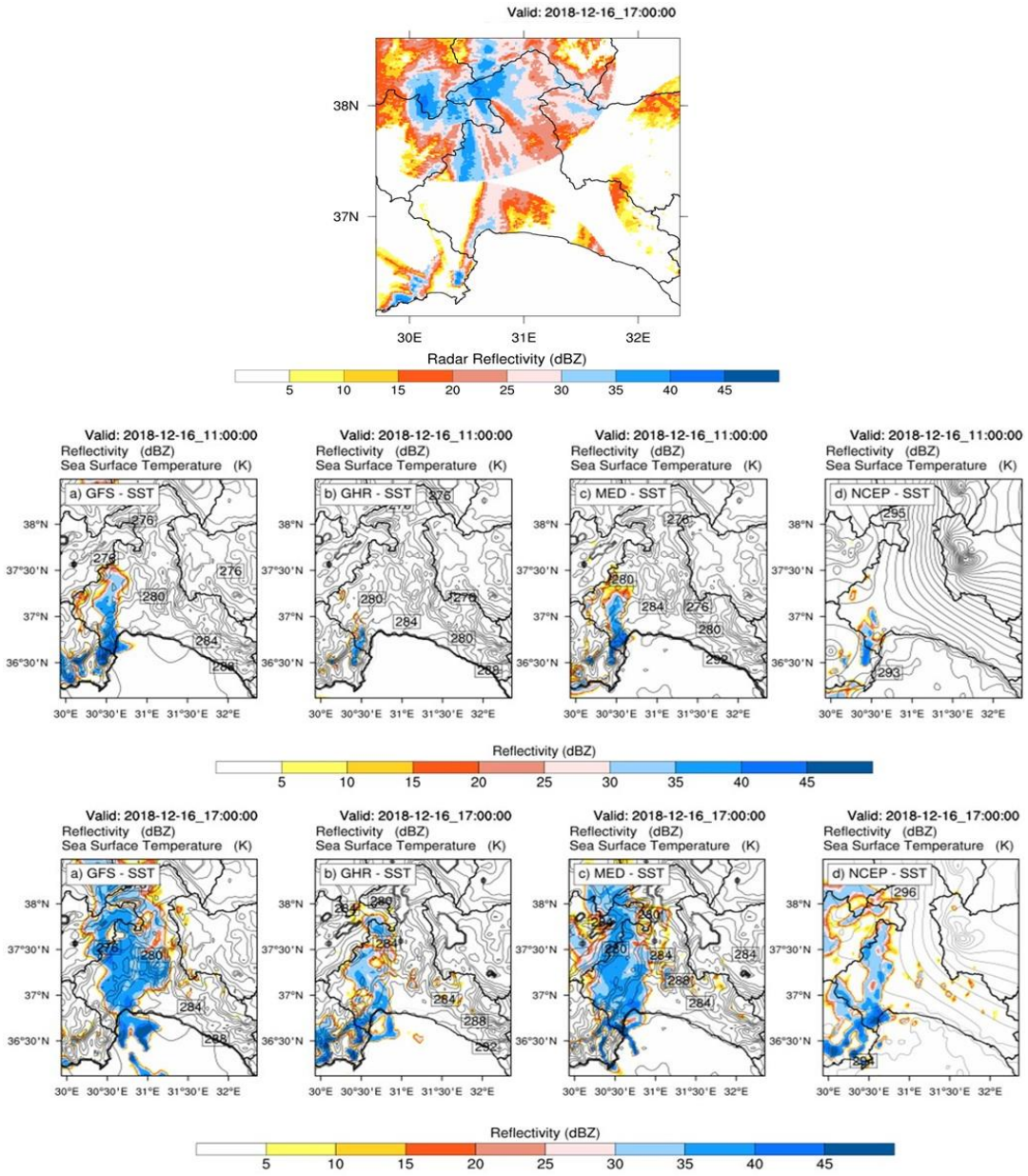

Figure 4.7.5 2018.12.10_00:00:00 – 2018.12.20_00:00:00 run period. The reflection and sea surface temperature (SST) maps with 3 km horizontal resolution of Mediterranean region. The map at the top shows the radar reflectivity data (dBZ) only at the peak hour (17:00 UTC of December 16) whereas the four maps of last two rows refer the WRF model predictions for both at 11:00 UTC and 17:00 UTC to observe the atmospheric evolution within the six hours. The shaded contours represent the reflection (dBZ) and the solid black contours indicate the SST (K). Each map in a row, illustrates the model forecast of the different SST data source: **a)** GFS, **b)** GHRSST, **c)** Medspiration and **d)** NCEP, respectively

From all of these aspects, it is clear that the model graphs on **Figure 4.7.5** meet the peak precipitation graphs on **Figure 4.7.4.**

Apart from the horizontal plane graphs over the region, the vertical condition of model predictions are also included under the scope of this study. For this purpose, the cross sectional lines from point A to point B and from point C to point D are taken to describe the vertical profile of the hotspot (around main station) where the highest precipitation takes in place, for this event.

Since the mountain effect is wanted to include into these graphs, it is planned that both the AB and CD lines are drawn in regard to pass over some part of the mountainous area. Therefore, the AB line (from south-west to north-east direction) starts from low height levels, incline the mountain heights and again reachs the plain levels while the CD line (from south-east to north-west direction) begins from the coastal side, climbs through the heights and ends at the peak point of mountains (**Figure 4.7.6** and **Figure 4.7.7**).

Once again, the cross sectional graphs are prepared for both peak hour and 6 hours before the peak time. The reason for that is observing how the atmospheric conditions in vertical axis has been changed through the hours until it reachs the peak hour's state. Additionally, the white colored gridded area at the bottom of these graphs show the topography elevation profile of the selected sections. As it can be observed from the terrain height representation on station graphs in **Figure 4.7.6** and **Figure 4.7.7**, 830 mb (~ 1.5 km height) from the ground in these vertical cross sectional graphs corresponds the peak points of the mountains.

All cross sectional graphs are analysed by using the vertical atmospheric components such as omega, combined wind velocity and equivalent potential temperature (EPT). The omega represents the upward motion in the atmosphere. Since the negative values indicate upward direction for omega, as the value gets smaller, the atmosphere becomes more unstable.

The equivalent potential temperature (EPT) is the temperature of air would have if all the moisture was condensed out by a pseudo-adiabatic process. EPT can be used to compare the temperature and moisture content among the model forecasts. High EPT values at pressure levels mean more water vapor has been carried to those levels within the air which makes the atmosphere unstable there. Upward wind velocity, on the other hand, can be considered as the flux carrier through the altitudes. All of these parameters are good indicators of the vertical turbulent mixing under the troposhere (Zhou et.al, 2009).

The first row of model forecasts on **Figure 4.7.6**, indicates the condition of atmosphere for the six hours before the peak by omega and EPT parameters whereas the second row represents how the air becomes unstable and where it dropped rain on the peak time. The last row also are drawn at this hour. Here the aim is to show the z direction wind velocity contours for the illustration of the system activity through the vertical layers.

Since the omega is the term used to describe vorticity advection in the atmosphere, it is an useful tool to observe the precipitation tendency of the cloud system. Here, the specific difference among the representations of vertical layers at 11:00 UTC and 17:00 UTC, is the power and impact area of the vorticity dynamics.

The white and blue colored sections in all four graphs at 11:00 UTC (**Figure 4.7.6** and **Figure 4.7.7**) indicate that even six hours before peak time, there were powerful vertical motions in the atmosphere. Probably, the models were producing high amounts of rain at this hour, too. If they did, it would not be wrong because through the records of the observation stations which are located on AB and CD lines, heavy precipitation continued all day along December 16.

Even though, the range of omega values shown on labelbars, meaning the intensity of vorticity, has decreased as the time flows to the peak hour, it can be easily seen that some of the configurations provide even more complex atmosphere through the vertical layers at 17:00 UTC. As from the Medspiration and NCEP scenarios (**Figure 4.7.6 c,d**), blue and white colored contours of omega has locally accumulated from higher pressure to lower pressure levels (especially for $\leq$ 500 mb).

This is important to look at because higher the magnitude of negative omega values indicate more atmospheric instability along the AB line (from point A to point B).

Additionally, the coordinates where the high magnitude of negative omega values (active vorticity advection) are obtained from Medspiration and NCEP graphs, can be easily matched with the map locations where the maximum amount of precipitation has dropped by the same options at peak hour by **Figure 4.7.4**. At this point of view, it can be seen that the Medspiration dataset model performed better than NCEP scenario for catching the hotspots of the event. Since from **Figure 4.7.4,** it can be observed that the coordinates of maximum rain received portion of the region (around the main station) should be somewhere between 30.2 – 30.4 ° Eastern longitudes. In this perspective, the strong omega forcing (white - blue colored portion on the graph) on Medspiration SST model forecast, from 780 mb up to 280 mb above the ground (**Figure 4.7.6 c**) meets the real conditions at the right coordinates.

When the combined wind speed graphs are investigated from the last column on **Figure 4.7.6**, the contour shapes are exactly the same with the omega's, shown at the top of it. As the wind is an essential component of the vertical and horizontal system of atmosphere, these graphs also provide the air circulation direction and power over the region.

Similar to omega, EPT contours' values and their intensities simulate the atmospheric system in model, too. As they kind of represent the moisture content of the current air. EPT has a direct relation with omega because if the upward dynamics accelerates among some pressure levels, the moisture concentration in those has also

enhanced and become more unstable to bring heavy precipitation over the region lie down.

The best example to prove this relation can be actually given again from the omega – EPT graphs in **Figure 4.7.6.** Since here, both the omega (the magnitude of negative values become higher and positive values start to dominate the region) and EPT (the values decreased) contours demonstrate that the GFS scenario lost its atmospheric complexity which means it turns more stable condition as the time moves to the peak hour of the event, 17:00 UTC. However, in other three options' graphs, the EPT values have risen within the same time interval, especially where the strong omega activity has observed.

Similar outcomes can be observed from CD line perspective (from point C to point D) on **Figure 4.7.7.** Here, the line starts from the coastal area and climb the mountain as it can be seen the longitudes shown on the x axis on these graphs.

Once again, omega forcing accelarates near to 30.4° Eastern longitude in the representation of Medspiration option at the peak time. However this time, from the areas covered by CD line, the upward motions also grow through the vertical levels in GFS scenario forecast for 17:00 UTC. Although these vertical local complexities in atmosphere refer heavy precipitation occurence for both four configurations, the locations where the precipitation takes place is quite different from each other. Since Medspiration option showed success for producing rain around main station; due to white – blue colored contours on 30.5° E, GFS dropped it over the sea and miss the actual hotspots of the event. GHRSST can catch the right coordinates to build unstable atmospheric system. Yet, because the upward forcing is not powerful as the others, the rain amount produced from it, is not much.

Or NCEP configuration spreads the atmospheric activity in vertical axis by larger inland portion of the region (through point D). The power of these forcings has not much enhanced via the surronding pressure levels, the system can be dynamic enough to bring heavy rainfalls like Medspiration over the area underneath. Once again, the combined wind speed contours reflect the omega patterns and by looking at the changes between this and EPT contours, it can be easily seen they share same behaviours with the previous figure.

From all of the vertical component aspects (omega, EPT and combined wind speed) of two lines, while the rising air on GHRSST, Medspitation and NCEP scenarios show strong differential positive vorticity advection (DPVA) which results dynamic precipitation, GFS scenario model draw comparatively stable and dry atmosphere by strong differential negative vorticity advection (DNVA). This may explain, why there is not much rain produced in GFS scenario, at the peak hour along the AB line on **Figure 4.7.6** and once more proves that the SST effect and the importance of using special SST source on these types of models.

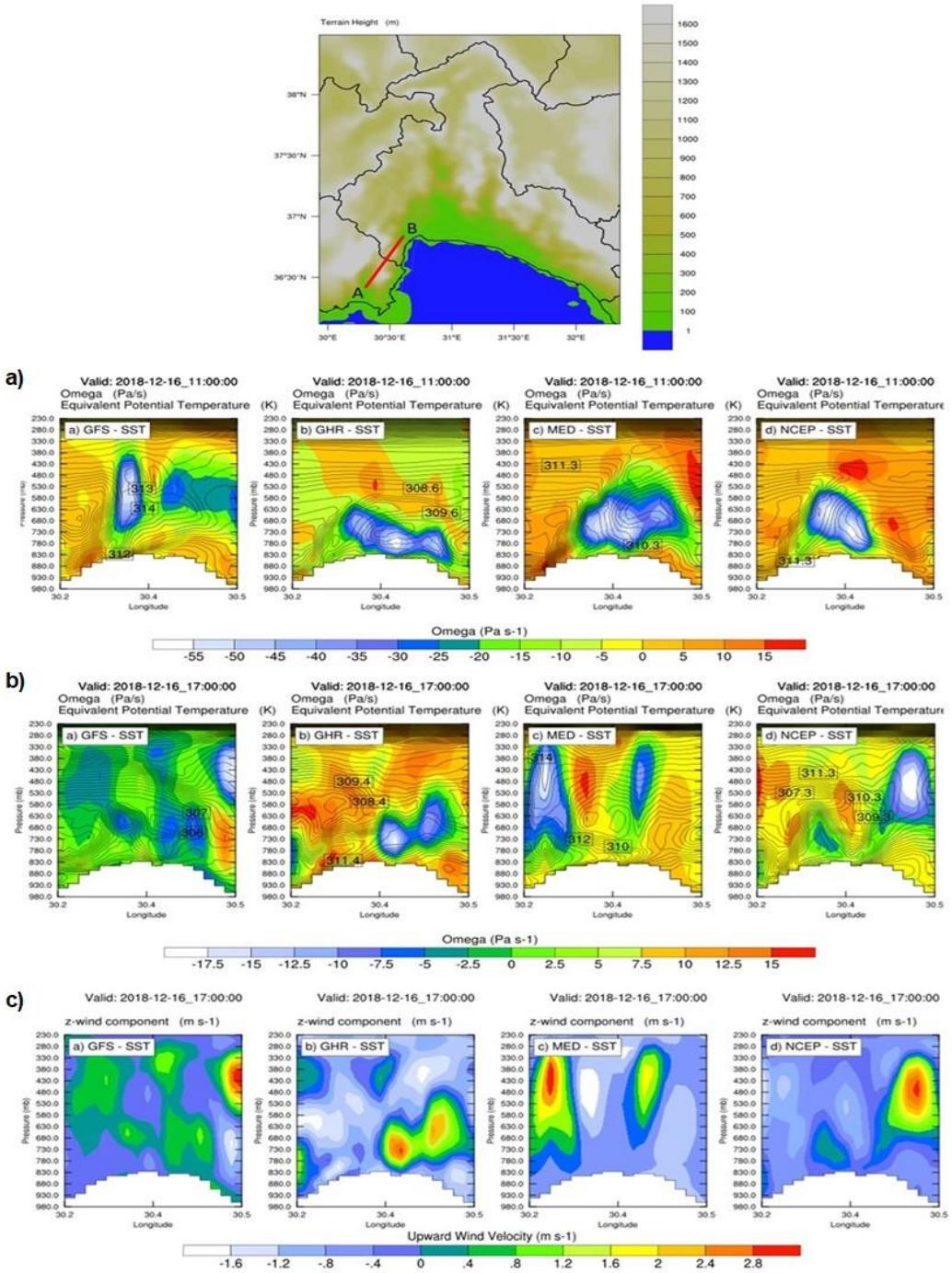

Figure 4.7.6 2018.12.10_00:00:00 – 2018.12.20_00:00:00 run period. The map at the top, shows the location and the terrain height that the AB line covers, the rest demonstrates the model forecasts by the vertical profile of atmosphere along AB line. The Y axis refers to the elevation levels (m) from the ground and the X axis shows the longitudes through the line.

Figure 4.7.6 (cont'd) The maps in the first two rows **(a & b)**, represent the omega (Shaded contours, Pa/s), the equivalent potential temperature (Solid black contours, K) for both at 11:00 UTC and 17:00 UTC to observe the change in atmosphere among the pressure levels within the six hours. Yet, the wind velocity (Shaded contours, m/s) has only drawn for the peak hour (17:00 UTC of December 16) via the last row **(c)**. The white colored gridded area at the bottom of each graph depicts the elevation profile of topography over the cross sectional area of AB line

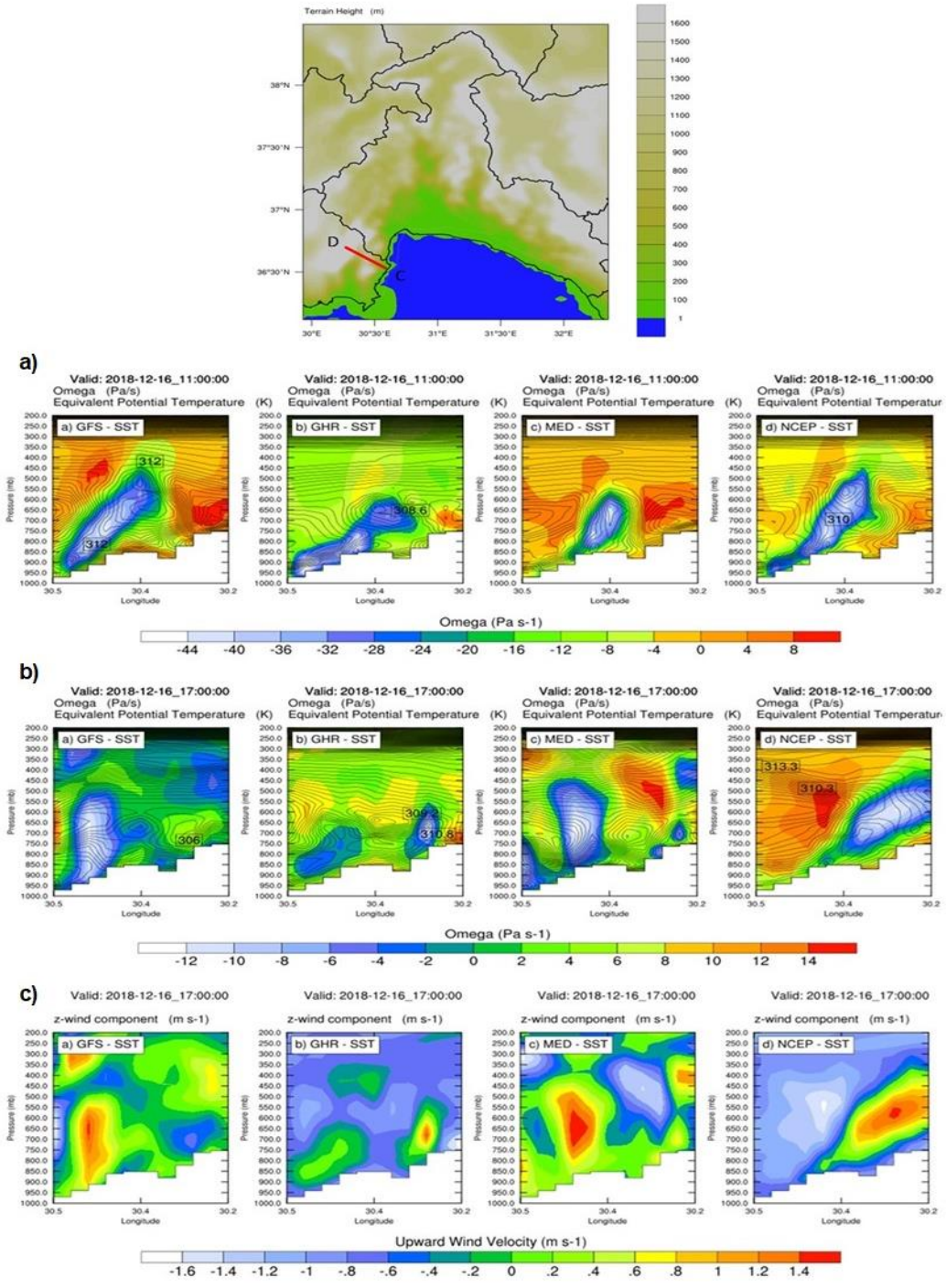

Figure 4.7.7 2018.12.10_00:00:00 – 2018.12.20_00:00:00 run period. The map at the top, shows the location and the terrain height that the CD line covers, the rest demonstrates the model forecasts by the vertical profile of atmosphere along CD line.

Figure 4.7.7 (cont'd) The Y axis refers to the elevation levels (m) from the ground and the X axis shows the longitudes through the line.The maps in the first two rows **(a & b)**, represent the omega (Shaded contours, Pa/s), the equivalent potential temperature (Solid black contours, K) for both at 11:00 UTC and 17:00 UTC to observe the change in atmosphere among the pressure levels within the six hours. Yet, the wind velocity (Shaded contours, m/s) has only drawn for the peak hour (17:00 UTC of December 16) via the last row **(c)**. The white colored gridded area at the bottom of each graph depicts the elevation profile of topography over the cross sectional area of CD line

4.8 Eastern Black Sea – Summer Event (2015/08/17 - 2015/08/27)

The second case is taken to investigate under this thesis, is the heavy precipitation event happened on Eastern Black Sea Basin, Black Sea region of Turkey. Once again, the observation station dataset are provided from the GDM. With 32.4 mm maximum precipitation production, the event date is defined as 23 – 24 August of 2015. The model for this event is run for 10 days like the Mediterranean region. To be able to observe the changing atmosphere through the event date, the starting point of the run period has decided as August 17. Hence, determined model period is 2015.08.17_00:00:00 – 2015.08.27_00:00:00.

According to the observed data, Arhavi station in Artvin has chosen as the 'main station' of this event. The peak rain amount that recorded in Arhavi station is 32.4 mm at the midnight of August 24 of 2015. The cumulative precipitation reachs almost 180 mm at the end of 10 days period. Comparing to these values with the Case 1, this event is not as intense as the previous one but considering seasonal difference among two cases, the current event is also powerful for a summer rainfall.

Figure 4.8.1 shows the temperature – precipitation time series of the main station for this event, where the highest rain amount has recorded. This graph has prepared for only 3 days (23 – 26 August) out of 10 days model period is because the event activity has started to observe in main station from the sixth day after August 17. While the black solid line represents precipitation amounts, the red dash line indicates temperature and the blue dash line on the right side depicts the change in cumulative rainfall collected of main station during the time period.

Here, temperature decreases by 4 to 5 °C before the peak hour. Yet, when it reachs the peak, there is a slight increase in temperature as well as the general precipitation pattern of this event. Through the graph on **Figure 4.8.1**, the temperature rises enhance the rainfall acitivities which may indicate the typical convective rain formation.

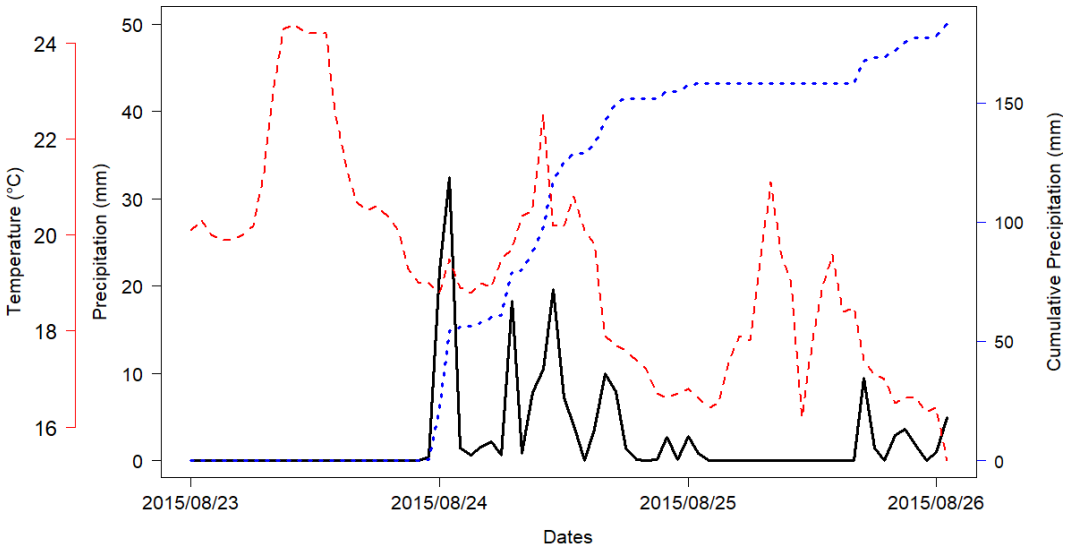

Figure 4.8.1 Precipitation and Temperature time series of the main station (Arhavi – Artvin) for Eastern Black Sea – Summer between 2015/08/23 – 2015/08/26. Black solid line refer precipitation amounts dropped over the station while the dashed red line indicates recorded temperature of the station. Dashed blue line represents the cumulative precipitation amounts through 3 days from total event period

Figure 4.8.2 and **Table 4.8.1** represent the model performances based on the important components of the tmospheric system that are known for their effects on precipitation formation. Likewise in Case 1, the first two days of 10 days run period are excluded from the analyses to keep the errors minimal as much as possible. Here, the precipitation graph on **Figure 4.8.2** depicts that the model scenarios are able to catch the closer pattern to the observation line. However, ECMWF, in which SST data has not been changed, and Medspiration scenarios have still some overpredictions in their forecasts during the period. The higher estimations in temperature and wind are valid but comparing to Mediterranean case, the gap between observation and the predictions is small. That's why, the correlations of those parameters are relatively higher than the rest.

The difference between the predictions and the recorded data at relative humidity graph can be easily observed from **Figure 4.8.2** and also proved by the statistics on **Table 4.8.1**. As the errors such as RMSE and MBE rise enormously while the correlations between the forecasts and observation diminish a lot. Although the temperature patterns are not much different from the observation, the fully humid and fast wind speed atmospheric environment created by the each scenario, in this event case predictions, the model tends to drop excess rainfall, especially for the last four days period (from August 24 to August 27).

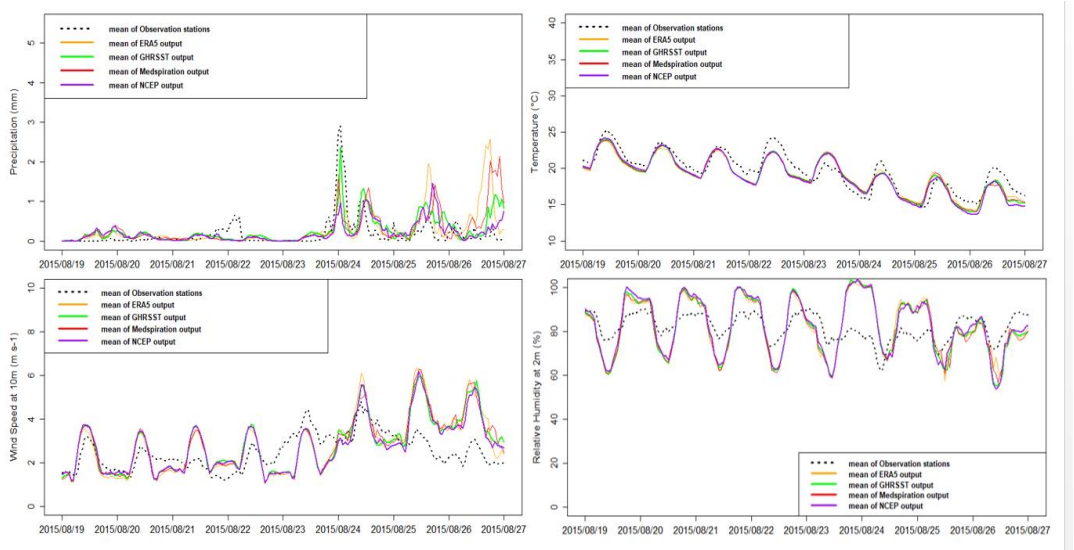

Figure 4.8.2 2015-08-19_00:00:00 – 2015-08-27_00:00:00 run period. The timeseries graphs of observation and SST model forecasts in terms of precipitation (mm), temperature (°C) , wind speed (m/s) and relative humidity (%). The solid colorful lines represent the each model prediction scenario while the dashed black line indicates the mean of observed precipitation regime in 10 days

Table 4.8.1 Statistical analysis of SST scenarios for 2015/08/19 – 2015/08/27 event period

Eastern Black Sea Region	RMSE	MBE	Standard Deviation	Correlation
Precipitation				
ECMWF	0.439	0.084	1.166	0.385
GHRSST	0.315	0.076	0.895	0.597
Medspiration	0.429	0.091	1.052	0.346
NCEP	0.347	0.350	0.706	0.396
Temperature				
ECMWF	1.441	-0.689	0.842	0.906
GHRSST	1.399	-0.687	0.889	0.911
Medspiration	1.425	-0.685	0.887	0.907
NCEP	1.426	-0.752	0.937	0.913
Combined Wind Speed				
ECMWF	1.021	0.273	1.568	0.612
GHRSST	0.995	0.305	1.471	0.590
Medspiration	1.008	0.307	1.510	0.600
NCEP	0.952	0.261	1.423	0.595
Relative Humidity				
ECMWF	10.454	0.367	2.015	0.497
GHRSST	10.763	0.135	2.116	0.528
Medspiration	10.718	0.043	2.071	0.500
NCEP	10.518	0.824	2.113	0.566

Just like **Figure 4.7.3**, **Figure 4.8.3** also represents the average precipitation and bias time series during 10 days event period. As it can be understood from the negative bias (colored in blue) at the midnigth of August 24, the observed data is much more higher than the four of models' predictions. Since this is the peak time of the current event, it can be considered that without depending on which SST dataset has been used, the four of models could achieve to catch the right time to form precipitation but miss the enough amount to drop. However, the small bias of GHRSST at this hour indicates that its scenario provided the most accurate prediction to the real conditions comparing to the rests. After the peak time, the models tend to overestimate the precipitation, especially ERA5 – ECMWF scenario.

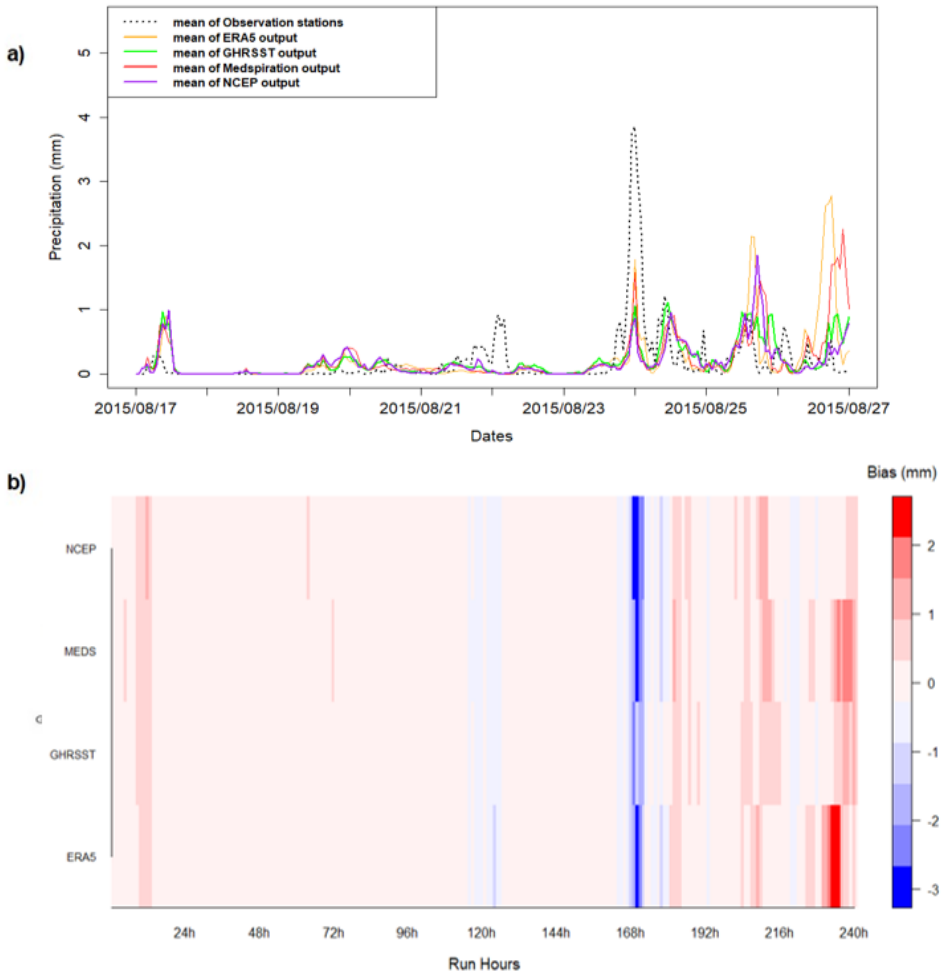

Figure 4.8.3 a) The average precipitation and **b)** bias raster plots of observation and SST model forecasts throughout the model run period. The dashed gray lines represent the each model prediction scenario while the red line indicates the mean of these model scenarios and the solid black line shows the mean of observed precipitation regime in 10 days

Figure 4.8.4 represents the observation station data and the WRF model forecasts at peak hour (2015.08.24_00:00 UTC). It has prepared by using the same approach in the **Figure 4.7.4**.

The highest precipitation with 32.4 mm dropped in main station which is colored in red on the 'Station Precipitation' map. The model predictions are able to catch the overall picture of the atmosphere. The maximum rain is usually achieved to be produced around the main station while the left side of basin is remained relatively

drier. Yet, the efficiency of the model predictions in terms of the amount and the right spot varies among the configurations.

Although ECMWF dataset model (**Figure 4.8.4a**) finds the most active area of the region right, the precipitation amount that is produced onto this area is way much higher than the reality. Based on the labelbar scale of 'Station Precipitation' and 'Hourly Precipitation', the model predicts more than 56 mm rain at and near to the main station whereas the actual range is 30 - 34 mm.

The NCEP (**Figure 4.8.4d**) model, on the other hand, has missed the right spot to pour the rain on. Besides, it does not provide enough precipitation on the region. Therefore, it shows poor performance for this event case.

Finally, GHRSST and Medspiration (**Figure 4.8.4b, c**) are both good at catching right spot and mimicing the real atmospheric condition for this hour. Nevertheless, GHRSST model forecasts overestimate the precipitation at inner portion of the region. Medspiration SST model gives the closest prediction to the observed and interpolated data over at the peak time of this event, comparing to the others.

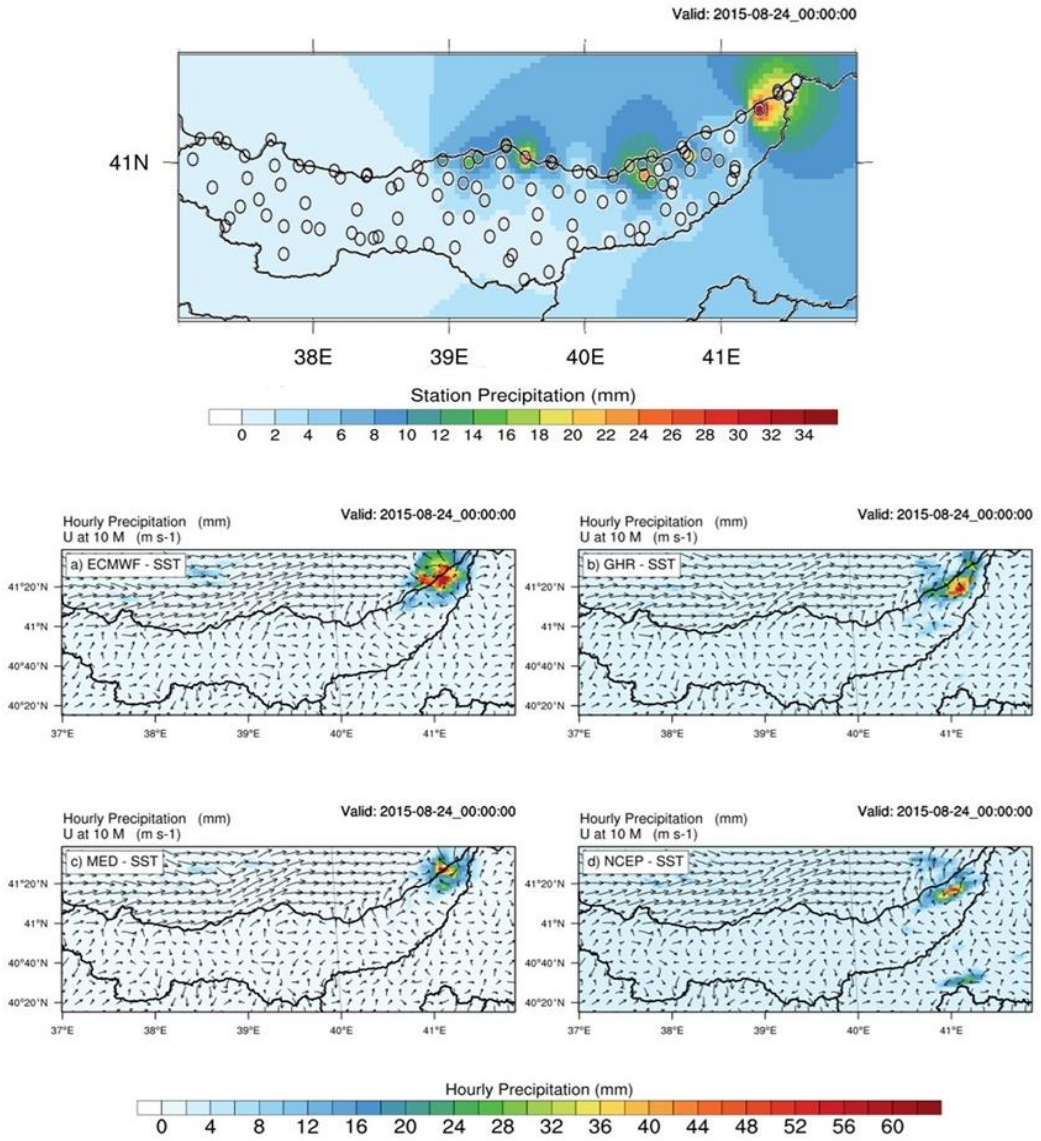

Figure 4.8.4 2015.08.17_00:00:00 – 2015.08.27_00:00:00 run period. The precipitation maps with 3 km horizontal resolution at the peak hour when the highest rain dropped over the Eastern Black Sea region. The map at the top shows the stations' precipitation data (m) and their interpolation throughout the whole domain once again for the peak time (00:00 UTC of August 24). The black circles indicate the locations of observation stations and the color scale of label bar determined according to the stations and their interpolated rain data together). The four maps at the bottom refer the WRF model precipitation forecasts (m) for the peak hour by working with different SST data sources: **a)** GFS, **b)** GHRSST, **c)** Medspiration and **d)** NCEP, respectively. Black colored vectors on each of these maps, demonstrate the wind speed (m/s) vector at 10 m above the ground

Reflectivity and SST improvements in atmosphere are shown once again on **Figure 4.8.5,** for the peak and six hours before. It is undeniable that, as time progressed to 00:00 UTC the reflectivity has grown over the right side of basin (near to main station) in all model forecasts.

The map at the top, on the other hand, represents the radar reflectivity (provided from Yousefi, 2020) at the peak hour only (the midnight of August 24). Since this data type offers 360 degree visual perception, it does not fully fill the whole region. Based on this radar data, reflectivity has shown at the center portion of region which is far away from the main station. Therefore, it can be compared with the model predictions for only that portion. According to this aspect, no common area can be observed between these two types of reflectivity outcomes. For the four scenarios showed at the bottom, the model misses the high cloudiness over the central coasts and the inlands but accumulates it around the main station.

Apart from that, the evolution of reflectivity demonstrates that the cloud activities at peak hour, have been accelerated in the model predictions due to the strong flux movements in vertical axis. Based on these, most unstable area (blue colored portion of the map, 40 - 55 dBZ) where the highest precipitation dropped at 00:00 UTC, is pointed out the top of northern east side of basin (near to main station) in all model graphs. Hence, the reflectivity contours of models are coherent with the precipitation maps in**.**

Nonetheless, SST performances of updated SST dataset used models in this event, are different from previous case study. As it can be observed from the first and second rows of satellite derived datasets, GHRSST and Medspiration, (**Figure 4.8.5b,c)**, SST contour values over the inland have decreased within six hours. Yet, even it drops a lot (around 10 K in GHRSST and 2-3 K in Medspiration) on the land, inluding the coastal area, it remains the same on the sea surface which is estimated as 300 K.

This may be related with the day time and climate effects of the region because due to its climate, the temperature on this region tends to drop sharply over the inlands at the night time of the day. Nevertheless, like GFS, the SSTs of ECMWF, have also not changed through the time. Therefore, in a way they ignore the SST impact on precipitation occurence in their forecasts. Additionally, the model worked with NCEP dataset is same in both six hours before and peak time in terms of SST values and they do not produce various contours over the region comparing to others. That may be one of the reasons of why its performance on this event is weak. Since the events on both regions are especially chosen to include this analysis because they are considered as SST triggered precipitation systems in the first place.

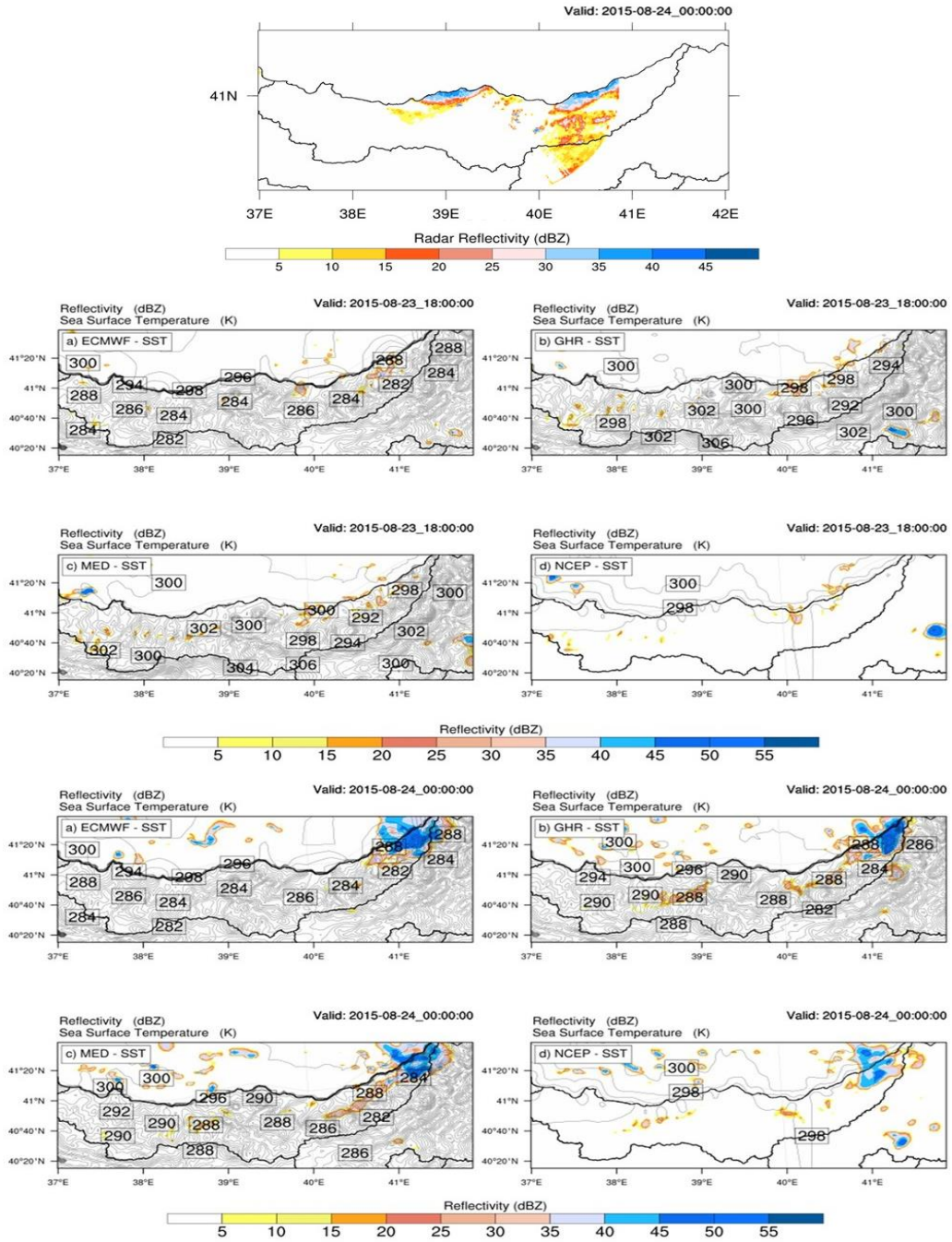

Figure 4.8.5 2015.08.17_00:00:00 – 2015.08.27_00:00:00 run period. The reflection and sea surface temperature (SST) maps with 3 km horizontal resolution of Eastern Black Sea region. The map at the top shows the radar reflectivity data (dBZ) only at the peak hour (00:00 UTC of August 24) whereas the four maps of last two rows refer the WRF model predictions for both at 18:00 UTC and 00:00 UTC to observe the atmospheric evolution within the six hours. The shaded contours represent the reflection (dBZ) and the solid black contours indicate the SST (K). Each map in a row, illustrates the model forecast of the different SST data source: **a)** GFS, **b)** GHRSST, **c)** Medspiration and **d)** NCEP, respectively

The cross sectional lines ,to observe vertical developments for this event, are again drawn as to cover some portion of mountainous area. Since the orographic impacts of the region on atmospheric system are wished to be seen. In this perspective, AB line in **Figure 4.8.6**, expands over the low heights in coastal area whereas CD line in **Figure 4.8.7** covers sea and mountain levels together.

Figure 4.8.6 and **Figure 4.8.7** are prepared to show the evolution of atmospheric stability based on the pressure levels. This type of graphs represent another perspective of complex atmospheric systems on vertical profile as omega with equivalent potential temperature (EPT) can give an idea about the possibility of precipitation and the strength of the event.

Different from the Mediterranean event, in this case the instability of atmosphere has enhanced as the time flows to peak hour in all four of model scenarios in **Figure 4.8.4**. As comparing to six hours before, the omega values at this hour's graphs have increased a lot. Here, both ECMWF, GHRSST and Medspiration options were able to create dense complex upward motions through various pressure levels. Particularly, strong omega forcing (with high magnitude of negative values) spreads over $\leq$ 500 mb on these graphs, indicate the locations where the possible extreme precipitation has produced.

By comparing the active portion of region on **Figure 4.8.4** with the cross sectional area covered by AB line on **Figure 4.8.6**, it can be seen that the rain mostly dropped towards the point B. That's why, the accelerated vertical motions (vertical vorticity advection) on GHRSST configuration could catch the right coordinates to establish the complex dynamics over. With respect to this approach, it represents the most realistic forecast among the four options for this event time. Yet, Medspiration scenario still could generate the similar vertical profiles around 41.3° E so it also provides high amounts of rain but it is not as intense as in GHRSST. Opposite to those, the other two scenarios (ECMWF and NCEP) grows the vorticity activity near to point A.

The combined wind velocities of the scenarios shown at the last row on **Figure 4.8.6**, draw the same patterns with omega forcings. As the upward motion accelerates, the wind velocity also speeds up in vertical axis (yellow to red colored contours on graphs).

Addition to all of these, the increased EPT contours at the peak hour, demonstrate the precipitation tendency of the atmospheric system of four SST scenarios. Since this parameter actually refers the moisture content of the air, higher the EPT value around powerful vorticity at the lower pressure levels, the more chance for that configuration to produce high amounts of precipitation.

If the same scenarios are investigated from CD line perspective (**Figure 4.8.7**); however, the general vertical profile patterns of atmosphere may perceptibly change. As now the cross sectional area covered by CD line, starts from the inlands and moves to sea side of the region. Therefore, the sea impact on air circulations can be observed better from this aspect.

According to that, in **Figure 4.8.7**, none of the SST configurations had strong upward motions which can bring intense rain, throughout the levels under troposhere for 18:00 UTC of August 23. As in this hour, the atmospheric activity has just started to produced.

Yet, this state has mostly changed at the peak hour's forecasts. White - blue colored contours of omega (high magnitude of negative values) again illustrate the rainy portion of the cross sectional area because they show the vertical complexity of atmosphere around there. As it can be verified from **Figure 4.8.7**, these parts in GHRSST and Medspiration scenarios correspond more commonly distributed precipitation from inlands to the sea whereas it mainly accumulates over inner portion of region (near to point C) in ECMWF option.

Moreover to this, because it exceeds 500 mb boundary and reachs lower pressures (~ 270 mb), the upward vorticity is much more strong in ECMWF configuration than the rest configurations for the peak hour. Both of these features are helpful to show the vertical atmospheric state of the large size red colored inland area on the first map (**Figure 4.8.4a**) in **Figure 4.8.4**.

Likewise to previous figures, the combined velocity speed graphs from the last row in **Figure 4.8.7**, again follow the same omega pattern and contribute the unstable air generation in the system according to that.

EPT contours for CD line perspective again become frequent and intense around the dynamic vertical motions by omega forcing. Here, it should be also observed that the EPT values generally rise towards to right side of graph (point D) as it moves to the sea side, the moisture content has increased.

Overall, the air lifting system in all four scenarios represents strong differential positive vorticity advection (DPVA) over the region.

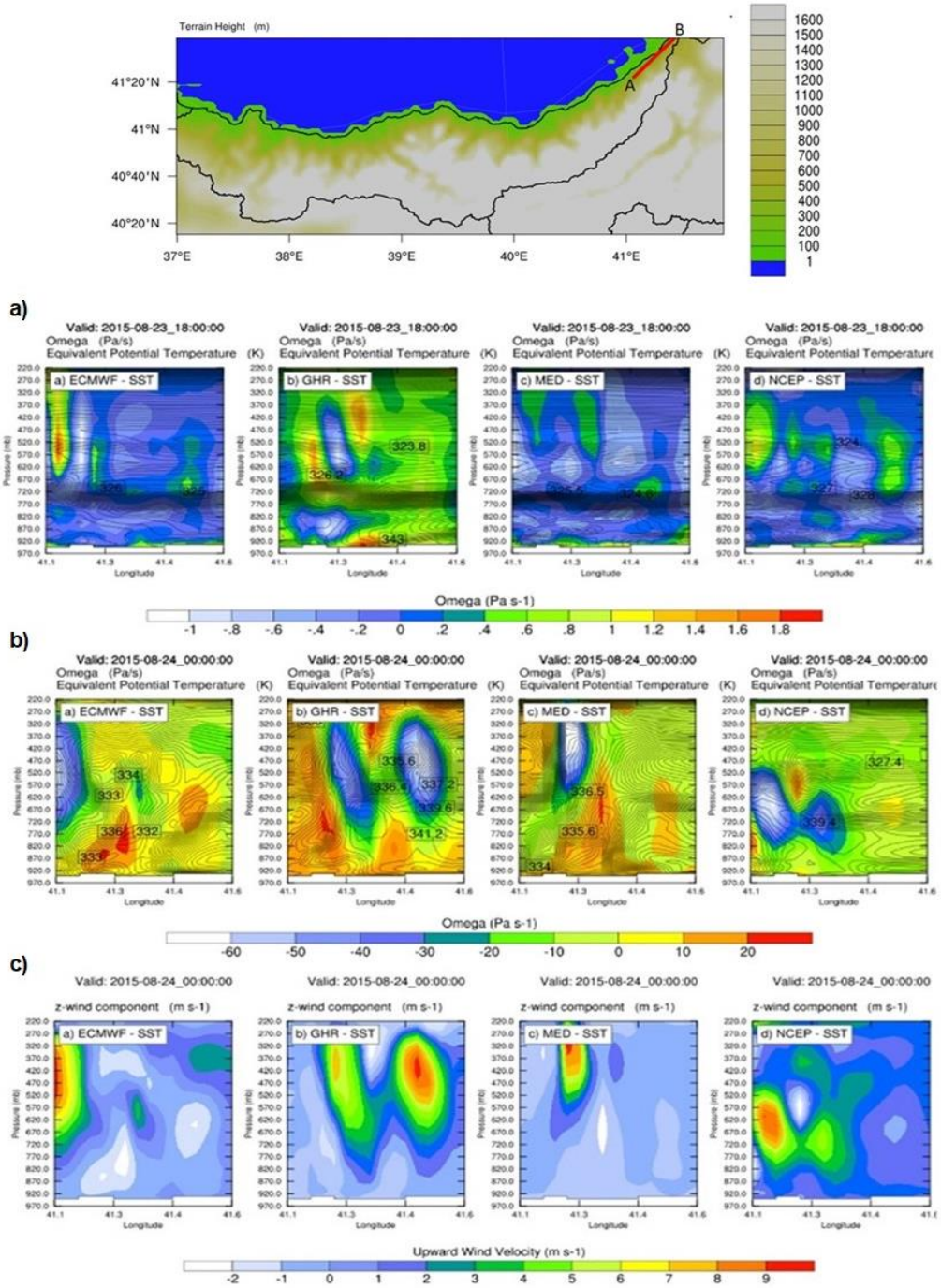

Figure 4.8.6 2015.08.17_00:00:00 – 2015.08.27_00:00:00 run period. The map at the top, shows the location and the terrain height that the AB line covers, the rest demonstrates the model forecasts by the vertical profile of atmosphere along AB line. The Y axis refers to the elevation levels (m) from the ground and the X axis shows the longitudes through the line.

Figure 4.8.6 (cont'd) The maps in the first two rows **(a & b)**, represent the omega (Shaded contours, Pa/s), the equivalent potential temperature (Solid black contours, K) for both at 18:00 UTC and 00:00 UTC to observe the change in atmosphere among the pressure levels within the six hours. Yet, the wind velocity (Shaded contours, m/s) has only drawn for the peak hour (00:00 UTC of August 24) via the last row **(c)**. The white colored gridded area at the bottom of each graph depicts the elevation profile of topography over the cross sectional area of AB line

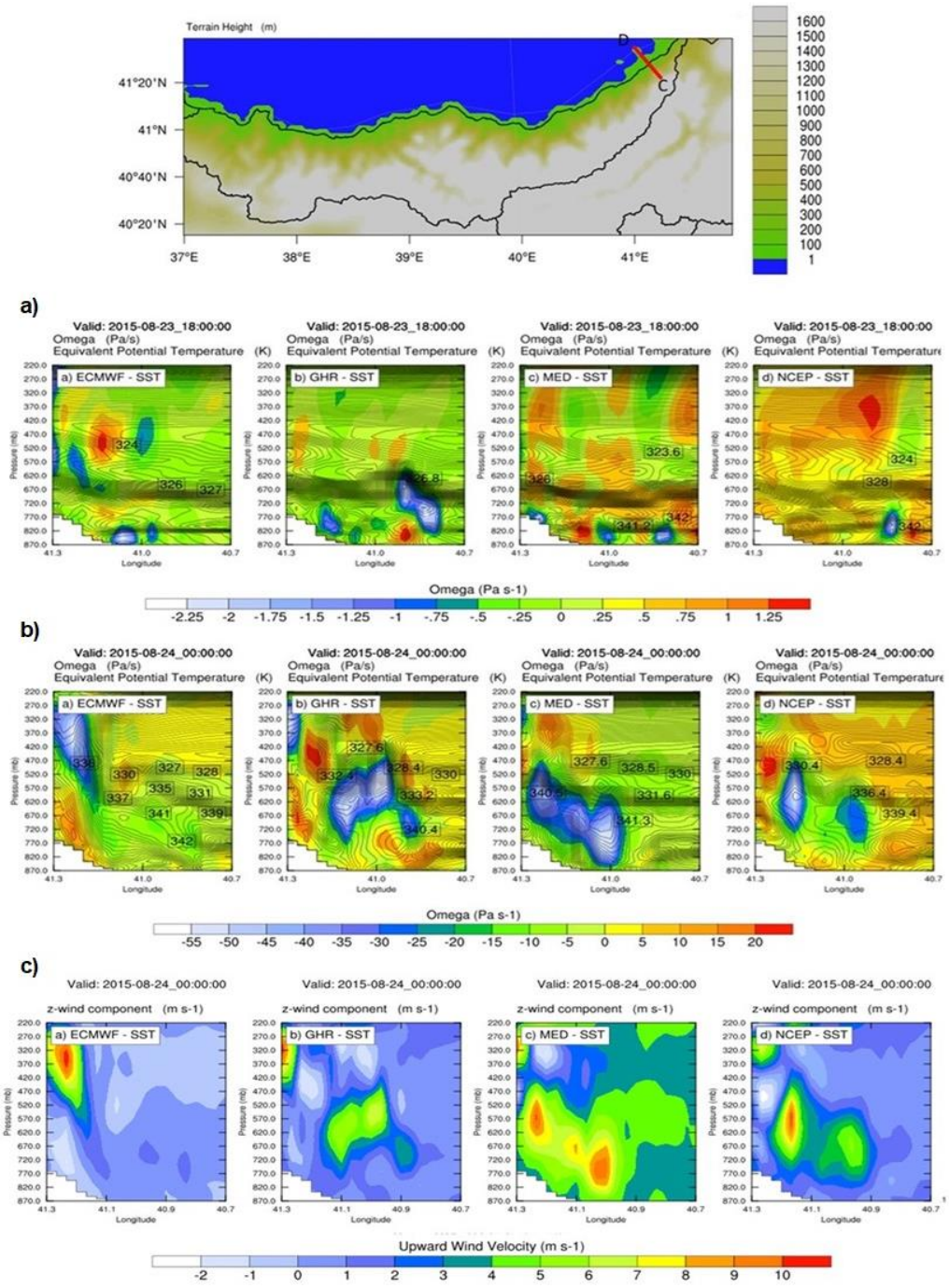

Figure 4.8.7 2015.08.17_00:00:00 – 2015.08.27_00:00:00 run period. The map at the top, shows the location and the terrain height that the CD line covers, the rest demonstrates the model forecasts by the vertical profile of atmosphere along CD line.

Figure 4.8.7 (cont'd) The Y axis refers to the elevation levels (m) from the ground and the X axis shows the longitudes through the line.The maps in the first two rows **(a & b)**, represent the omega (Shaded contours, Pa/s), the equivalent potential temperature (Solid black contours, K) for both at 18:00 UTC and 00:00 UTC to observe the change in atmosphere among the pressure levels within the six hours. Yet, the wind velocity (Shaded contours, m/s) has only drawn for the peak hour (00:00 UTC of August 24) via the last row **(c)**. The white colored gridded area at the bottom of each graph depicts the elevation profile of topography over the cross sectional area of CD line

CHAPTER 5

DISCUSSION AND CONCLUSION

5.1 Discussion of Sensitivity Analysis

Through the different perspectives of illustrations that had been applied in Sensitivity analysis so far, there is not a certain answer to describe 'best and worst' configuration options for the event predictions via the model on Mediterranean and Eastern Black Sea regions. Nonetheless, the perspectives of these illustrations still can assist some idea about the overall performance of each parameters and their options.

From all of the rankings (in **Table 4.1.3** and **Table 4.1.5)**, TOPSIS analysis, Taylor diagrams (in **Figure 4.6.1 - Figure 4.6.4)** and the visual maps, the final remarks of Sensitivity analysis can be done as follows: Eta (Ferrier, ES) scheme has already shown its great impact on Mediterranean autumn event's predictions. Here, either GFS or ERA5 input data source had been used, the model was able to build the right atmospheric conditions over the region during the event period.

These results seem comprehensible with Mediterranean climate as the ES physical mechanism is suitable for heavy precipitation but not much snow or icing occurence. However, for the summer event of the same region, Aerosol Aware Thompson (AATS) holds the higher places among the other microphysics' scenarios. As mentioned before, this event was not very successfully run by the model. The overall performances of all scenarios, even if it was chosen as 'the best configuration' by the TOPSIS Analysis, were not good enough to generate the peak precipitation amount of rain to the reality on precipitation maps. Yet, when the individual performances of microphysical schemes are considered for the 'MED – Summer' event, Taylor diagram in **Figure 4.6.1b** can be beneficial to decide which of them is

‘the best’. Based on this aspect, it can be easily seen that once again the ES scheme performed much better than the other options. Therefore, the working mechanism of ES scheme can be taken as the appropiate microphysical option to work on Mediterranean climate.

Microphysics in Eastern Black Sea events, on the contrary, the results usually proved what had been expected. Here, Aerosol Aware Thompson (AATS) and WRF Single Moment 6 (WSM6) achieved the closest forecasts to the real conditions. The general performances of these model configurations stepped forth among the other two options. This situation was expected before, as it was mentioned in Chapter 3.2.2, both of the schemes work with various type of water species including snow, ice, graupel which lead them to provide more realistic forecasts that match with the seasonal event characteristics of autumn and winter in Black Sea region.

For PBL, it can not be said that the impact of this physical parameter on WRF model is as high as microphysics. Accordingly, the best and worst scenario rankings among 96 scenarios is not significantly seperated. Although Mellor Yamada Janjic (MYJ) dominates the upper places, Yonsei University (YSU) can also perform well in some circumstances.

Unfortunately, the cumulus scheme comparison can be done by only looking at the parent domain configurations (9 km) as cumulus parameterization did not applied on nest (3 km) scenarios. The overall performances of parent domain’s scenarios points out the GFES scheme for both regional predictions.

Lastly, it is obvious that the model showed great sensitivity to the used input meteorological dataset type which defines the initial boundary conditions. For Mediterranean region, GFS dataset performed better whereas ERA5 used configurations could create more realistic events for Eastern Black Sea region.

5.2 Discussion of SST Analysis

From the obtained results, it is undeniable that the SST is quite effective atmopsheric component on the weather forecasts, especially for Mediterranean region. When the SST dataset has not been updated, the model generally tends to overestimate precipitation over the sea or miss the right location where the event is mainly occured. This happens probably because the rapid rises or drops in SST can not be supplied from the meterological input datasets as it does when the case where the external updated SST source datasets have been used. Therefore, the model fails to produce vertical movements, builds up the right atmospheric conditions under troposhere.

Through the multiple horizontal and vertical plane analyses on Mediterranean region, the overall performance of each model can be determined. Although all of the three models run by external SST datasets are able to achieve simulating the system well, the model used Medspiration SST source seems usually one step ahead from the others. As it can be observed from peak hour maps on **Figure 4.7.4d** or the vertical profiles of models in **Figure 4.7.6d** and **Figure 4.7.7d**, when the model worked with NCEP SST dataset, it provided high amounts of precipitation on the northern and western parts of the actual spot whereas GHRSST was able to catch the actual spot but it could not form enough rain over there. For the case where the SST values are not updated by an additional source (GFS – SST scenario), the clouds were mostly accumulated on the sea. This cause the model to provide more precipitation over there, overestimate the amounts. Thus, it diminishes the forecast performance (**Figure 4.7.4a**).

For Eastern Black Sea region, however, the order of models' performances is not the same with Mediterranean. Firstly, the ECMWF scenario which does not contain updated SST source, did not offer the worst prediction. Even though it overestimated the precipitation amounts at peak hour (**Figure 4.8.4a**), especially over the sea, it

succeded to find the hot spot area (around main station). Yet still, other datasets could create apparent differences from this forecast. The models run by GHRSST and Medspiration sources provide similar forecasts, only divergence is that GHRSST has more accurate prediction near to the main station. NCEP dataset model, on the other hand, could not catch the right spot to build up the unstable atmosphere and estimate enough rain. Hence, it underestimated the rain at peak time as well as brought the most of it towards to the inland part of the region.

5.3 Summary, Conclusions and Recommendations

The Sensitivity Analysis of this thesis once again reveals one fact that has been already known for NWP model predictions: the model makes better predictions for synoptic / frontal precipitation systems rather than convective systems. Since the dropped amount of rain is much more small, the rain received area is relatively large (recorded by many stations) and the precipitation does not suddenly occur and stop like in the convective system, the frontal characteristic events are generally much easy to predict by the NWP models. This may be why the WRF predictions were generally more successful at the maximum mean precipitation hour maps of each event case in Sensitivity Analysis. Additionally, it may be also one of the reasons why ERA5 dataset performed better at Eastern Black Sea region but not on Mediterranean. The precipitation system in Eastern Black Sea region is generally frontal whereas in Mediterranean region, the convective systems are usually observed.

Table 5.3.1 represents a summary of the best options obtained from both Sensitivity and SST analyses. According to this, the various options of each parameter are evaluated based their performances on two regions, for both autumn and summer seasons and the different aspects of examinations conducted under this thesis such as TOPSIS analysis, Taylor diagrams or the precipitation maps. Eventually, the option that contributes the most accurate

precipitation forecast and gives the optimal results for both seasons, are selected and listed on **Table 5.3.1**. Since there was no cumulus parameterization had been applied on domain 2 (3 km) scenarios in Sensitivity and SST Analyses, 'Precipitation maps' column of the cumulus parameter is empty for both regions. As it can be observed from the previous chapter, 'Precipitation maps' were only prepared for domain 2 scenarios not domain 1. Therefore, the best cumulus option could not be determined from the 'precipitation maps. Similarly, Taylor diagrams were not used during the examination of SST Analysis. Hence, that column of 'SST Source' parameter could not be filled with any option.

Table 5.3.1 Summary Table of the Best Options for Sensitivity and SST Analyses

	Region	TOPSIS Analysis	Statistical Parameters	Precipitation maps	Taylor Diagrams
Microphysic	MED	ES	ES	ES	ES
	EBLS	WSM6/ AATS	ES	WSM6/ AATS	ES
Cumulus	MED	GFES	GFES	-	GFES
	EBLS	GFES	GFES	-	KFS
PBL	MED	MYJ	MYJ	MYJ	MYJ
	EBLS	MYJ	MYJ	YSU	MYJ
Input Dataset Type	MED	GFS	ERA5	GFS	ERA5
	EBLS	ERA5	GFS	ERA5	GFS
SST Source	MED	NCEP	GHRSST	MEDS/ NCEP	-
	EBLS	ECMWF	NCEP	ECMWF/ GHRSST	-

Based on the two analyses conducted so far, the impacts of region, climate, physical schemes and initial boundary conditions were found to have strong impact on the WRF model predictions. The amount of precipitation as well as its distribution throughout the domains varies a lot by these parameters. Besides that, the coherence

among the options in the model configuration is crucial for WRF model. Since sometimes even the working mechanism of a physical scheme or the input data source suits well with the event or the climate characteristic on that region because the other configuration options do not cooperate with this mechanism good enough, that scenario does not provide successful predictions. That's actually why, 96 different model configurations were run by the model in Sensitivity analysis. Since even though certain schemes and datasets are selected to use, their performance together as an ensemble in the model will change from one scenario to other.

This outcome proves the theory (Chapter 1.3) about the GDM's one model configuration application for the whole regions in Turkey. Since the results obtained from the Sensitivity Analysis, indicate that using only one standard model configuration ensemble may not always provide the best weather forecasts for different climates, the orographies and the even seasons. Therefore, it may be a better idea to determine the new model configurations that are special to each regions in Turkey. These configuration options can be determined based on their weather prediction performances on every region and for mainly two seasons (winter and summer or autumn - summer). Since generally, the precipitation characteristics and the recorded temperature of winter - autumn and summer - spring are similar in many regions of this country. Hence, changing the used configuration ensemble even for only two seasons among four, can create great improvements in prediction accuracy.

When the GDM's configurations are compared with the results of Sensitivity Analysis, it can be easily noticed that there are major differences between them. For instance, in Sensitivity Analysis ES for Mediterranean region and AATS's performances for Eastern Black Sea region become prominent among other microphysics schemes, while the GDM only use WRF Single Moment 3 or 5 (WSM3 or WSM5) schemes. In terms of the working mechanisms of these schemes, it is possible to think WSM5 might be a good alternative option to use in the model for Eastern Black Sea region. Since WSM5, WSM6 and AATS share similar approachs and relations among hydrometeors to make calculations. However, by looking at

WSM6 and AATS performances on Mediterranean event cases, WSM5 may not provide same success for Mediterranean region's forecasts. At this point, WSM3 can be better alternative to use.

The GDM uses YSU as PBL scheme whereas the general outcome of four event cases taken under Sensitivity Analysis, points out MYJ. Even though this again creates difference, best PBL approach on each region may vary from one season to another or even the time of day. Since PBL parameter is highly related with the event characteristics. If the event is dominated with strong turbulence and drops heavy rainfalls after (mostly happens in winter), probably YSU approach can solve that atmospheric system better than MYJ. However, if the air is relatively stable and not surronded by great temperature changes (mostly happens in summer or night time in a day) then MYJ scheme might be more appropiate to use.

From **Table 1.3.1**, it can be observed that GDM only use IFS meteorological dataset to define the initial boundary conditions of WRF model. Similar to ERA5, IFS is also a product of ECMWF and contains data assimilation for observation and forecasted data. With this perspective, it may show similar prediction successes at Eastern Black Sea region as ERA5 dataset did. Yet, for Mediterranean weather events, especially fo the heavy convective precipitations, it may not provide the same forecast performance. As if it is remembered from the results of Sensitivity Analysis, GFS meteorological dataset usually becomes prominent on Mediterranean region. Hence, it may be more appropiate to consider the prediction performance of each datasets on a region before using it for the operational studies.

The same outcomes were obtained from SST Analysis, too. Here, it has been proved that SST also contributes to the weather predictions a lot for shaping the atmospheric system in the model. Hence, using daily updated SST source where both satellite and in-situ observation data included, is very important on the heavy precipitation occurences especially for hot the climates and the omplex topographical regions such as Mediterranean. Therefore, the results obtained from the conducted SST Analysis can be beneficial for the GDM's future studies. They can use satellite derived

updated SST sources during the weather predictions in Turkey. For instance, on Mediterranean region the Medspiration dataset but on Easter Black Sea region, GHRSST dataset can be preferred.

At the end of many examinations applied on both analyses, some recommendations are offered for possible future studies. The recommendations are listed as follows:

- Cumulus parameterization may be opened for scale aware schemes (e.g. Grell Freitas)
- Model run periods may be arranged based on the precipitation existence

First recommendation is using the cumulus parameterization for some specific conditions. As mentioned before, the cumulus parameterization has been usually turned off for the higher horizontal resolution domains ($\leq$ 4 km). However according to some studies (Jeworrek et al., 2019; Moya-Álvarez et al., 2018; Mayor & Mesquita, 2015; Gilliland & Rowe, 2007; Bister, 1998), this may create one of the weakness of Sensitivity analysis because by looking at the cumulus effects on domain 1 (parent, 9 km) forecasts, it can be considered that the usage of cumulus parameterization may change entire forecast performances of the domain 2, too (nest, 3 km) (Moya-Álvarez et al., 2018). This claim is especially valid for the scale aware cumulus schemes (Jeworrek et al., 2019) such as Grell Freitas (GFES). As this type of schemes calculate the effective radius of updraft mechanism based on the entrainment rate while the other schemes generally cover < 10 % of horizontal area of grid cell with updraft (Jeworrek et al., 2019). Yet, when the resolution gets higher, the updraft usually becomes strong and complex by occuring different sizes from the deep convections to the turbulent eddies during the extreme precipitations. Therefore, most of the cumulus scheme assumptions are usually suitable for the coarse domain resolutions (15 – 30 km) whereas with their working mechanisms, the scale aware cumulus schemes offer more realistic atmospheric system over high resolution domains.

The second recommendation is the importance for the starting day of the model run period. Since it was found out that this factor has an impact on WRF model prediction accuracy. If there is rain on the region at the very first hour of the model run period then probably when the peak hour has come, the model may underestimate the rain amount produced or miss the actual spots to drop precipitation, as it happened in Eastern Black Sea region – Autumn event case. This may be related with the initial unstable atmospheric conditions are missed by the spin up time of the model.

REFERENCES

Abualkishik, A. Z. (2018). A comparative study on the software architecture of WRF and other numerical weather prediction models. *Journal of Theoretical and Applied Information Technology*, *96*(24), 8244–8254.

Argüeso, D., Hidalgo & Muñoz, J., M., Gámiz & Fortis, S. R., Esteban & Parra, M., J., Dudhia, J., Castro & Diez, Y. (2011). Evaluation of WRF Parameterizations for Climate Studies over Southern Spain Using a Multistep Regionalization, *J. Amer. Meteor. Soc.*, 24, 5633 – 5651, doi: 10.1175/JCLI-D-11-00073.1 Ó.

Arthur, R. S., Lundquist, K. A., Mirocha, J. D., & Chow, F. K. (2018). Topographic effects on radiation in the WRF model with the immersed boundary method: Implementation, validation, and application to complex terrain. *Monthly Weather Review*, *146*(10), 3277–3292. https://doi.org/10.1175/MWR-D-18-0108.1

Arakawa, A., Schubert, W.H. (1974) Interaction of a cumulus cloud ensemble with the large-scale environment, part 1. *J. Atmos. Sci*. 31, 674–701.

Balseiro, C., F. (2008). Final Report MeteoGalicia – Consellería de Medio Ambiente Xunta de Galicia, European Atlantic Forecasting System, 7-8.

Bao, J.-W., Michelson, S. A., McKeen, S. A., Grell, G. A. (2005) Meteorological evaluation of a weather-chemistry forecasting model using observations from the TEXAS AQS 2000 field experiment. *J. Geophys. Res.*, 110, D21105, doi:10.1029/2004JD005024.

Bernardet, L., Wolf, J., Nance, L., & Loughe, A. (2006). *Comparison between WRF-ARW and WRF-NMM objective forecast verification scores a b a b*.

Betts, A. K. (1982) Saturation point analysis of moist convective overturning. *J. Atmos. Sci.*, 39, 1484–1505.

Betts, A. K. (1986a) A new convective adjustment scheme. Part I: Observational and theoretical basis. *Quart. J. Roy. Meteor. Soc.*, 112, 677–691.

Betts, A. K., Miller, M. J. (1986b) A new convective adjustment scheme. Part II: single column test using Gate wave, BOBMEX, ATEX and arctic air-mass data sets, Q. J. R. Meteorol. Soc., 112, 693–709.

Bianco, L. (2008). Surface layer parameterization in WRF. ATOC 7500: Mesoscale Meteorological Modeling, 1–23. http://cires1.colorado.edu/science/groups/pielke/classes/at7500/Bianco_SFC.pdf. Accessed 15 May 2020

Bigg, G. R., Jickells, T. D., Liss, P. S., & Osborn, T. J. (2003). The role of the oceans in climate. *International Journal of Climatology*, *23*(10), 1127–1159. https://doi.org/10.1002/joc.926

Bister, M. (1998). Cumulus Parameterisation in Regional Forecast Models: A Review. In *Hirlam Techinal Report* (Issue 35, pp. 1–31). http://scholar.google.com/scholar?hl=en&btnG=Search&q=intitle:Cumulus+parameterisation+in+regional+forecast+models:+A+Review#1

Bonekamp, P. N. J., Collier, E., Immerzeel, W. W. (2018). *The Impact of Spatial Resolution , Land Use , and Spinup Time on Resolving Spatial Precipitation Patterns in the Himalayas*. *Whiteman 2000*, 1565–1581. https://doi.org/10.1175/JHM-D-17-0212.1

Bright, D. R., Mullen, S. L. (2002) The sensitivity of the numerical simulation of the southwest monsoon boundary layer to the choice of PBL turbulence parameterization in MM5. *Wea. Forecasting*, 17, 99–114.

Brown, A. R. (1996) Evaluation of parameterization schemes for the convective boundary layer using large-eddy simulation results. *Bound.-Layer Meteor.*, 81, 167–200.

CERSAT (2012) MEDSPIRATION project background. http://cersat.ifremer.fr/thematic-portals/projects/medspiration/medspiration-project-background. Accessed 23 December 2019

Chen, F., Dudhia, J. (2001) Coupling an Advanced Land Surface - HydrologyModel with the Penn State–NCARMM5 Modeling System. Part I: Model implementation and sensitivity. *Mon.Wea. Rev.*, 129, 569–585.

Cisneros, M., Cacho, I., Frigola, J., Canals, M., Masqué, P., Martrat, B., Casado, M., Grimalt, J. O., Pena, L. D.,Margaritelli, G., & Lirer, F. (2016) Sea surface temperature variability in the central-western Mediterranean Sea during the last 2700 years: A multi-proxy and multi-record approach. *Climate of the Past*, *12*(4), 849–869. https://doi.org/10.5194/cp-12-849-2016

Conforti, P., Ahmed, S. and Markova, G. (2018). The impact of disasters and crises on agriculture and food security - 2017. In *Food and Agriculture Organization of the United Nations*. https://doi.org/978-92-5-130359-7

Conley, A., Collins, W.D., Iacono, M.J. (2011) Impacts of the Rapid Radiative Transfer Model (RRTMG) on CAM5 simulations, in preparation for *J. Climate* CESM1 special issue.

Davies, T. (2014). *Lateral boundary conditions for limited area models*. *January*,

185–196. https://doi.org/10.1002/qj.2127

Done, J., Davis, C. A., Weisman, M. (2004) "*e next generation of NWP: explicit forecasts of convection using the weather research and forecasting (WRF) model," *Atmospheric Science Letters*, vol. 5, no. 6, pp. 110–117.

Dudhia, J. (1989) Numerical study of convection observed during the winter monsoon experiment using a mesoscale two dimensional model. J. Atmos. Sci., 46, 3077–3107.

Dudhia, J. (n.d.). Overview of WRF Physics NCAR.. http://homepages.see.leeds.ac.uk/~lecag/wiser/sample_wiser_files.dir/Physics Dudhia.ppt.pdf. Accessed 15 May 2020

European Centre for Medium-Range Weather Forecasts, ECMWF (2020) ERA5 https://www.ecmwf.int/en/forecasts/datasets/reanalysis-datasets/era5. Accessed 15 May 2020

Ek, M. (2013). Land Surface in Weather and Climate Models, "IV WorkEta: Esquema de superfície", Environmental Modeling Center (EMC). National Centers for Environmental Prediction (NCEP). NOAA Center for Weather and Climate Prediction (NCWCP). 5830 University Research Court College Park, MD 20740 National Weather Service (NWS). National Oceanic and Atmospheric Administration (NOAA). IV WorkEta – Workshop em Modelagem Numérica de Tempo e Clima em Mesoescala utilizando o Modelo Eta: Aspectos Físicos e Numéricos CPTEC/INPE, Cachoeira Paulista, São Paulo, 3-8 de Março de 20131

Elvidge, A. D., Sandu, I., Wedi, N., Vosper, S. B., Zadra, A., Boussetta, S., et al. (2019). Uncertainty in the representation of orography in weather and climate models and implications for parameterized drag. *Journal of Advanced in*

Modelling Earth Systems, 11, 2567 – 2585. https://doi.org/10.1029/2019MS001661

Ferrier, B.S., Jin, Y., Lin, Y., Black, T., Rogers, Eric & Dimego, Geoff. (2002) Implementation of a new grid-scale cloud and precipitation scheme in the NCEP Eta model. 15th Conf. on Numerical Weather Prediction. 280-283.

Flesch, T. K., and G. W. Reuter, 2012: WRF Model simulation of two Alberta flooding events and the impact of topography. *J. Hydrometeor.*, **13**, 695–708, doi:https://doi.org/10.1175/JHM-D-11-035.1.

Fritsch, J. M., Chapell, C. G. (1980) Numerical prediction of convectively driven mesoscale pressure systems, Part 1: Convective parameterization, *J. Atmos. Sci.*, 37, 1722–1733.

Gelpi, I .R., Gaztelumendi, S., Carreño, S., Hernández, R., Egaña, J. (2016). Study of NWP parameterizations on extreme precipitation events over Basque Country, *J. Adv. Sci. Res.*, 13, 137–144, doi:10.5194/asr-13-137-2016.

Gerard, L., Phillips, V. T. J., Barkidija, S., & Piriou, J. (2013). *Phenomenology of convection-parameterization closure*. 4111–4131. https://doi.org/10.5194/acp-13-4111-2013

GHRSST Science Team (2010), The Recommended GHRSST Data Specification (GDS) 2.0, document revision 4, available from the GHRSST International Project Office, 2011, pp 123

Gilliland, E. K., Rowe, C. M. (2007) "A comparison of cumulus parameterization schemes in the WRF model," in *Proceedings of the 87th AMS Annual Meeting and 21st Conference on Hydrology*, San Antonia, TX, USA.

Grell, G. A. (1993) Prognostic evaluation of assumptions used by cumulus parameterization. *Mon. Wea. Rev.*, 121, 764–787.

Grell, G. A., Freitas, S. R. (2014) A scale and aerosol aware stochastic convective parameterization for weather and air quality modeling. Atmospheric Chemistry and Physics, 14, 5233–5250. https://doi.org/10.5194/acp-14-5233-2014

Hanna, S. R., and R. Yang, 2001: Evaluations of mesoscale models'simulations of near-surface winds, temperature gradients, and mixing depths. J. Appl. Meteor., 40, 1095–1104.

Hart, K. A., W. J. Steenburgh, and D. J. Onton, 2005: Model forecast improvements with decreased horizontal grid spacing over finescale intermountain orography during the2002 Olympic Winter Games. Wea. Forecasting, 20, 558–576.

Hersbach, H., Bell, B., Berrisford, P., Hirahara, S., Horányi, A., Nicolas, J., Peubey, C., Radu, R., Bonavita, M., Dee, D., Dragani, R., Flemming, J., Forbes, R., Geer, A., Hogan, R. J., Janisková, H. M., Keeley, S., Laloyaux, P., Cristina, P. L., & Thépaut, J. (2020). *The ERA5 global reanalysis*. *March*, 1–51. https://doi.org/10.1002/qj.3803

Hong, S. Y., and J. W. Lee (2009a) Assessment of the WRF Model in reproducing a flash-flood heavy rainfall event over Korea. *Atmos. Res.*, 93, 818–831, doi:https://doi.org/10.1016/j.atmosres.2009.03.015.

Hong, S.–Y., Dudhia, J., Chen, S.–H. (2004) A revised approach to ice microphysical processes for the bulk parameterization of clouds and precipitation. *Mon. Wea. Rev.*, 132, 103–120.

Hong, S.–Y., Lim, J.–O. J. (2006a) The WRF single–moment 6–class microphysics scheme (WSM6). *J. Korean Meteor. Soc.*, 42, 129–151.

Hong, S. – Y., Lim, K. S. S., Kim, J. H., Lim, J. O. J., Dudhia, J. (2009b) Sensitivity study of cloud-resolving convective simulations with WRF using two bulk microphysical parameterizations: Ice-phase microphysics versus sedimentation effects. *J. Appl. Meteor. Climatol.*, 48, 61–76.

Hong, S.–Y. (2010), A new stable boundary layer mixing scheme and its impact on the simulated East Asian summer monsoon, Quart. J. Roy. Meteor. Soc., 136(651), 1481–1496, doi:10.1002/Qj.665.

Hong, S.-Y., Pan, H.-L. (1996) Nonlocal boundary layer vertical diffusion in a medium-range forecast model. *Mon. Wea. Rev.*, 124, 2322–2339.

——, Noh, Y., Dudhia, J. (2006b) A new vertical diffusion package with explicit treatment of entrainment processes. *Mon. Wea.Rev.*, 134, 2318–2341.

Iacono, M. J. (2011). Final Report: Application of Improved Radiation Modeling to General Circulation Models, Atmospheric and Environmental Research, Inc. 131 Hartwell Avenue, Lexington, Massachusetts

IPCC, 2014: Climate Change 2014: Impacts, Adaptation, and Vulnerability. Part A: Global and Sectoral Aspects. Contribution of Working Group II to the Fifth Assessment Report of the Intergovernmental Panel on Climate Change [Field, C.B., V.R. Barros, D.J. Dokken, K.J. Mach, M.D. Mastrandrea, T.E. Bilir, M.

Chatterjee, K.L. Ebi, Y.O. Estrada, R.C. Genova, B. Girma, E.S. Kissel, A.N. Levy, S. MacCracken, P.R. Mastrandrea, and L.L.White (eds.)]. Cambridge University Press, Cambridge, United Kingdom and New York, NY, USA, 1132 pp.Pratolongo, P., Leonardi, N., Kirby,J. R.,Plater, A.. (2019). Temperate Coastal Wetlands: Morphology, Sediment Processes, and Plant Communities, Elsevier, Chapter 3, 105 – 152. https://doi.org/10.1016/B978-0-444-63893-9.00003-4

Iracema, L., Pinto, C., Costa, M. H., De, F. Z., Mara, L., Diniz, F., Sediyama, G. C., Falco, E. F., Aires, B., Gerais, M., Lin, H., Brunet, G., Derome, J., McGuffie, K., Henderson-Sellers, A., Saha, S., Moorthi, S., Wu, X., Wang, J., … Cataldi, M. (2014). What ' s the difference between FNL and GFS ? *Journal of Climate*, *27*(2), 1–15. https://doi.org/10.1118/1.3685581

Iriza, Amalia & Dumitrache, Rodica & Lupascu, Aura. (2015). The influence of topography characteristics on the numerical weather forecast with the WRF model in cases of severe weather. *Romanian Reports in Physics*. *67*. 1128–1137

Janjic, Z. I. (1994) The step-mountain eta coordinate model: Further development of the convection, viscous sublayer, and turbulence closure schemes. *Mon. Wea. Rev.*, 122, 927–945.

Janjic, Z., Gall, R., & Pyle, M. E. (2010). *Scientific Documentation for the NMM Solver* (No. NCAR/TN-477+STR). National Center for Atmospheric Research University Corporation for Atmospheric Research. doi:10.5065/D6MW2F3Z

Jankov, I., Gallus Jr., W. A., Segal, M., Shaw, B., Koch, S. E. (2005) The impact of different WRF model physical parameterizations and their interactions on warm season MCS rainfall. *Wea. Forecasting*, 20, 1048–1060.

——, Schultz, P. J., Anderson, C. J., Koch, S. E. (2007) The impact of different physical parameterizations and their interactions on cold season QPF in the American river basin. *J. Hydrometeor.*, 8, 1141–1151.

Jarno Mielikainen, Bormin Huang, and Allen Huang "Optimizing Weather and Research Forecast (WRF) Thompson cloud microphysics on Intel Many Integrated Core (MIC)", Proc. SPIE 9124, Satellite Data Compression, Communications, and Processing X, 91240Q (28 May 2014); https://doi.org/10.1117/12.2055038

Jee, J.-B., Kim, S. (2016). Sensitivity Study on High-Resolution Numerical Modeling of Static Topographic Data.
Atmosphere, 7, 86.

Jee, J. B., & Kim, S. (2017). Sensitivity sudy on high-resolution WRF precipitation forecast for a heavy rainfall event. *Atmosphere*, *8*(6).
https://doi.org/10.3390/atmos8060096

Jeworrek, J., West, G., & Stull, R. (2019). Evaluation of cumulus and microphysics parameterizations in WRF across the convective gray zone. *Weather and Forecasting*, *34*(4), 1097–1115. https://doi.org/10.1175/WAF-D-18-0178.1

Kain, J. S., Fritsch, J. M. (1990), A one-dimensional entraining/detraining plumemodel and its application in convective parameterization,
J. Atmos. Sci., 47, 2784–2802.

Kain, J. S., Fritsch, J. M. (1993) Convective parameterization for mesoscale models: The Kain–Fritsch scheme. *The Representation of Cumulus Convection in Numerical Models, Meteor. Monogr.*, No. 24, Amer. Meteor. Soc., 165–170.

Kain, J. S. (2004), The Kain-Fritsch convective parameterization: An update, *J. Appl. Meteorol.*, 43, 170–181.

Kessler, E. (1995) On the continuity and distribution of water substance in atmospheric circulations, *Atmospheric Research*, 38 (1995) 109-145

Li, R., Jin, J., Wang, S. Y., & Gillies, R. R. (2015). Significant impacts of radiation physics in the Weather Research and Forecasting model on the precipitation and dynamics of the West African Monsoon. *Climate Dynamics*, *44*(5–6), 1583–1594. https://doi.org/10.1007/s00382-014-2294-2

Li, Y., Lu, G., Wu, Z., He, H., Shi, J.,Ma, Y., Weng, S. (2016) Evaluation of Optimized WRF Precipitation Forecast over a Complex Topography Region during Flood Season. Atmosphere, 7, 145.

Lim, K. - S.S., Hong, S.-Y. (2010) Development of an effective double-moment cloud microphysics scheme with prognostic cloud condensation nuclei (CCN) for weather and climate models. *Mon. Weather Rev*. 138, 1587–1612.

Lin, Y. – L., Farley, R. – D., Orville, H. – D. (1983) Bulk Parameterization of the Snow Field in a Cloud Model. *J.Climate Appl. Met.*, 22, 1065–1092

Mayor, Y. G., & Mesquita, M. D. S. (2015). Numerical simulations of the 1 May 2012 deep convection event over Cuba: Sensitivity to cumulus and microphysical schemes in a high-resolution model. *Advances in Meteorology, 2015*. https://doi.org/10.1155/2015/973151

Mellor, G. L., Yamada, T. (1982) 'Development of a Turbulence Closure Model for Geophysical Fluid Problems', *Rev. Geophys. Space Phys.* 20, 851–875.

Merchant, C. J., Filipiak, M. J., Le Borgne, P., Roquet, H., Autret,E., Piolle, J. F., and Lavender, S. (2008) Diurnal warm-layer events inthe western Mediterranean and European shelf seas, *Geophys.Res. Lett.*, 35, L04601, https://doi.org/10.1029/2007GL033071

Miao, C., Ye, A., & Tong, C. (2014). *in the Greater Beijing Area*. 579–587. https://doi.org/10.1002/2014GL061623.

Min, J.-S., Rho, J.-W., Jee, J.-B., Kim, S. (2016) A study on sensitivity of heavy precipitation to domain size with a regional numerical weather prediction model. Atmosphere, 26, 85–95.

Ministry of Forestry and Water Affairs & General Directorate of Meteorology. (2013). DENİZ SUYU SICAKLIK VERİSİNİN İSTATİSTİKSEL ANALİZİ

Ministry of Forestry and Water Affairs & Directorate General for Water Management. (2016). *Antalya Havzası Taşkın Yönetim Planı*.

Ministry of Forestry and Water Affairs & General Directorate of Meteorology. (2019). DENİZ SUYU SICAKLIK VERİSİNİN İSTATİSTİKSEL ANALİZİ

Ministry of Forestry and Water Affairs & Directorate General for Water Management. Kuraklik. (2019). *S TRATEJİK ÇEVRESEL DEĞERLENDİRME*.

Ministry of Forestry and Water Affairs & Directorate General for Water Management. (2019). DOĞU KARADENİZ HAVZASI TAŞKIN YÖNETİM PLANI STRATEJİK ÇEVRESEL DEĞERLENDİRME TASLAK KAPSAM BELİRLEME RAPORU

Minnett, P. J. (2014). Sea surface temperature. *Encyclopedia of Earth Sciences Series, Exhibit 1*, 754–759. https://doi.org/10.1007/978-0-387-36699-9_166

Mironov, D. V. (2015). Parameterization of Cumulus Convection, COSMO-CLM-ART Training, Langen, Germany, 23 – 31 March 2015

Moya-Álvarez, A. S., Martínez-Castro, D., Flores, J. L., & Silva, Y. (2018). Sensitivity Study on the Influence of Parameterization Schemes in WRF-ARW Model on Short- and Medium-Range Precipitation Forecasts in the Central Andes of Peru. *Advances in Meteorology, 2018*. https://doi.org/10.1155/2018/1381092

National Centers for Environmental Prediction (NCEP), National Oceanic and Atmospheric Administration (NOAA) (2014) https://polar.ncep.noaa.gov/sst/rtg_high_res/description.shtml. Accessed 23 December 2019

Nurmi, P. (2007). *Verification of Categorical Forecasts*. Meteorological Research & Development Finnish Meteorological Institute, 3rd International Verification Methods Workshop. https://www.ecmwf.int/sites/default/files/elibrary/2007/15490-verification-categorical-forecasts.pdf Accessed 15 May 2020

Pleim, J. E. (2007a) A combined local and nonlocal closure model for the atmospheric boundary layer. Part I: Model description and testing. *J. Appl. Meteor. Climatol.*, 46, 1383–1395.

——, 2007b: A combined local and nonlocal closure model for the atmospheric boundary layer. Part II: Application and evaluation in a mesoscale meteorological model. *J. Appl. Meteor. Climatol.*, 46, 1396–1409.

——, Chang, J. S (1992) A non-local closure model for vertical mixing in the convective boundary layer. *Atmos. Environ.*, 26A, 965–981.

Peng, G. (2014a) What's the difference between FNL and GFS ?. National Center for Atmospheric Research. https://rda.ucar.edu/datasets/ds083.2/docs/FNLvGFS.pdf. Accessed 15 May 2020

Peng, G. (2014b) Analysis, reanalysis, forecast—what's the difference?. National Center for Atmospheric Research. https://rda.ucar.edu/datasets/ds083.2/docs/Analysis.pdf. Accessed 15 May 2020

Rebora, N., Molini, L., Casella, E., Comellas, A., Fiori, E., Pignone, F., Siccardi, F., Silvestro, F., Tanelli, S., Parodi, A. (2013) Extreme Rainfall in the

Mediterranean: What Can We Learn from Observations?, *Journal of Hydrometeorology*, 14(3):906-922. https://doi.org/10.1175/JHM-D-12-083.1

Robinson, I., Piolle, J. F., Leborgne, P., Poulter, D., Donlon,C., and Arino, O. (2012) Widening the application of AATSR SST data to operational tasks through the Medspiration Service, *Remote Sens. Environ.*, 116, 126–139. https://doi.org/10.1016/j.rse.2010.12.019

Rontu, L. (2013). Studies on orographic effects in a numerical weather prediction model.

Senatore, A., Mendicino, G., Knoche, H. R., & Kunstmann, H. (2014). Sensitivity of modeled precipitation to sea surface temperature in regions with complex topography and coastlines: A case study for the Mediterranean. *Journal of Hydrometeorology*, *15*(6), 2370–2396. https://doi.org/10.1175/JHM-D-13-089.1

Senatore, A., Furnari, L., & Mendicino, G. (2020). Impact of high-resolution sea surface temperature representation on the forecast of small Mediterranean catchments' hydrological responses to heavy precipitation. *Hydrology and Earth System Sciences*, *24*(1), 269–291. https://doi.org/10.5194/hess-24-269-2020

Sikder, S., and F. Hossain (2016), Assessment of the weather research and forecasting model generalized parameterization schemes for advancement of precipitation forecasting in monsoon-driven river basins, *J. Adv. Model. Earth Syst.*, 8, 1210–1228, doi:10.1002/2016MS000678.

Skamarock, W. C., Klemp, J. B., Dudhia, J., Gill, D. O., Liu, Z., Berner, J., … Huang, X. -yu. (2019). *A Description of the Advanced Research WRF Model Version 4* (No. NCAR/TN-556+STR). doi:10.5065/1dfh-6p97

Smith, B. L., Yuter, S. E., Neiman, P. J., Kingsmill, D. E. (2010) Water vapor fluxes and orographic precipitation over Northern California associated with a landfalling atmospheric river. Mon. Wea. Rev., 138, 74–100. doi:https://doi.org/10.1175/2009MWR2939.1

Song, X., & Zhang, G. J. (2011). Microphysics parameterization for convective clouds in a global climate model: Description and single-column model tests. *Journal of Geophysical Research Atmospheres*, *116*(2), 1–17. https://doi.org/10.1029/2010JD014833

Stensrud, D. – J. (2007) Parameterization Schemes: Keys to Understanding Numerical Weather Prediction Models, Cambridge University Press, New York, USA

Stensrud, D., Morrison, H., (2010), Parameterization Schemes, Chapter 7.

Suhas, E., & Zhang, G. J. (1955). Journal of geophysical research. *Nature*, *175*(4449), 238. https://doi.org/10.1038/175238c0

Szoke, E., Koch, S., E., Barjenbruch, D., Wesley, D.A. (2007) Evaluation of the NCEP WRF NMM and ARW models for some recent high-impact weather events, 22nd Analysis and Forecasting/18th Conference on Numerical Weather Prediction, American Meteorological Society, Park City, Utah

Szunyogh, I., (2015). Techniques For The Exploration Of Atmospheric Dynamics: Applicable Atmospheric Dynamics, World Scientific Publishing, 337.

Thompson, G., Field, P. R., Rasmussen, R. M., Hall, W. D. (2008) Explicit Forecasts of Winter Precipitation Using an Improved Bulk Microphysics Scheme. Part II: Implementation of a New Snow Parameterization. *Mon. Wea. Rev.*, 136, 5095–5115.

Thompson, G., Eidhammer, T. (2014) A Study of Aerosol Impacts on Clouds and Precipitation Development in a Large Winter Cyclone. Journal of the Atmospheric Sciences. 71. 3636. 10.1175/JAS-D-13-0305.1.

Senatore, A., Mendicino, G., Knoche, H. R., & Kunstmann, H. (2014). Sensitivity of modeled precipitation to sea surface temperature in regions with complex topography and coastlines: A case study for the Mediterranean. *Journal of Hydrometeorology*, *15*(6), 2370–2396. https://doi.org/10.1175/JHM-D-13-089.1

Song, X., & Zhang, G. J. (2011). Microphysics parameterization for convective clouds in a global climate model: Description and single-column model tests. *Journal of Geophysical Research Atmospheres*, *116*(2), 1–17. https://doi.org/10.1029/2010JD014833

Suhas, E., & Zhang, G. J. (1955). Journal of geophysical research. *Nature*, *175*(4449), 238. https://doi.org/10.1038/175238c0

Team, G. S. (2010). *The Recommended GHRSST Data Specification (GDS) Revision 2.0 Technical Specifications*. *2010*.

UCAR. (2019). *WRF - Weather Research & Forecasting Model*. *January*, 1–456.

Ve, T., Bakanli, O., Kuraklik, K. I. N. V. E., & Ba, R. E. (2019). *S TRATEJİK ÇEVRESEL DEĞERLENDİRME*.

Yilmaz, A. G. (2015). The effects of climate change on historical and future extreme rainfall in Antalya , Turkey. *Hydrological Sciences Journal*, *60*(12), 2148–2162. https://doi.org/10.1080/02626667.2014.945455

Yousefi, K. et al. (2020) 'Production of a High-Resolution Improved Radar Precipitation Estimation Map Using Gauge Adjustment Bias Correction Methods', in EGU2020. EGU Sharing Geosciences Online. doi: https://doi.org/10.5194/egusphere-egu2020-18780

Yucel, I., & Onen, A. (2014). *Evaluating a mesoscale atmosphere model and a satellite-based algorithm in estimating extreme rainfall events in northwestern Turkey*. 611–624. https://doi.org/10.5194/nhess-14-611-2014

Zhou, Y ., Liu, L., Deng, G. (2009) Comparisons of the Generalized Potential Temperature in Moist Atmosphere with the Equivalent Potential Temperature in Saturated Moist Atmosphere, Hindawi Publishing Corporation Advances in Meteorology Volume 2009, Article ID 105265, 9 pages doi:10.1155/2009/105265

Zhou, Y., & Mu, Z. (2018). Impact of different reanalysis data and parameterization schemes on WRF dynamic downscaling in the Ili Region. *Water (Switzerland)*, *10*(12). https://doi.org/10.3390/w10121729

Zeyaeyan, S., Fattahi, E., SaadatAbadi, A. R., Azadi, M., & Vazifedoust, M. (2017). Evaluating the effect of physics schemes in WRF simulations of summer rainfall in North West Iran. *Climate*, *5*(3). https://doi.org/10.3390/cli5030048